Lactide Polymerization Kinetic Studies and Development of Flow NMR Instrumentation

By

Anna Louise Dunn

A dissertation submitted in partial fulfillment of

the requirements for the degree of

Doctor of Philosophy

(Chemistry)

at the

UNIVERSITY OF WISCONSIN-MADISON

2015

Date of final oral examination: 8/11/2015

The dissertation is to be approved by the following members of the Final Oral Committee:

Clark R. Landis, Professor, Chemistry
Ive Hermans, Associate Professor, Chemistry
Thomas C. Brunold, Professor, Chemistry
Shannon S. Stahl, Professor, Chemistry
Thatcher W. Root, Professor, Chemical and Biological Engineering

Lactide Polymerization Kinetic Studies and Development of Flow NMR Instrumentation

Anna L. Dunn

Under the supervision of Professor Clark R. Landis

At the University of Wisconsin-Madison

Stopped-flow (SF) NMR spectroscopy is an information-rich technique that allows direct spectroscopic observation of fast, irreversible reaction progression on millisecond time scales by mixing reagents within the spectrometer. The initiated reaction mixture flows into the NMR detection region and stops for NMR acquisition. A new design of SF NMR probe enables accurate examination of reactions on short time regimes at variable temperatures by utilizing a coiled, temperature-controlled tube reservoir at the center of the NMR spectrometer that permits reagent magnetization and temperature equilibration prior to mixing. A modified wide-bore 360 MHz NMR probe utilizes a two-jet mixer which allows complete mixing of substrates with a short transport time (2.6 ms) and fast flow rate (14.5 mL/s). ^{1}H NMR spectra for the polymerization of lactide with an air-sensitive catalyst 1,3-dimesitylimidazol-2-ylidene (IMes) are acquired over the temperature range of -30 to 40 °C. SF NMR enables direct observation of lactide epimerization in the zwitterionic polymerization of lactide as catalyzed by IMes. Data for both monomer consumption and molecular weight distribution as a function of time are examined with a kinetic model featuring slow initiation, rapid propagation, and reversible elimination of free IMes to form cyclic polylactide. In collaboration with Pfizer, online NMR spectroscopy, a technique for observing reaction progression where the reaction mixture is continuously flowing (*ca.* 4 mL/min) from a reaction vessel to the NMR probe for analysis then returned to the reaction vessel, is directly compared with the basic method of reaction monitoring in an NMR tube. Additionally, online NMR spectroscopy is utilized for reaction monitoring and mechanistic characterization of the reaction of 3-methylpentanoic acid with Meldrum's acid.

Acknowledgements

I am extremely grateful to have so many supportive people in my life. Clark always advocated for me and taught me that "NMR doesn't lie", a lesson I will never forget. Charlie Fry is an excellent mentor and friend who always supported my research and hankerings for wedge fries. David Foley, Mark Zell, and Ron Morris taught me a lot about "real life" and encouraged me to have more confidence in my abilities. Tracy Drier allowed me to express my creativity and performed many glassblowing miracles. I would like to thank Thomas Brunold for helping my development at Wisconsin. I also appreciate the time Hans Reich, Shannon Stahl, Ive Hermans, and Thatcher Root have devoted to my education.

Thank you to the past and present members of the Landis group for all the conversations, spontaneous ice cream runs, inside jokes, and thesis editing. To GWW – your scientific enthusiasm is hard to match. I wish I could still learn from you. The many friends I made in the department taught me a lot about chemistry, video games, and how to be a bro. Amanda Corcos and I have many cheap dates and bottles of wine in our future. I was fortunate enough to make great friends outside of the department who forced me to enjoy fresh air and furthered my appreciation for baked goods.

My family has relentlessly supported me in all my endeavors. Thank you for instilling a love of science in me from such a young age. My grandmother Louise inspires me each day to be full of kindness and good humor. I hope I can live up to her memory.

My partner Alex Meyer has an incredible amount of patience and has been a constant cheerleader and source of support. My furry companion Poe is always feisty and full of love. I am so excited for the many adventures that lie ahead.

Table of Contents

Chapter 1

Introduction for a Non-Chemist Audience

1.1. NMR (Nuclear Magnetic Resonance)

Just as MRI (Magnetic Resonance Imaging) helps doctors to see what is going on inside your body, NMR (Nuclear Magnetic Resonance) helps chemists to see what is going on in a reaction. Much of the theory behind MRI and NMR is the same – you can think of NMR as being a two-dimensional MRI. Most of my dissertation deals with using NMR instrumentation. We will not go into the theory and the physics behind NMR; instead, I will describe how to perform NMR measurements. When I have an unknown sample, I dissolve it in a liquid (make a *solution*) and place the solution in a glass tube (an *NMR tube*). I then place the NMR tube in the middle of a giant magnet, known as the *spectrometer*, and tell the computer to collect data (acquire an *NMR spectrum*) on the sample in order to get the information I need.

1.2. Studying Reactions

Chemists are typically concerned with what happens when you mix two or more things together. The things that we mix together are known as *reagents*, and they will often combine to make a new thing, known as a *product*. The act of going from reagents to products is known as a *reaction*. See Figure 1.1 for an example.

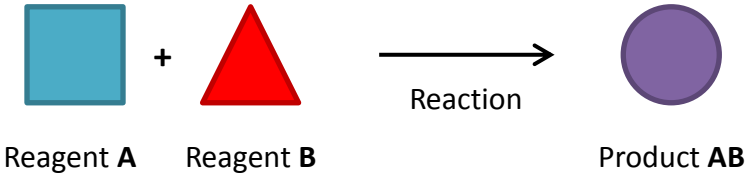

Figure 1.1. The reaction of Reagent **A** and Reagent **B** to form Product **AB**.

My work is concerned with being able to watch the reaction happen in real time, under real-life conditions, to understand exactly how the reaction proceeds. We need to be able to

watch reactions because what we call *intermediates* are often formed from the reagents and later transformed into the products (Figure 1.2). By understanding what intermediates are formed, and how quickly they are formed, we learn a lot more about how the reaction actually works. The tricky thing is that these intermediates are often formed very quickly and disappear too quickly for us to see them.

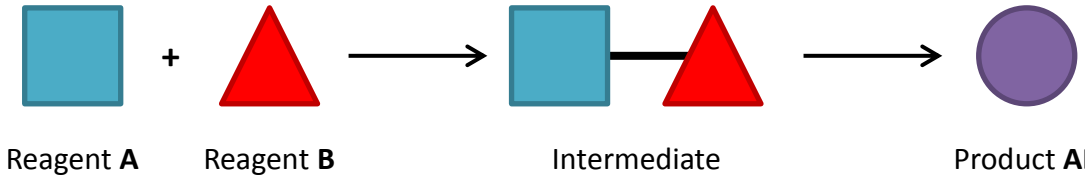

Figure 1.2. Reagent **A** and Reagent **B** first form an intermediate, which then forms Product **AB**.

Reactions that have halfway transformed into products within 10 seconds are very difficult to study by NMR. Even experienced NMR users need around 30 seconds to mix two reagents together and put the NMR tube in the spectrometer before they can take an NMR spectrum. By that time, the reaction is finished and we do not know what intermediates were formed! We therefore need a technique that allows mixing of two reagents quickly enough to observe intermediates by NMR of these very fast reactions.

1.3. Stopped-Flow NMR

If we want to study extremely fast reactions, we need to be able to acquire an NMR spectrum within a few milliseconds of reagent mixing. Our approach is called *stopped-flow* NMR because we flow the reagents into the spectrometer where we then stop the flow and take NMR spectra. Figure 1.3 is a drawing of what goes inside the NMR spectrometer. Each reagent (blue and red) flows into a T-shape design. When the reagents hit one another, they immediately

mix together (purple) and flow into the region where we can see (*detect*) them by NMR (where the magnet is strongest is known as the *detection region*). If the reagents flow quickly enough, they will mix and reach the detection region in a few milliseconds. Once the reagents reach the detection region, flow must stop before acquiring NMR spectra. The mixed reagents need to stop within the detection region because it takes a few seconds to acquire an NMR spectrum.

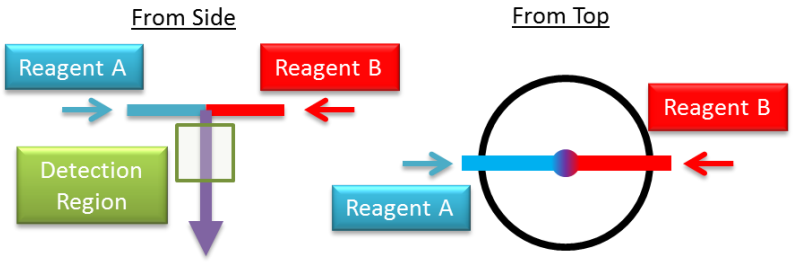

Figure 1.3. How the reagent solutions mix within the NMR spectrometer.

By mixing the two reagents together right above the detection region, we can take NMR spectra less than 100 milliseconds after the reaction begins! This allows me to study very fast reactions that I would not be able to understand without this instrumentation. The main reaction that I study in my graduate work is the polymerization of lactide, which I will talk about next.

1.4. Lactide Polymerization

A *polymerization* is a reaction where many *monomers* (smaller molecules) connect to form a larger molecule known as a *polymer*. A polymerization of green circles is displayed in Figure 1.4.

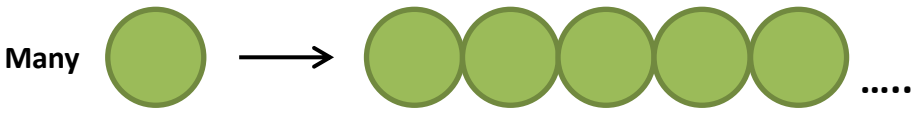

Figure 1.4. The polymerization of many monomers to form a larger polymer.

All of the plastics you encounter on a daily basis are different types of polymers. The reason why soda bottles are clear and milk jugs are cloudy, even though they are both made of plastic, is because different monomers are used to make the polymers. *Polylactide*, what I study, is biodegradable and decomposes to become nontoxic material. The environmental and medical applications for polylactide are wide-spread. Imagine if you could use biodegradable forks at your next picnic instead of contributing to the landfill, or if heart stints were biodegradable, eliminating a second surgery to remove the stint after the heart heals.

The monomer used in my research is called *lactide*, which comes from lactic acid - something your body produces when you work out that makes your muscles hurt. We get lactide from lots of renewable resources, such as corn and sugar beets. My goal is to watch the polymerization of lactide into polylactide by using NMR. Knowing more information about the process of polymerization allows us to have more control over the final polymer product. Understanding the steps from monomer to intermediate(s) to polymer (known as the *mechanism*) and how fast each step is (known as the *kinetics*) is extremely powerful knowledge! With that information it is much easier to influence the resulting polymer, making it be either thin and pliable or thick and tough, depending on what application we desire.

Chapter 2

Stopped-Flow NMR Spectroscopy: Recent Developments in Instrumentation and Application to Fast, Irreversible Reactions

2.1. Introduction

Direct spectroscopic observation of reaction progress over time affords valuable mechanistic and kinetic information. To observe reaction progression with minimal perturbations to the system, many tools have been implemented, commonly utilizing optical spectroscopy (UV-Vis, IR, Raman) or calorimetry.[1–11] Although these methods work well for monitoring reaction progress for many reactions and over broad time scales, they are not ideally suited to provide easily interpreted information about intermediates or unexpected mechanistic pathways. Limitations arise with these methods because not all reactions have suitable chromophores, quantitation of concentrations requires tedious calibrations, and the information is generally insufficient to make clear structural assignments for reactions that produce multiple products and intermediates. In contrast, Nuclear Magnetic Resonance (NMR) spectroscopy provides, in principle and often in practice, quantitative information about the structures and concentrations all reagents, intermediates, and products generated that have NMR active nuclei during a reaction. For these reasons, NMR spectroscopy is a preferred method for obtaining mechanistic and kinetic insight into chemical reactions.[12]

Despite the widespread utility of NMR spectroscopy for mechanistic examination, traditional NMR techniques cannot be applied to the investigation of fast, irreversible reactions. By traditional NMR we mean mixing reagents into an NMR tube which is then inserted into the instrument followed by data collection (perhaps with locking and shimming of the magnetic field preceding data gathering). This process precludes collecting data in the first *ca.* 10-30 seconds of a reaction. Processes that occur on faster time scales can be probed by NMR exchange techniques, but such methods are limited to studying systems in equilibrium, in other words fast, *reversible* reactions.[13–17] For fast, irreversible reactions, where monitoring of the first few

seconds of reaction time is essential, two main classes of NMR methods have been developed: rapid-injection and stopped-flow NMR spectroscopy.

Rapid-injection experiments involve injecting and mixing a reactant solution into an NMR tube containing the other reactant solution.[18–29] Rapid-injection techniques have reported dead times, the minimal amount of time necessary between reaction initiation and data acquisition, as fast as *ca.* 100 ms. With the exception of nuclei with very short longitudinal relaxation times (T_1), the time interval between spectra during a reaction followed by rapid injection NMR generally is greater than a few seconds because the nuclei must relax to equilibrium before the next pulse.[18,25,29] This represents a fundamental limitation on the time resolution of the experiment. In principle, one could achieve finer time resolution by running multiple experiments with different delays between injection and the collection of the first spectrum while maintaining, say 2 s delays between subsequent spectra (Figure 2.1). However, the rapid-injection method as practiced is a batch process that requires slow and inconvenient setup of a new batch reaction for each experiment.

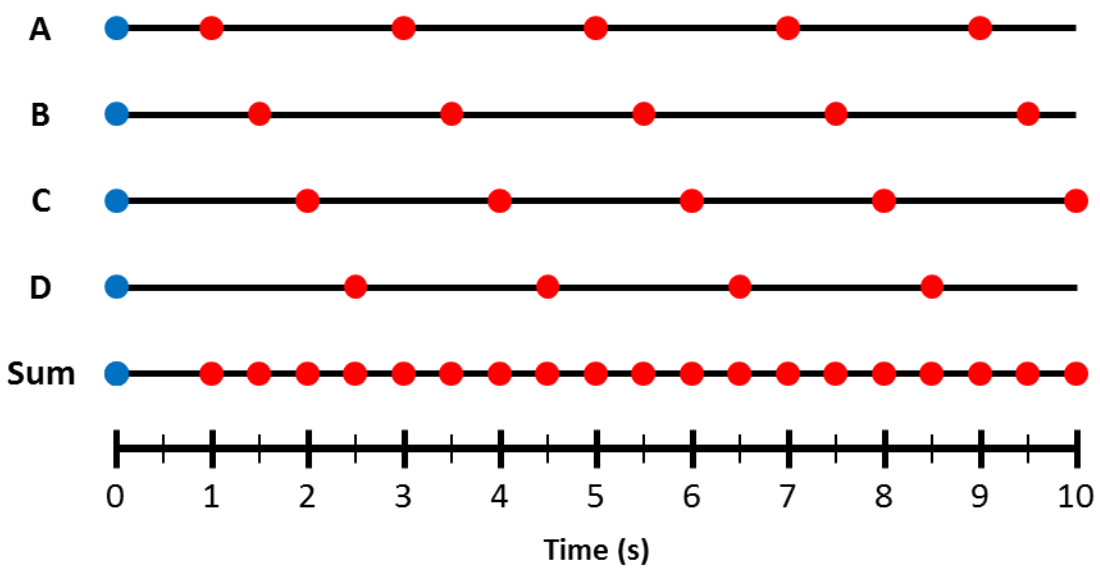

Figure 2.1. Example of the method for collecting data on a finer time resolution by combining data from multiple experiments (**A**-**D**) with different delay times between injection and acquisition of the first spectrum. The injection time (blue) is at t = 0 s. The first experiment (**A**) has an initial delay of 1 s before the first spectrum (red) is collected, with a 2 s delay between spectra. Experiments **B**, **C**, and **D** have initial delays of 1.5, 2, and 2.5 s, respectively, and each have a 2 s delay between spectra. Interleaving data from experiments **A**-**D** results in data collected at 0.5 s intervals, displayed in **Sum**.

Flow techniques enable multiple experiments to be performed more conveniently and with higher throughput than batch methods. Many examples of reactions that use optical spectroscopy in flow systems have been reported over the last 90 years; the stopped-flow (SF) method is very popular for fast reactions.[30–32] Stopped-flow implementation of NMR spectroscopy (SF NMR) involves injecting two reagent solutions into a mixer, and then directing the mixed solutions into the detection region of the NMR spectrometer, stopping the flow prior to acquisition. A general scheme of typical SF NMR instrumentation is displayed in Figure 2.2. Two drive syringes push reagent solutions into the mixing and detection regions, which in turn fills a stopping syringe. Once the stopping syringe is full, it hits a stop plate causing the flow to stop and often triggers an electronic switch to send a signal to the spectrometer to begin acquisition.

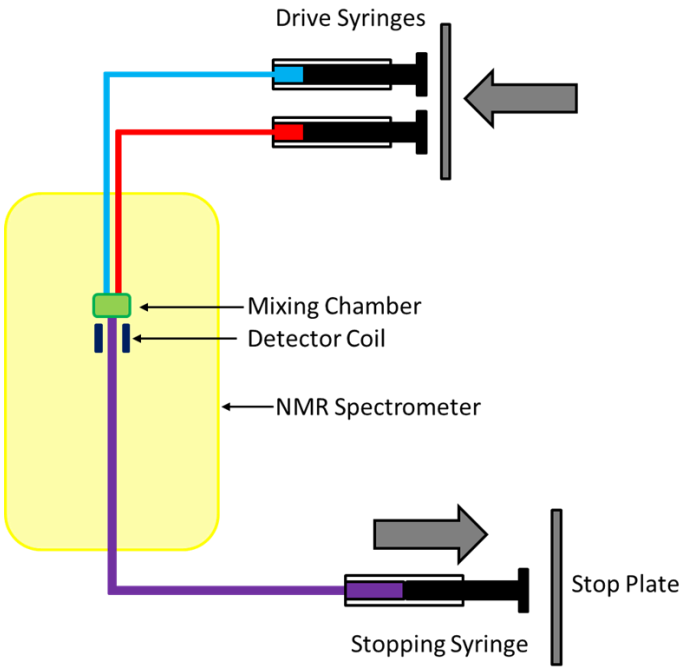

Figure 2.2. General scheme of stopped-flow NMR spectroscopy.

The history of SF NMR spectroscopy and all older designs was well-reviewed by Fyfe, *et al.* in 1978,[33] Parkhurst, *et al.* in 1990,[34] and SF NMR as it relates to protein folding by Ropson, *et al.* in 1993.[35] There are several key challenges that must be addressed in a SF NMR design: (i) loss of signal strength due to the reagent solutions not being fully magnetized prior to acquisition; (ii) reducing the time necessary to transport the mixed reaction solution to the active region; (iii) rapid mixing to achieve complete homogeneity of sample on the timescale of interest; and (iv) stopping the flow of freshly mixed solutions in the active region rapidly and with minimal impact on lineshapes. Multiple designs have been proposed in the literature (with dead times as low as *ca.* 3 ms) to address these issues with varying success.[33–35]

This introduction will focus on the more recent instrumentation developments since those reviewed by Parkhust and Ropson more than 20 years ago.[34,35] Our review will focus on recent changes in the design of the stopped-flow reactor for application in NMR and how these changes addressed some of the challenges described above.

2.2. Stopped-Flow NMR Instrumentation Developments:

There are two approaches to adding stopped-flow capability to NMR instrumentation: stopped-flow inserts that are used with any conventional NMR probe, and modified NMR probes that are solely dedicated to SF or flow measurements. The ability to use conventional NMR probes is an important advantage of stopped-flow inserts, particularly to individuals using shared NMR facilities. Due to the limited space available, sacrifices are often made when designing stopped-flow inserts that limit the effectiveness in one or more areas; therefore, for some applications a modified, dedicated SF NMR probe is necessary. In general, the design of the SF probe or SF insert is highly dependent upon the chemical reaction to be studied, as will be discussed in the applications section.

SF NMR Probe Inserts:

Frieden, *et al.* reported a stopped-flow device that could be easily inserted into a conventional NMR probe in 1994.[36] Their system utilized a commercial drive system which is connected to a mixer placed above a 5 mm NMR tube in the spectrometer. They used a four-jet tangential mixer (Figure 2.3) and minimized the amount of solution that needed to be pushed into the system to 0.7-0.9 mL, meaning a smaller quantity of reagents is needed per experiment.

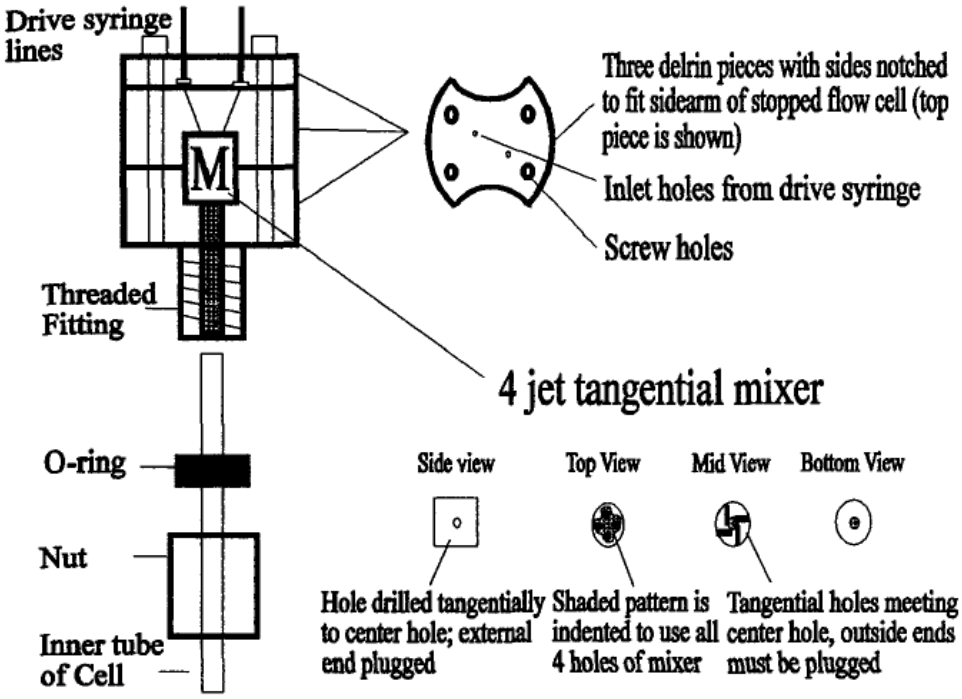

Figure 2.3. Diagram of the Frieden SF insert design with four-jet tangential mixer.[36]

The outlet was connected to a stop syringe, which triggers acquisition upon filling. The dead time was estimated to be *ca.* 100 ms. However, their system did not allow for premagnetization of reagent solutions, decreasing the sensitivity of the method and giving rise to post-mixing magnetization artifacts that arise because the sample is initially at low field and then placed in a high magnetic field after mixing. Additionally, there was no temperature control over the drive system, so all experiments were conducted at room temperature.

In 2005, another SF NMR device for conventional NMR probes was reported by Furó, *et al.*[37] Their system enabled premagnetization of reactant solutions up to 90-95% of the active region magnetization level, thus minimizing post-mixing magnetization artifacts. Valves were used to control driving and stopping, rather than the syringe system typically utilized in SF systems (Figure 1). Their valve design, rather than the typical syringe design, causes variation of

the volumes of liquids by a few percent between separate experiments, leading to larger errors. A diagram of their system is summarized in Figure 2.4, with main components labeled.

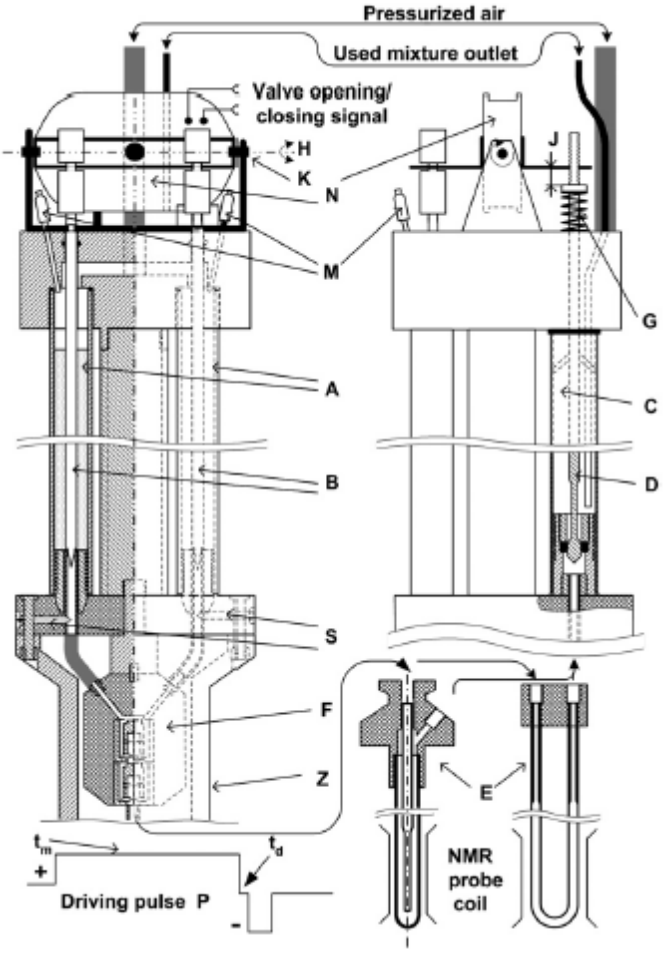

Figure 2.4. Furó, *et al.* stopped-flow design for conventional NMR probes.[37] Premagnetization occurs in the reagent chambers **A**. Upon opening of valves **B** and **D**, reagents are mixed with four-jet tangential jet mixer blocks (**F**) before reaching the NMR tube **E**.

Furó reported dead times of *ca.* 100 ms, with good mixing 20 ms after flowing through two serial four-jet tangential mixing blocks. A disadvantage to their system is that reagents were added to the SF NMR *via* standard glass pipettes and the reagents were driven through the system with pressurized air, precluding the study of moisture- and/or oxygen-sensitive reactions. There is no mention of temperature control of reactant solutions in these studies.

Modified NMR Probes:

Parkhurst, *et al.* reported in 1990 a combined NMR and absorbance stopped-flow device.[34] Their device was unique in that reagents approached the active region from drive syringes at the bottom of the spectrometer, using glass balls as check valves to prevent diffusion of the reacting mixture into the reagent lines (Figure 2.5).

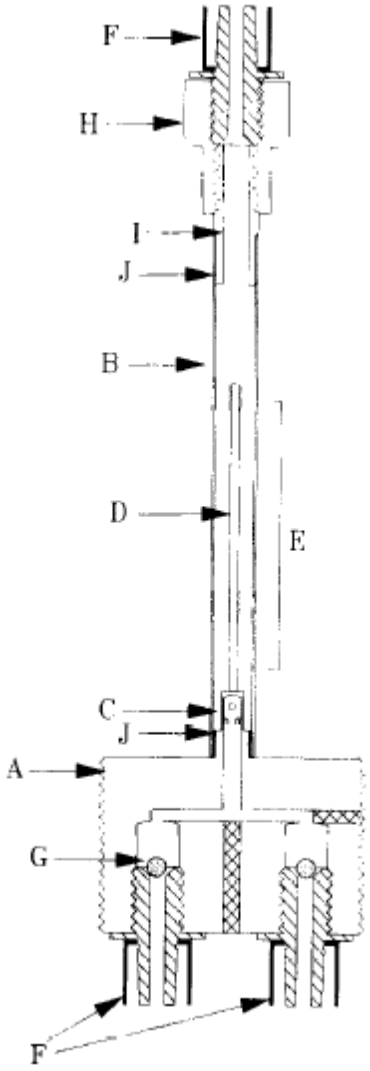

Figure 2.5. The NMR section of the Parkhurst design.[34] Each reagent flows up past a glass ball check valve (**G**) into an 8 jet mixer (**C**) before reaching the NMR detection region (**E**).

In the Parkhurst design the reagents are not completely magnetized before mixing and there is no temperature control over the reagent lines. After flowing through the NMR active

region, the solution reaches an optical cell to perform simultaneous NMR and absorbance measurements. They reported a 60 ms dead time to reach the center of the NMR active region. The ability to measure NMR and optical changes on the same sample allows more information to be gathered at once, particularly for complex systems such as protein folding.

In 1993, Tanaka, *et al.* reported the first high-pressure stopped-flow (HP-SF) NMR device that could monitor reactions under pressures up to 200 MPa (Figure 2.6).[38] In order to sustain such pressures, the high-pressure NMR vessel was constructed of tantalum reinforced with stainless steel. The reagents are pushed into the active region by high-pressure driving syringes. The system utilized a pressure transmitting fluid (in this case, poly(chlorotrifluoroethylene)) around the NMR tube. Both the pressure transmitting fluid and the sample within the NMR tube were pressurized, resulting in no pressure differential on the NMR tube.

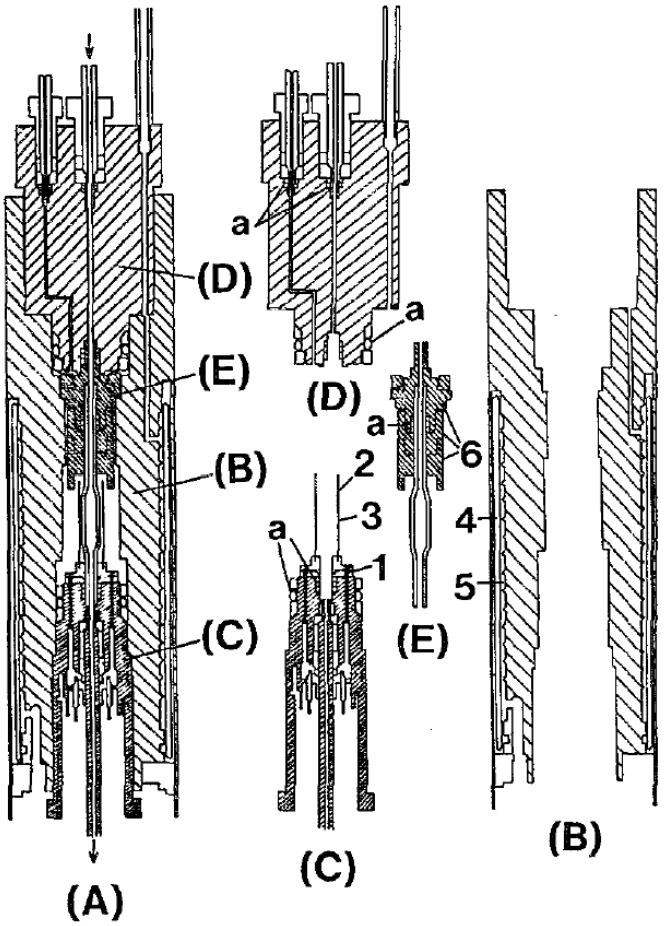

Figure 2.6. Tanaka HP-SF NMR diagram. The entire probe is on the left (**A**) and each part **B**-**E** is displayed larger to the right. The reagents flow from the top left in (**D**), a plug adapted for flow, through the flowtube (**E**). The HP NMR vessel (**B**) includes a Dewar (**4**) and grooves for thermostated N_2 gas (**5**) to provide temperature control. (**C**) represents the electrical terminal, and each place marked with (**a**) is an o-ring seal.[38]

Tanaka, *et al.* reported a dead time of several hundred ms. Two mL of sample is required per run, so only two runs can be measured per filling of the reagent syringes. They achieve temperature regulation of reagents by regulating the temperature of the reagent syringes and the high-pressure tube leading to the NMR detection region. This is the only system reported that is able to study high pressure reactions using stopped-flow NMR spectroscopy.

Landis, *et al.* reported in 2010 a slight modification of a commercial flow probe to allow for stopped-flow use.[39] The reagent lines led to a four-jet mixer, after mixing, the reacting

solution flowed through a glass flow tube comprised of 3 mm NMR tube in the active region fused to glass tubing which extended through the probe (Figure 2.7).

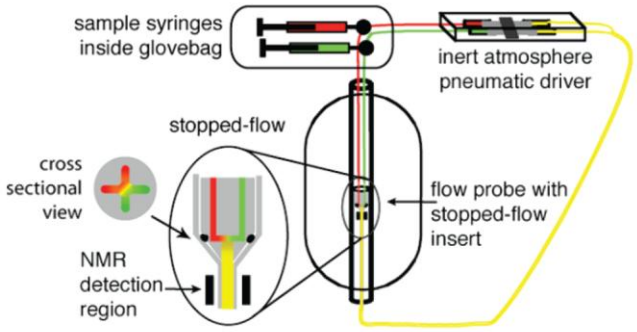

Figure 2.7. The Landis SF modification on a commercial flow probe.[39]

The Landis system had a dead time of ca. 35 ms. The design did not allow for premagnetization of reagents or for temperature control of reagent lines, so reactions were limited to room temperature. Additionally, the system is completely air and moisture free, allowing the ability to study moisture sensitive reactions such as complex organometallic pathways.

2.3. Recent Applications of Stopped-Flow NMR Spectroscopy

Each of the stopped-flow NMR systems mentioned above has their own advantages and disadvantages, and were often built with a specific type of system in mind. The faster reactions require premagnetization of reagents, as in the Furó system,[37] to acquire quantitative data at very short dead times. The Frieden[36] and Parkhurst[34] systems are similar in that they are optimized for room temperature reactions that do not require premagnetization of reagents, so those authors used their systems for slower protein and micelle applications. Tanaka's device[38] is unique in that it can obtain information about reactions under pressure. The Landis instrument[39] reports

the lowest dead time of all the mentioned devices while additionally allowing for air-free systems that are necessary for many organometallic reactions.

Parkhurst, *et al.* used their combination SF NMR and absorbance device to study the denaturation of ^{19}F-labeled hemoglobin by sodium hydroxide.[34] Although the absorbance data did not indicate any intermediates during the reaction, the ^{19}F SF NMR data clearly displayed an intermediate that quickly grew in, maximizing 20 s after reaction initiation, and decayed over the course of the reaction (200 s), allowing insight into the denaturation mechanism.

In addition to the stopped-flow protein folding studies mentioned by Frieden, Hoeltzli, and Ropson in 1993,[35] these authors reported another study in 1994 using fluorine labeled amino acids to watch the folding behavior of *E. coli* dihydrofolate reductase (DHFR) with ^{19}F SF NMR.[36] Using this technique, they examined fluorine labeled amino acid side chains during protein denaturation. The ability to discern specific information about the individual amino acid side chains gave essential insight into the folding mechanisms of a variety of proteins.

The pressure dependence of reaction rates were studied using the HP-SF NMR device mentioned above.[38] Tanaka, *et al.* used their device to study the reaction of tetramethyltin with iodine, noting a significant rate acceleration upon pressurization with nitrogen gas. In addition, they studied the solvent exchange of $[Al(DMF\text{-}d_0)_6](ClO_4)_3$ and DMF-d_6 in CD_3NO_2. In order to differentiate between free and bound DMF, they added a solution of paramagnetic manganese (II) ions to broaden and deshield free DMF. They followed the fast solvent exchange reaction by monitoring the decrease in ^{1}H NMR of bound DMF molecules at 141 MPa and obtained an exchange rate constant.

Another recent application of stopped-flow NMR spectroscopy is the study of the dynamics of micellar changes that occur upon dilution, reported by Furo, *et al.* in 2006.[40] The

authors studied the micelle behavior of aqueous solutions of the surfactant sodium perfluorooctanoate (NaPFO) upon dilution with water. They were able to monitor micellar behavior by observing changes in chemical shift and transverse relaxation time (T_2) with ^{19}F SF NMR. The ^{19}F NMR chemical shift is sensitive to the average intermolecular environment, so changes in chemical shift displayed changes in aggregation of micelles. The T_2 is dependent upon the average size and/or shape of the micelles, but the error of T_2 measurement in their system is on the same order as the expected T_2 change. They reported no changes in ^{19}F NMR chemical shift or T_2 within their first time point (100 ms), so they concluded that the equilibration upon dilution occurs in less than 100 ms. This result was in contradiction to another study of the system using small-angle X-ray scattering (SAXS) which saw much slower time to equilibration,[41] and the authors attributed this to the fact that NMR is sensitive to the average molecular environment, but that there could be a low-amplitude, slower relaxation process that is not observable via NMR.

Surfactant phase change kinetics can also be studied by SF NMR spectroscopy, as demonstrated in 2006 by Stilbs, *et al.*[42] The authors monitored precipitation and crystal growth upon addition of sodium chloride to aqueous solutions of NaPFO in micellar form. Crystallization was observed with time by observing signal loss due to the rotational hindrance of crystalline solids, which causes significant line broadening in the ^{19}F SF NMR spectrum. The authors noted that reproducible results were only obtained after a first, irreproducible run. They attributed this behavior to the first run leaving crystallization seeds within the SF NMR system, allowing crystal growth upon pre-existing nuclei. The main crystallization pathway was observed to be due to incorporation of monomers, not whole micelles, into the crystal by observing change in ^{19}F chemical shift with time.

Additionally, catalyst speciation of an organometallic zirconium-catalyzed polymerization of 1-hexene as observed by stopped-flow NMR was reported in 2010 by Landis, *et al.*[39] Following reaction progress with time *via* ^{1}H NMR allowed direct observation of three Zr-containing species with respect to time. With accurate concentrations of intermediate catalyst species, all rate constants of the Zr-catalyzed polymerization were determined by fitting to a kinetic model.

2.4. Conclusion

Over the past 25 years, multiple designs of stopped-flow NMR instrumentation have been reported, all of which have different advantages and disadvantages. The applications of stopped-flow NMR in the literature are widespread, gathering information about fast reactions at high pressures, protein folding, micellar kinetics, surfactant precipitation, and organometallic polymerizations. The ability of stopped-flow NMR to give crucial information from the first milliseconds of a reaction will be essential to understanding the mechanism and kinetics of fast, irreversible reactions.

The remaining challenges left to the stopped-flow NMR community are to design and build a probe that allows for *all* of the following in order to allow study of a wide variety of reactions with a single piece of instrumentation: (i) premagnetization of reagents; (ii) temperature control of the reagent lines and active region; (iii) air-free design; and (iv) complete mixing of reagents. Additionally, an extremely powerful stopped-flow NMR field is opened if a design that incorporates both all of above and dead times below 5 ms is introduced into the literature. First reported experimentally by Ernst, *et al.*, and further elaborated on computationally by Landis, *et al.*, a stopped-flow NMR probe with a dead time below 5 ms gives

rise to NMR lineshape information that allows the kinetics of very fast reactions to be elucidated from single scan NMR spectra.[43,44] My efforts to construct a SF NMR probe that addresses many of these problems is detailed in Chapter 3.

2.5. References:

(1) Rao, C. N. R. *Ultra-Violet and Visible Spectroscopy: Chemical Applications*, 3rd ed.; London, 1975.

(2) Connolly, T. J.; Matchett, M.; Mcgarry, P.; Sukhtankar, S.; Zhu, J. *Org. Process Res. Dev.* **2006**, *10* (3), 586.

(3) Denmark, S. E.; Pham, S. M.; Stavenger, R. a.; Su, X.; Wong, K. T.; Nishigaichi, Y. *J. Org. Chem.* **2006**, *71* (10), 3904.

(4) Blackmond, D. G. *Angew. Chemie - Int. Ed.* **2005**, *44* (28), 4302.

(5) Blackmond, D. G.; Rosner, T.; Pfaltz, A. *Org. Process Res. Dev.* **1999**, *3* (4), 275.

(6) LeBlond, C.; Wang, J.; Larsen, R. D.; Orella, C. J.; Forman, A. L.; Landau, R. N.; Laquidara, J.; Sowa, J. R.; Blackmond, D. G.; Sun, Y. K. *Thermochim. Acta* **1996**, *289* (2), 189.

(7) Eisenbeis, S. A.; Chen, R.; Kang, M.; Barrila, M.; Buzon, R. *Org. Process Res. Dev.* **2014**, *19*, 244.

(8) Le Gall, E.; Sengmany, S.; Hauréna, C.; Léonel, E.; Martens, T. *J. Organomet. Chem.* **2013**, *736*, 27.

(9) Sniady, A.; Durham, A.; Morreale, M. S.; Marcinek, A.; Szafert, S.; Lis, T.; Brzezinska, K. R.; Iwasaki, T.; Ohshima, T.; Mashima, K.; Dembinski, R. *J. Org. Chem.* **2008**, *73* (15), 5881.

(10) Korshin, G. V.; Li, C. W.; Benjamin, M. M. *Water Res.* **1997**, *31* (7), 1787.

(11) Aarnoutse, P. J.; Westerhuis, J. A. *Anal. Chem.* **2005**, *77* (5), 1228.

(12) Chamberlain, N. F. *The Practice of NMR Spectroscopy*; Plenum Press: New York, NY, 1974.

(13) *Dynamic Nuclear Magnetic Resonance Spectroscopy*; Jackman, L. M., Cotton, F. A., Eds.; Academic Press: New York, NY, 1975.

(14) Alexander, S. *J. Chem. Phys.* **1962**, *37* (5), 967.

(15) Alexander, S. *J. Chem. Phys.* **1962**, *37* (5), 974.

(16) Gutowsky, H. S.; Vold, R. L.; Wells, E. J. *J. Chem. Phys.* **1965**, *43* (11), 4107.

(17) McConnell, H. M. *J. Chem. Phys.* **1958**, *28* (3), 430.

(18) Jones, A. C.; Sanders, A. W.; Bevan, M. J.; Reich, H. J. *J. Am. Chem. Soc.* **2007**, *129* (12), 3492.

(19) McGarrity, J. F.; Prodolliet, J. *J. Org. Chem.* **1984**, No. 3, 4465.

(20) McGarrity, J. F.; Prodolliet, J.; Smyth, T. *Org. Magn. Reson.* **1981**, *17* (1), 59.

(21) Mok, K. H.; Nagashima, T.; Day, I. J.; Jones, J. A.; Jones, C. J. V; Dobson, C. M.; Hore, P. J. *J. Am. Chem. Soc.* **2003**, *125* (41), 12484.

(22) Bertz, S. H.; Carlin, C. M.; Deadwyler, D. A.; Murphy, M. D.; Ogle, C. A.; Seagle, P. H. *J. Am. Chem. Soc.* **2002**, *124* (46), 13650.

(23) Bertz, S. H.; Cope, S.; Dorton, D.; Murphy, M.; Ogle, C. A. *Angew. Chemie - Int. Ed.* **2007**, *46* (37), 7082.

(24) Bertz, S. H.; Cope, S.; Murphy, M.; Ogle, C. A.; Taylor, B. J. *J. Am. Chem. Soc.* **2007**, *129*, 7208.

(25) Klein, R.; Gawley, R. E. *J. Am. Chem. Soc.* **2007**, *129* (14), 4126.

(26) Mcgarrity, J. F.; Ogle, C. A.; Brich, Z.; Loosli, H.-R. *J. Am. Chem. Soc.* **1985**, *107* (9), 1810.

(27) Mcgarrity, J. F. *Tetrahedron Lett.* **1982**, *23* (4), 417.

(28) Plessel, K. N.; Jones, A. C.; Wherritt, D. J.; Maksymowicz, R. M.; Poweleit, E.; Reich, H. J. *Org. Lett.* **2015**, 2310.

(29) Denmark, S. E.; Williams, B. J.; Eklov, B. M.; Pham, S. M.; Beutner, G. L. *J. Org. Chem.* **2010**, *75* (16), 5558.

(30) Hartridge, H.; Roughton, F. J. W. *Proc. R. Soc. A Math. Phys. Eng. Sci.* **1923**, *104* (726), 376.

(31) Hartridge, H.; Roughton, F. J. W. *Proc. R. Soc. A Math. Phys. Eng. Sci.* **1923**, *104* (726), 395.

(32) Gibson, Q. H. *Methods Enzymol.* **1969**, *16* (C), 187.

(33) Fyfe, C. A.; Cocivera, M.; Damji, S. W. H. *Acc. Chem. Res.* **1978**, *11* (7), 277.

(34) McGee, W. a; Parkhurst, L. J. *Anal. Biochem.* **1990**, *189* (2), 267.

(35) Frieden, C.; Hoeltzli, S. D.; Ropson, I. J. *Protein Sci.* **1993**, *2* (12), 2007.

(36) Hoeltzli, S. D.; Ropson, I. J.; Frieden, C. In *Techniques in Protein Chemistry V*; Crabb, J. W., Ed.; Academic Press: San Diego, CA, 1994; pp 455–465.

(37) Yushmanov, P. V.; Furó, I. *J. Magn. Reson.* **2005**, *175* (1), 264.

(38) Funahashi, S.; Ishihara, K.; Aizawa, S.; Sugata, T.; Ishii, M.; Inada, Y.; Tanaka, M. *Rev. Sci. Instrum.* **1993**, *64* (1), 130.

(39) Christianson, M. D.; Tan, E. H. P.; Landis, C. R. *J. Am. Chem. Soc.* **2010**, *132* (33), 11461.

(40) Yushmanov, P. V.; Furó, I.; Stilbs, P. *Langmuir* **2006**, *22* (5), 2002.

(41) Eastoe, J.; Dalton, J.; Downer, A.; Jones, G. *Langmuir* **1998**, *53* (97), 1937.

(42) Yushmanov, P. V.; Furó, I.; Stilbs, P. *Colloids Surfaces A Physicochem. Eng. Asp.* **2006**, *291* (1-3), 59.

(43) Kühne, R. O.; Schaffhauser, T.; Wokaun, A.; Ernst, R. R. *J. Magn. Reson.* **1979**, *35* (1), 39.

(44) Christianson, M. D.; Landis, C. R. *Concepts Magn. Reson. Part A Bridg. Educ. Res.* **2007**, *30* (4), 165.

Chapter 3

Stopped-Flow NMR Probe Design for Reaction Monitoring at Variable Temperatures

Helen Yan built the first generation device and performed initial testing on the design. Anton Mlinar and Dr. Matthew Christianson built the original pneumatic drive system. Much of the difficult machining was performed by machine shop personnel. The custom flowtube was built by Tracy Drier. Dr. Rob McClain and the electrical shop personnel helped with soldering and electronic components. Dr. Emily Tan was the first to observe lactide epimerization in this system with stopped-flow NMR spectroscopy.

3.1. Introduction

NMR spectroscopy provides detailed kinetic and mechanistic information and, hence, is one of the most valuable techniques for monitoring chemical reactions in solution.[1] However, the most common technique for following reactions by NMR spectroscopy, by which reagents are injected into an NMR tube then placed in the spectrometer for measurement, is blind to the first ~30 s of reaction. Therefore, other methods for introduction of the sample into the NMR instrument are needed to observe faster time scales.

Common methods for accessing fast reactions include variable temperature (VT) NMR, rapid injection NMR, and stopped-flow NMR. The VT approach to following fast reactions by NMR is to slow the reaction by lowering the temperature. Variable temperature (VT) NMR limits the choice of solvent and may move the reaction conditions outside the region of interest. (We note that NMR exchange spectroscopy in combination with VT measurements provides detailed kinetic information over a broad temperature range but only for reversible reactions.[2–6])

Several rapid injection methods have been developed that allow kinetic elucidation for irreversible reactions with half-lives in the sub-second regime.[7–17] Rapid injection techniques include methods that effect mixing through mechanical stirrers or through the impact of the jet of fast moving reagent. In the latter case it appears that mixing times can be as short as 30 ms. Advantages of the rapid injection technique include compatibility with standard NMR probes and standard temperature control systems. However, the rapid injection technique is a batch method, which makes high throughput data collection more difficult than flow systems.

Stopped-flow (SF) NMR spectrometry enables rapid measurement of fast reactions with the convenience of a flow system.[18–23] SF NMR involves pushing two solutions rapidly through an efficient mixer and then the detection region of the NMR instrument. After the active region

has been completely flushed by the flowing solution, the flow is rapidly stopped and data acquisition is initiated. An important consideration is the amount of time which it takes the solutions to mix and reach the middle of the active region, known as the transport time. In addition, the solutions must stop flowing prior to data collection; this time is defined as the stop time. The dead time, the shortest time necessary to wait before a spectrum is acquired, is the sum of stop and transport times. A related measure is the mixing time, which represents the time need to achieve complete mixing of the two reactant solutions.

Applications of SF NMR in the literature are wide-spread and include biological, organic and inorganic reactions.[22–29] Dead times as low as a few milliseconds have been reported, but mixing efficiency, the extent of sample magnetization, and ability to operate with variable temperatures are not always addressed. Previously our group described a simple stopped-flow NMR apparatus that incorporates a mixer assembly into a flow NMR probe and a pneumatic drive system. A disadvantage of this design was the lack of temperature control. In this paper we describe a custom modification of an NMR probe that enables improved reagent magnetization, high flow rates, fast mixing, and variable temperature capabilities.

3.2. Results and Discussion

The stopped-flow NMR system comprises a solution drive system, an NMR probe that has been modified to accommodate the mixer and reaction zone, and an electronic signal system that detects stoppage of flow and communicates to the NMR console through a TTL circuit. The solution drive system, which is mounted to a plastic cart that is placed close to the NMR magnet, has been described by us in previous publications. For the data reported herein, the originally described drive system was modified slightly by minimizing turns in the flow path and

maintaining more constant cross sectional areas throughout the flow lines (Figure 3.1). The drive design is based on a push-pull mechanism that pushes reactant solutions through the mixer and detection with one pair of syringes and pulls the collection syringes on the back side of the NMR probe. Both reactant and collection syringes are attached to a metal plate that is driven by a pneumatic piston. When the plate strikes a mechanical stopping plate an optical trigger switch sends signal to the NMR console that initiates data acquisition.[26]

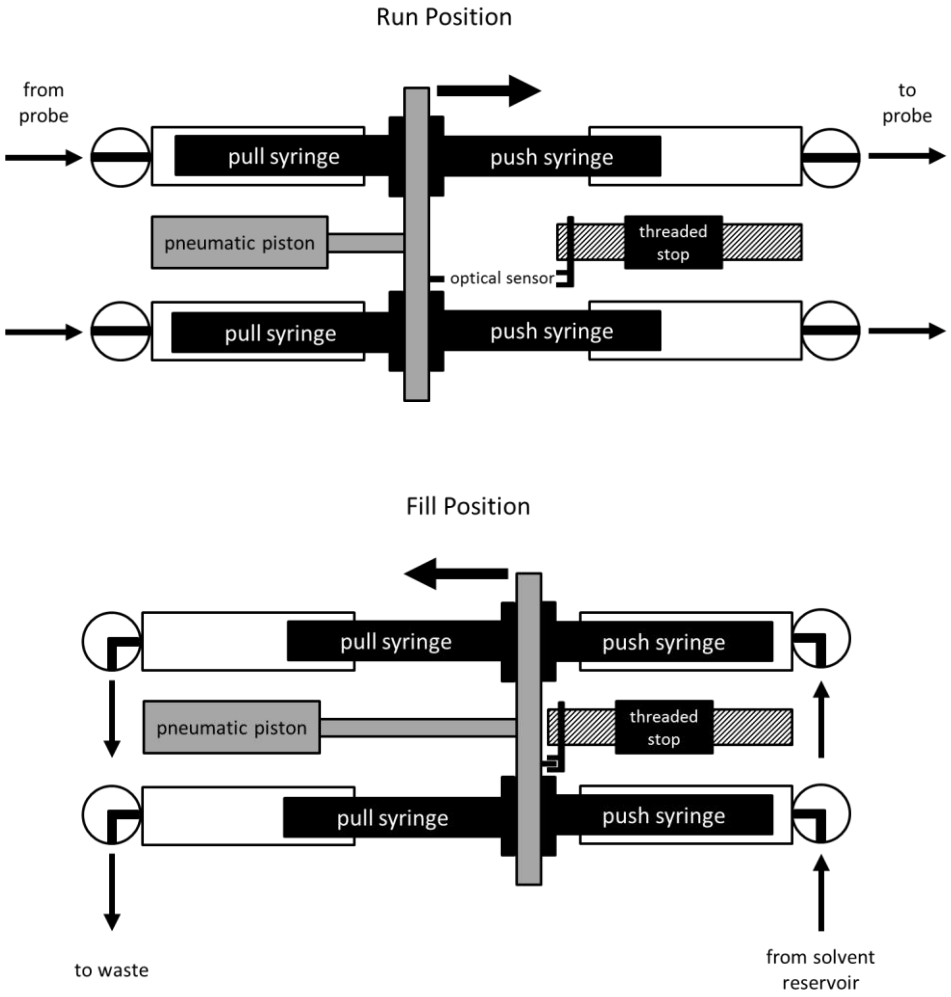

Figure 3.1. The pneumatic drive system described herein. In the run position (top), the pneumatic piston pushes the coupled syringes from left to right, which simultaneously empties the push syringes into the SF NMR probe while filling the pull syringes from the outlet of the probe. In the fill position (bottom), the syringes move from right to left, simultaneously filling the push syringes with fresh solvent and emptying the pull syringes into a waste container.

Commonly the drive syringes are filled with solvent. To conserve reagents, the actual reaction solutions fill about 3 mL each of the tubing volume located just before the stopped flow NMR probe. Two three-way fill valves (one for each reactant line) are located in an inert atmosphere glove bag that is placed about 20 inches below the NMR magnet. Through these valves the flow lines can be filled with reactants such that the volume between the valves and stopped-flow mixer contains solutions of the two reactants with known concentrations. Thus, pure solvents are located in the drive syringe and tubing volume up to the fill valves. Movement of the plungers in the drive syringes displaces solvent which forces the reactant solutions through the mixer and detection region of the stopped-flow NMR probe. The "pull" of the collection syringes prevents any build-up of pressure in the flow lines and stopped-flow NMR probe.

The pulse sequenced used herein is a simple 30° pulse with a prepulse delay, acquisition time, and post-acquisition delay. Commonly we use a 4 s acquisition time, 1 s prepulse delay, and 0.5 s post-acquisition delay. Thus spectra may be collected every 5.5 s. In order to collect data with a sampling frequency greater than 5.5 s, multiple runs are performed with different prepulse delay times. To obtain data for each second of the reaction, five runs would be performed with 0, 1, 2, 3, and 4 s prepulse delays with a 0 s post-acquisition delay, collecting 1 pulse spectra at 5 s intervals through the course of the reaction. Interleaving the data from each run allows reaction observation at intervals that would be otherwise unattainable due to incomplete relaxation between spectra.

3.3. Stopped-Flow NMR Probe Design

The SF NMR probe described herein is based on a standard wide-bore Bruker 360 MHz NMR probe that has been modified. Overall the flow path consists of the reactant lines that enter

the probe body through the bottom and emerge at the probe top, a rapid mixing cell, and a single glass flowtube reactor that begins at the mixer, passes through the NMR detection coils, and continues down through the bottom of the probe body.

The stopped flow mixer is a T-shaped, two jet (two reagent streams) mixer that allow for high flow rates and low transport times. The T-shape flow path generates high turbulence at the junction that facilitates rapid mixing of the reagents prior to reaching the detection region. The mixer is composed of three main parts: the cap, body, and base (Figure 3.2) that are custom machined out of polychlorotrifluoroethylene (PCTFE).

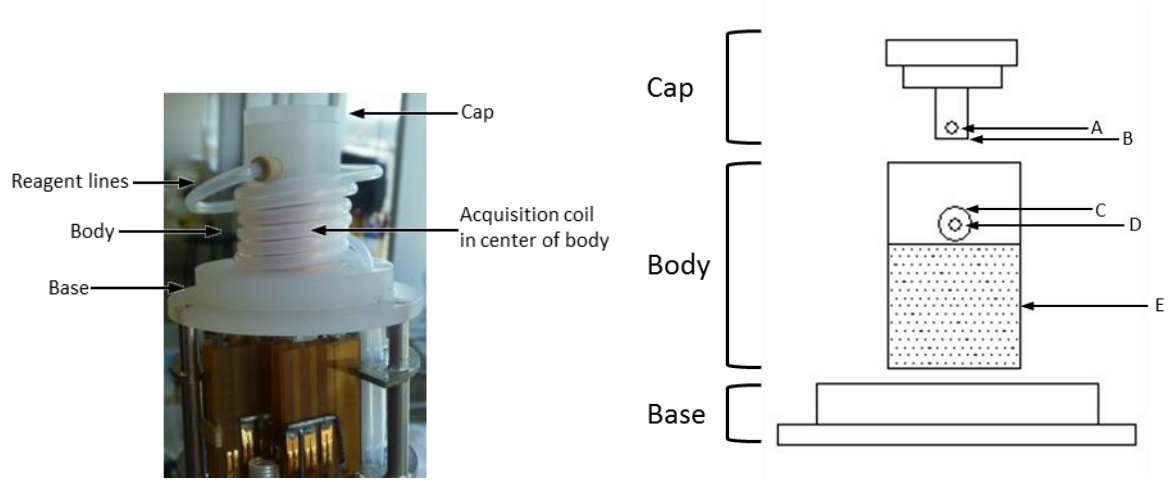

Figure 3.2. a) Photograph and b) diagram of the constructed SF NMR mixer. The cap inserts into the body such that the thru holes **A** and **D** line up to allow flow of each reagent stream into the mixer. There is a shallow indentation at the bottom of the cap (**B**) to allow for mixing of reagents. The reagent lines are screwed directly into the mixer at **C**. The dotted section (**E**) has spiraling guides for the reagent lines. The diameter of the cap and body is 1 inch.

The reagents flow through holes **A** and **D** once the cap is secured to the body with four PCTFE screws. Reagent lines (ETFE, 1/8 inch OD, 0.062 inch ID, IDEX 1530) screw into the body of the mixer with PEEK flangeless fitings (IDEX XP-348) and ETFE ferrules (IDEX P-300) at **C**. A seal between the glass flowtube and the mixer is achieved with an o-ring compressed by the cap. Grooves in the body serve as guides to allow the reagent lines (ETFE,

1/8 inch OD, 0.062 inch ID, IDEX 1530) to coil in an alternating fashion about the detection region. The acquisition coil (3 mm) is located about the flowtube in the center of the hollow cylinder body. Copper foil is wrapped around the inside of the hollow cylinder to provide shielding of the reagents from the detection coil. The hollow cylinder is press fit into the PCTFE base.

The coiling of the reagent flow lines around the outside of the mixer assembly was incorporated to facilitate thermal and magnetic equilibration of the reactants prior to mixing. When a stopped-flow "shot" is executed, the volume of reagents that mix and enter the NMR detection region are wholly contained within the coiled delivery lines. Because these lines lie in a temperature controlled region at the center of the magnetic field, both the temperature and magnetization of the reactants are equilibrated prior to reaction initiation.

The flowtube consists of a 6 cm length of 3 mm OD NMR tube (Wilmad, 335-PP-7) within the detection region which is fused with 3 mm glass tubing to extend through the entire NMR probe. At the bottom of the NMR probe a Cajon-type o-ring fitting secures the flowtube to the NMR probe. The flowtube is connected with HPLC fittings to ETFE tubing (1/8" OD, 0.093" ID, IDEX 1648) which is connected to the pull side of the push-pull pneumatic driver. Temperature control is achieved by using the standard Bruker gas purge system equipped with a heating coil; for subambient temperatures the gas first circulates through coils submerged in a low temperature and the gas temperature is controlled by the subsequent heating coil. Temperature control of the reagent lines, mixer assembly, and reactor zone is facilitated by capping the top of the probe with a glass dewar (Figure 3.3). A thermocouple (PT-6, ThermoWorks) is routed from the bottom of the probe to the base of the reactor zone to measure the temperature within the dewar cap. It is connected to a standard Bruker thermocouple

connection (LEMO, ERA.0S. 302.CLL) to allow the spectrometer to monitor the temperature inside the dewar cap for calibration.

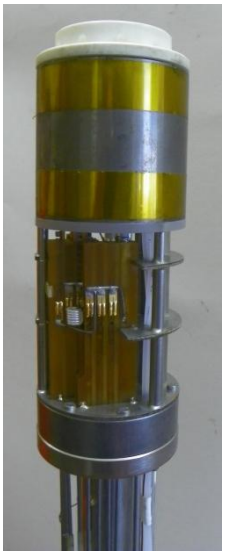

Figure 3.3. Temperature equilibration of the reagent lines is achieved by placing a Dewar around the mixer.

The entire SF NMR setup is displayed in Figure 3.4. The pneumatic driver described above is mounted on the cart to the left. Two lines flow into the probe, and one line connects the outlet of the glass flowtube to the pull syringes.

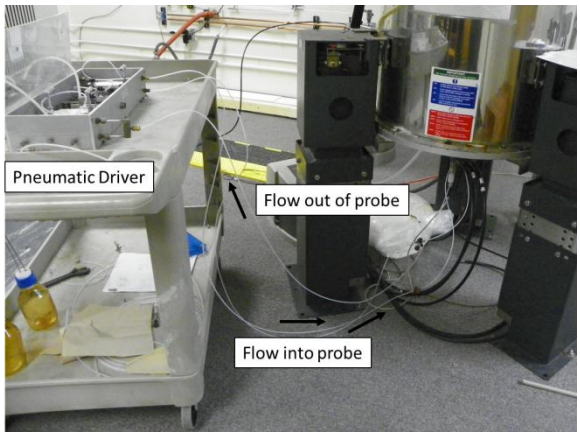

Figure 3.4. Photograph of the installed SF NMR probe.

3.4. Stopped-Flow NMR Probe Testing

The mixing capability of a T-shaped mixer design was tested with a prototype built by Helen Yan (Figure 3.5). A basic indicator solution of bromothymol blue (left) was mixed with an acidic solution (right) at a flow rate of ~8-10 mL/s. The rapid acid-base reaction results in a color change, so any blue color in the center region would be indicative of incomplete mixing. The photo shows no blue solution after leaving the mixer, indicating that the T-shape mixing design results in complete mixing of the two solutions.

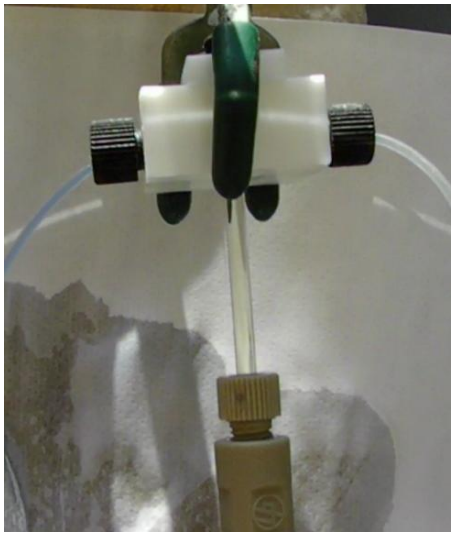

Figure 3.5. Photograph of the T-shaped mixer prototype. A basic solution with bromothymol blue indicator flows into the mixer from the left and an acidic solution flows into the mixer from the right. The absence of blue color from the mixed solution indicates complete mixing. This test was performed by Helen Yan.

Another test of mixing capability is to observe ^{1}H NMR spectra resulting from mixing acetone and chloroform. The chemical shift of neat chloroform is different by almost 1 ppm from the chemical shift of chloroform in a homogenous solution with acetone. Incomplete mixing of chloroform and acetone results in distinctive broadening of the peaks (Figure 3.6).

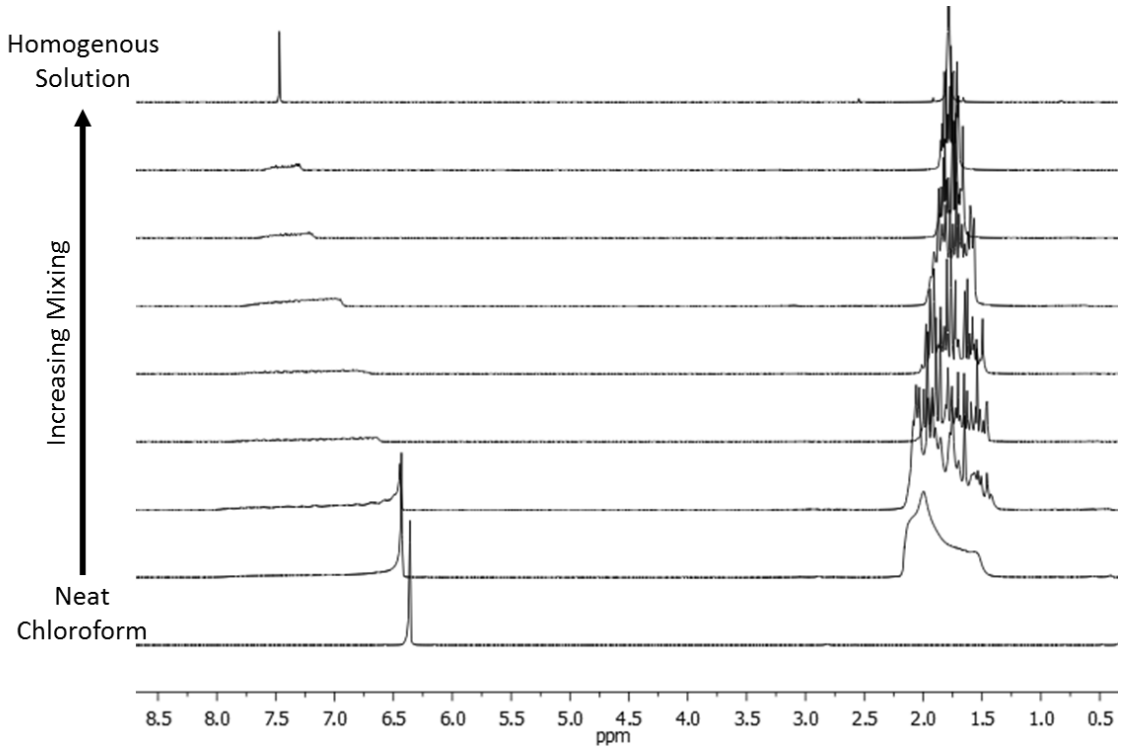

Figure 3.6. ^{1}H NMR spectra of neat chloroform (bottom) which was layered with acetone (next) and increasingly mixed until a homogeneous solution (top) is formed. All spectra were acquired at 24 °C on a 500 MHz spectrometer and externally referenced to a neat acetone sample.

Thus, passing chloroform and acetone solutions through the mixer in a stopped-flow experiment enables the mixing efficiency to be gauged from the line width of the chloroform signal. The mixing test was first performed by filling the entire system with acetone, then injecting chloroform into one of the reagent lines. Upon mixing, one signal for chloroform was observed which slightly shifts upfield with time (Figure 3.7). However, it is likely that the chloroform mixed with the acetone that was previously in the reagent line. The integrations of the two signals display that there is much more acetone in solution than chloroform, which supports the premixing hypothesis. If the chloroform did not mix with the acetone in the reagent lines, the spectra would display a 1:1 mixture of chloroform:acetone. Therefore, this approach is not a conclusive test of mixing ability.

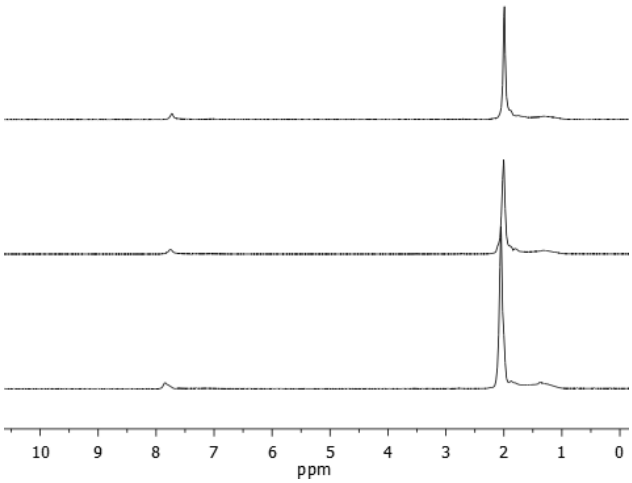

Figure 3.7. ^{1}H NMR spectra after mixing of chloroform and acetone. The first spectrum (bottom) was acquired 1 s after mixing, each subsequent spectrum was acquired 2 s later.

The next approach to perform the chloroform and acetone mixing test was to fill the system with a third solvent and inject equal amounts of chloroform and acetone in order to obtain a 1:1 mixture. The system was filled with toluene and chloroform and acetone were injected into separate reagent lines. Upon mixing, one signal for chloroform was observed (Figure 3.8), but there is a significant amount of toluene in solution. The presence of toluene will change the chemical shift values of chloroform and acetone, making it difficult to interpret chemical shift changes upon mixing. Although the chloroform and acetone mixing test was unsuccessful for this system, the bromothymol blue indicator test (Figure 3.5) indicates that a T-shape mixer provides efficient mixing of two solutions.

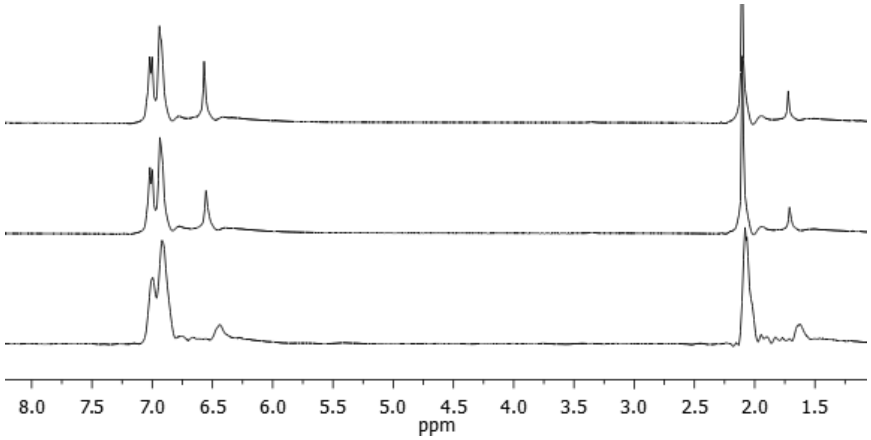

Figure 3.8. ^{1}H NMR spectra after mixing chloroform and acetone. The first spectrum (bottom) was acquired 200 ms after mixing, each subsequent spectrum was acquired 14.2 s later.

High flow rates of solution through the probe result in significant line broadening of the NMR signal if the NMR excitation pulse occurs prior to flow stoppage. Therefore, the time for the solution to stop flowing (known as the stop time) must be determined to obtain quality spectra. To measure the stop time, the system was filled with toluene and a short delay prior to a 30° excitation pulse was varied. Zero time (time = 0) was defined as the time when the pneumatic driver had pushed solvent into the system, hit the physical stop, and activated the optical trigger. At time = 0 the optical trigger signaled the spectrometer to start the pulse sequence. The stop time was determined by monitoring the width at half height ($w_{1/2}$) of the toluene methyl signal as measured at different delay times for three different flow rates. The stop time was estimated by noting the minimal delay needed to maintain narrow peak widths at half height (Figure 3.9).

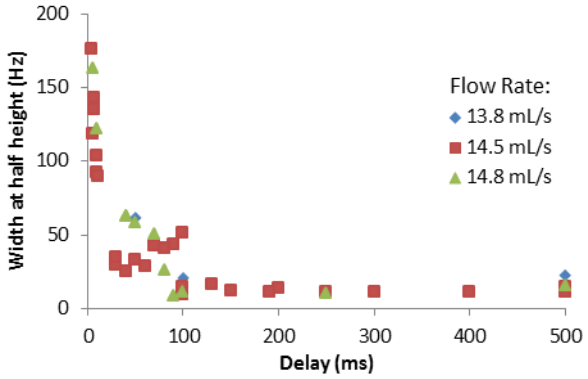

Figure 3.9. Estimation of the stop time by altering the delay prior to the 30° pulse and measuring the width of half height of the toluene methyl ^{1}H NMR signal.

As displayed in Figure 3.9, a 30 ms stop time is necessary to obtain protio solvent peak widths less than 50 Hz. A 100 ms stop time is required to obtain protio solvent peak widths less than 20 Hz, which is more relevant for reaction monitoring. The phenomenological stop-time represents the pulse delay required to obtain spectra of a given quality. It should be noted that a variety of factors influence the effective stop-time, including the time for vibrations of the detection coil and reactor tubes to ring down. Also, the tubing in the probe expands during high pressure flow and contracts after liquid flow slows down, contributing to movement of solution through the active region. At a flow rate of 14.5 mL/s, the transport time was estimated to be 2.6 ms.

To test the variable temperature capabilities of the probe, a temperature calibration was computed using the difference of the chemical shifts of neat methanol (Figure 3.10).[30] Spectra were successfully measured at a temperature range of -43 to 46 °C with no observable problems.

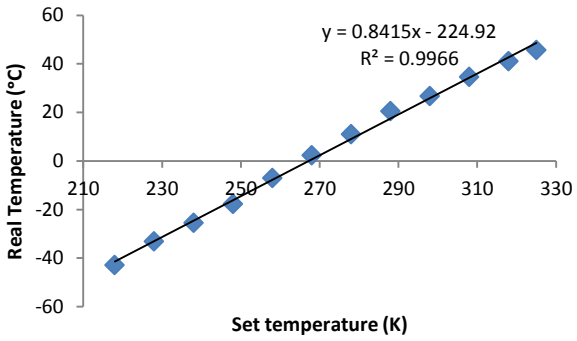

Figure 3.10. Calibration curve comparing the real temperature of the detection region as measured by the peak distance of pure methanol (°C) to the set temperature of the NMR spectrometer (K).

The temperatures of the reagent lines within the Dewared cap and the active region within the mixer body, which is not directly exposed to the cooling gas, could be different. If the reagent lines and active region are at different temperatures, there will be a temperature gradient upon solvent push. In order to measure the temperature change upon solvent push into the detection region, the system was filled with neat methanol and set to 0 °C. Methanol (0.2 mL per line, 0.4 mL total) was pushed through the system and a series of spectra was acquired to allow measurement of the temperature variation upon solvent push and time to temperature equilibrium (Figure 3.11).

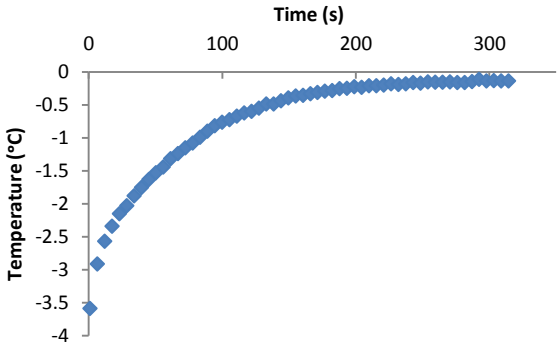

Figure 3.11. Temperature variation upon solvent push as measured by methanol ^{1}H NMR chemical shifts. The spectrometer was set to regulate the temperature at 0 °C.

As displayed in Figure 3.11, with a total solvent push of 0.4 mL, the temperature gradient is less than 4 °C. The time for temperature equilibration to the set 0 °C is observed to be approximately 300 seconds. The small (< 4 °C) temperature gradient observed upon solvent push should not cause a problem for most kinetic measurements.

In order to demonstrate the capabilities of our stopped-flow NMR probe, we elected to study a reaction which has a rate that is mostly independent to temperature, the polymerization of lactide by the organocatalyst 1,3-dimesitylimidazol-2-ylidene (IMes). The polymerization of lactide by IMes has been well studied in the literature (Scheme 3.1).[31,32] The NHC catalyst IMes quickly deactivates upon exposure to moisture, so successful polymerizations demonstrate that this SF NMR system is moisture-free and presumably air-free.

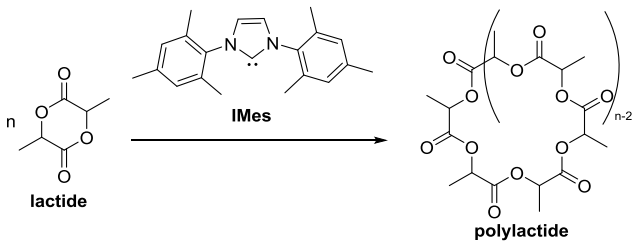

Scheme 3.1. The polymerization of lactide to polylactide by 1,3-dimesitylimidazol-2-ylidene (IMes).

For detailed mechanistic or kinetic studies, it is necessary to collect NMR spectra with a high S/N ratio to allow for accuracy of integrations. To provide evidence that this probe is capable of such work, reagent solutions were prepared in toluene-d_8 (a total of 10 mL toluene-d8) to reduce the toluene signal and allow for better S/N. The ^{1}H NMR spectra and reaction progression are displayed in Figure 3.12. The monomer used was 89% *meso*-lactide and 11% *rac*-lactide, and equilibration to the more thermodynamically favorable *rac*-lactide via epimerization is observed over the course of the first few spectra (first observed by Dr. Emily

Tan). Observation of the *rac-meso* equilibration is not possible using traditional NMR techniques because equilibration is complete within ten seconds. Growth of polymer with time was clearly observed, demonstrating the fast time resolution and inert conditions that can be achieved with this probe. Addition of known amounts of internal standard 1,4-bis(trimethylsilyl)benzene (BTMSB) allowed for the determination of the absolute concentration of each species in solution. However, it should be noted that these concentrations are based upon no dilution of each reagent solution. There is likely dilution of the reagent solutions with the solvent due to mixing upon injection of reagent solutions.

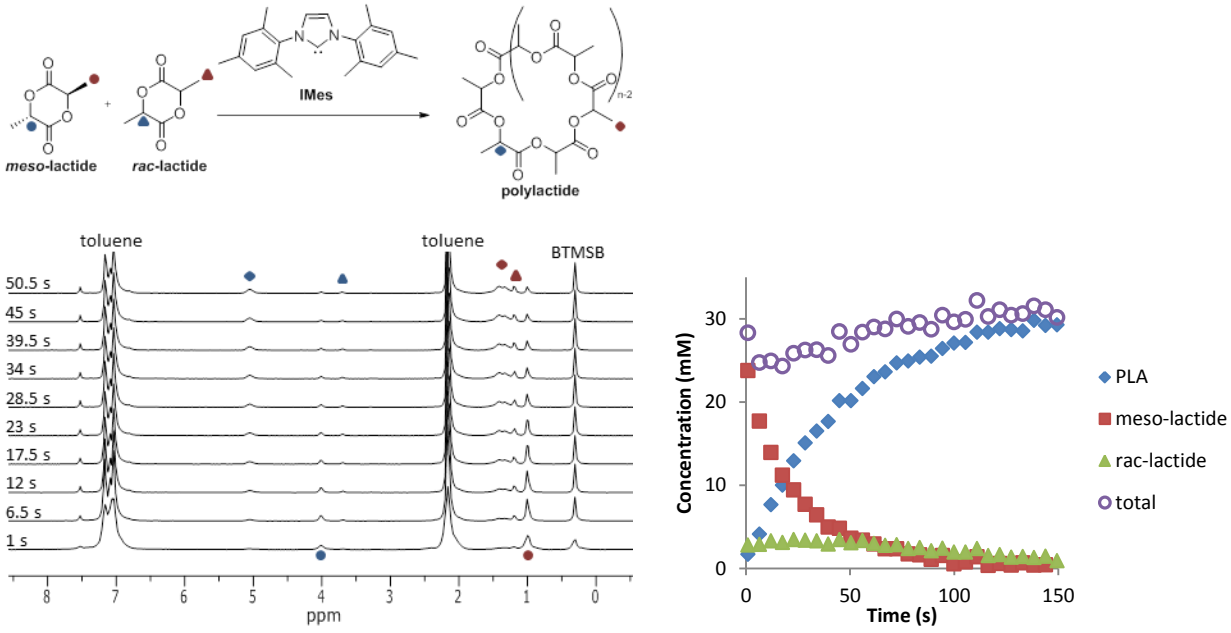

Figure 3.12. ^{1}H NMR spectra and reaction progression demonstrating the polymerization of *meso*-enriched lactide (30.1 mM) as catalyzed by IMes (1.0 mM) at 0 °C using toluene-d_8 as solvent.

To test the optimal solvent push volume (the volume of reagent solution needed to completely displace the detection region with fresh reagents), the polymerization was performed using the following total solvent push volumes: 0.4, 0.5, 0.6, and 0.7 mL (Figure 3.13). PLA

was not observed at the first time point for each push volume. In addition, the reaction rate and final PLA concentration is the same for each push volume, indicating all the reacted solution is removed from the detection region. Therefore under these conditions, 0.4 mL total push volume is sufficient to completely replace the solution in the active region with unreacted reagent solutions; however, this push volume may vary with solvent choice, temperature, or viscosity of the final product solution.

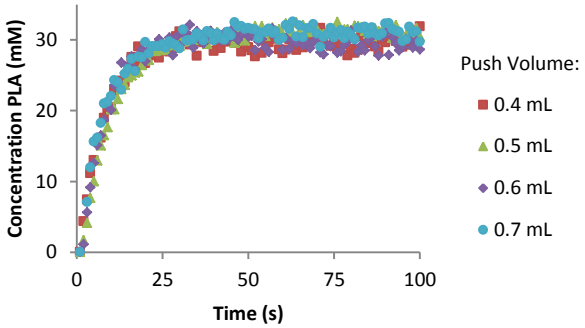

Figure 3.13. Growth of PLA with time for different solvent push volumes. Each reaction was performed at 0 °C in toluene-d_8 with [*meso*-enriched lactide]$_0$ = 30.1 mM, [IMes]$_0$ = 1.0 mM.

Additionally, lactide polymerizations were run in protio toluene to demonstrate more relevant, cost-effective reaction monitoring conditions, albeit with lower S/N resulting from the use of protio solvent. Figure 3.14 displays the reaction progression at 0 °C.

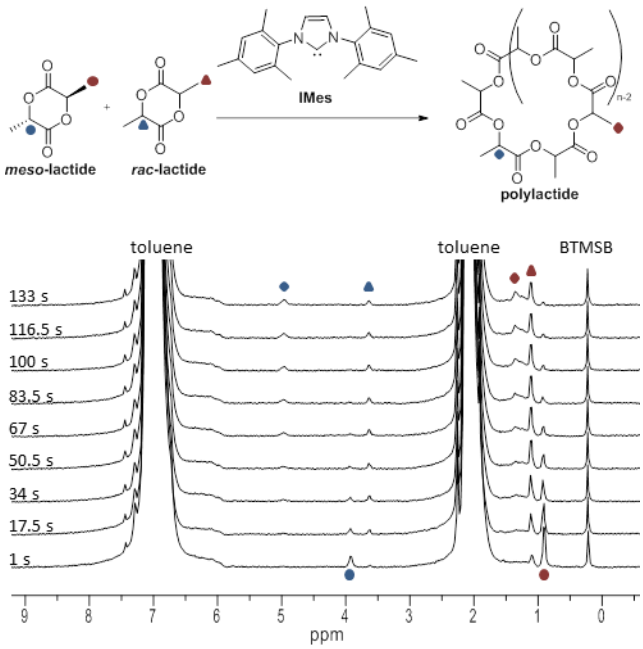

Figure 3.14. ^{1}H NMR reaction progression of polymerization of *meso*-enriched lactide (29.8 mM) catalyzed by IMes (1.0 mM) at 0 °C in protio-toluene.

Even with the lower S/N, lactide epimerization is still observed at early time points. To further demonstrate the utility of the stopped-flow NMR probe, lactide polymerization was performed at -30, -10, 0, 25 and 40 °C. The growth of polymer with time at each temperature is displayed in Figure 3.15. As shown by these data, there is not a strong temperature dependence for the rate of polymerization.

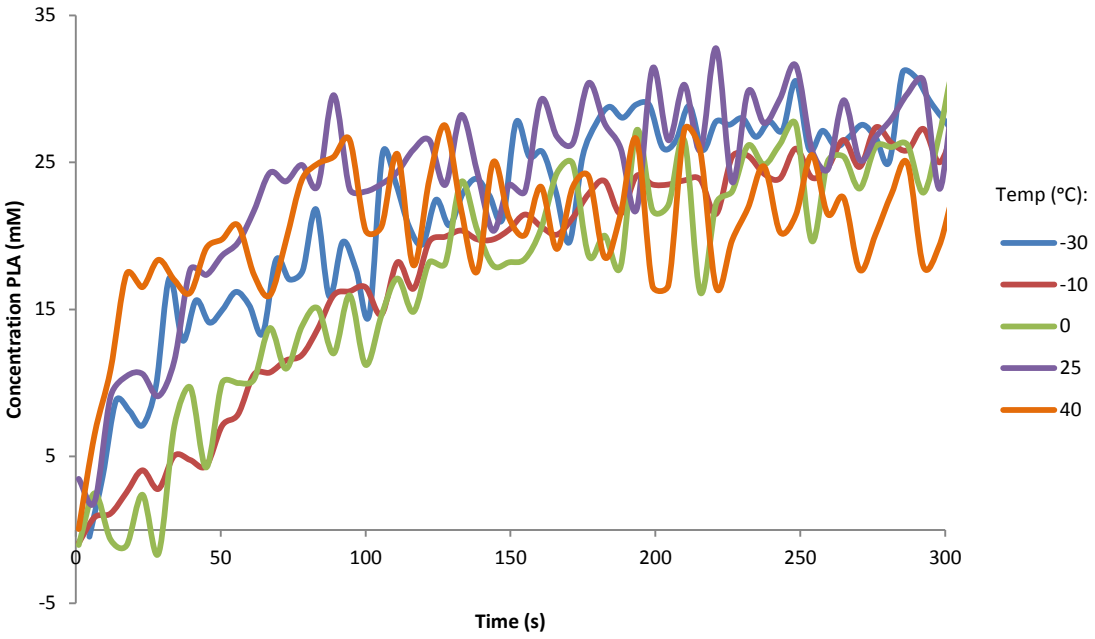

Figure 3.15. Growth of PLA with time at several different temperatures collected on the SF NMR probe. Concentrations obtained by comparison with internal standard BTMSB. All polymerizations were performed in protio toluene with the following initial concentrations: [*meso*-enriched lactide]$_0$ = 29.8 mM, [IMes]$_0$ = 1.0 mM.

The ability to successfully monitor lactide polymerization at a variety of temperatures indicates that the SF probe is suitable to study a wide variety of reactions. Deutero solvent is not necessary for reaction monitoring, allowing cost-effective studies.

3.5. Conclusion

Stopped-flow NMR enables the high intrinsic information content of NMR spectroscopy to fast reactions. We have designed a new stopped-flow NMR probe by modifying an existing wide-bore probe. The new stopped-flow NMR probe is designed with a coiled tube reservoir located near the center of the magnet that enables reagent magnetization and temperature equilibration prior to mixing. The probe exhibits a fast flow rate (14.5 mL/s) and short transport time (2.6 ms) that assure rapid and complete mixing for fast reactions. However, the signal

quality as revealed by NMR linewidths is deteriorated for the first *ca.* 100 ms after the stopped-flow trigger activates. This signal deterioration may reflect some residual flow through the active region and/or vibrations of the detection coil and reactor tube. The difference in temperature between the coiled tube reservoir and the NMR-detected active region is less than 4 °C. The polymerization of lactide with the air-sensitive catalyst IMes has been performed over the temperature range of -30 to 40 °C. The stopped flow NMR probe is especially valuable for monitoring of fast reactions where traditional NMR techniques would suffer from incomplete mixing, poor temperature control, and missing the first 30 s or so of reaction.

3.6. Experimental

General Experimental Methods

Stopped-Flow NMR was performed on a Bruker AV 360 MHz spectrometer. Toluene, THF, and hexanes were each distilled under N_2 from sodium benzophenone and stored over molecular sieves. Toluene-d_8 was stored over molecular sieves prior to use. IMes was synthesized according to literature procedure, except the deprotonation step was performed by stirring with NaH overnight, and recrystallized with THF/hexanes.[33] *Meso*-enriched lactide (89% *meso*-, 11% *rac*-lactide) was purchased from Natureworks LLC and dried over activated alumina. $Al(^{i}Bu)_2$(BHT) (BHT = 2,6 di-tert-butyl-4-methylphenol) was synthesized according to the literature procedure.[34] 1,4-bis(trimethylsilyl)benzene (BTMSB) was sublimed and stored in a N_2 glovebox.

General Stopped-Flow Procedure

The stopped-flow procedure was previously described, and the procedure was followed as described except where noted.[26] Three syringes were prepared in an N_2 atmosphere glovebox:

(a) meso-enriched lactide (43.4 mg, 0.301 mmol) and BTMSB (10.1 mg, 0.045 mmol) in 5 mL toluene-d_8, (b) IMes (3.00 mg, 9.88 μmol) in 5 mL toluene-d_8, (c) Al(^{i}Bu)$_2$(BHT) (110.6 mg, 0.308 mmol) in 5 mL toluene. The syringes were sealed in plastic bags in the glovebox and transferred to a N_2-purged glovebag. The drive system and NMR probe were filled with toluene and each reagent line was injected with 2.5 mL of syringe (c) and allowed to stand for 30 minutes to remove trace water. 10 mL toluene was pushed through the system to remove Al(^{i}Bu)$_2$(BHT) from the reactant lines. Syringes (a) and (b) were then simultaneously injected into the separate reagent lines. Each SF run used 0.2 mL of each solution (0.4 mL total volume) unless otherwise noted. The delay prior to the 30° pulse was set to one second, acquisition time was 4 seconds, and the delay after acquisition was 0.5 seconds, unless otherwise noted.

3.7. References

(1) Chamberlain, N. F. *The Practice of NMR Spectroscopy*; Plenum Press: New York, NY, 1974.

(2) Alexander, S. *J. Chem. Phys.* **1962**, *37*, 967–974.

(3) Alexander, S. *J. Chem. Phys.* **1962**, *37*, 974–980.

(4) Gutowsky, H. S.; Vold, R. L.; Wells, E. J. *J. Chem. Phys.* **1965**, *43*, 4107–4125.

(5) McConnell, H. M. *J. Chem. Phys.* **1958**, *28*, 430–431.

(6) *Dynamic Nuclear Magnetic Resonance Spectroscopy*; Jackman, L. M., Cotton, F. A., Eds.; Academic Press: New York, NY, 1975.

(7) Jones, A. C.; Sanders, A. W.; Bevan, M. J.; Reich, H. J. *J. Am. Chem. Soc.* **2007**, *129*, 3492–3493.

(8) McGarrity, J. F.; Prodolliet, J. *J. Org. Chem.* **1984**, *3*, 4465–4470.

(9) McGarrity, J. F.; Prodolliet, J.; Smyth, T. *Org. Magn. Reson.* **1981**, *17*, 59–65.

(10) Mok, K. H.; Nagashima, T.; Day, I. J.; Jones, J. A.; Jones, C. J. V.; Dobson, C. M.; Hore, P. J. *J. Am. Chem. Soc.* **2003**, *125*, 12484–12492.

(11) Bertz, S. H.; Carlin, C. M.; Deadwyler, D. A.; Murphy, M. D.; Ogle, C. A.; Seagle, P. H. *J. Am. Chem. Soc.* **2002**, *124*, 13650–13651.

(12) Bertz, S. H.; Cope, S.; Murphy, M.; Ogle, C. A.; Taylor, B. J. *J. Am. Chem. Soc.* **2007**, *129*, 7208–7209.

(13) Bertz, S. H.; Cope, S.; Dorton, D.; Murphy, M.; Ogle, C. A. *Angew. Chemie - Int. Ed.* **2007**, *46*, 7082–7085.

(14) Klein, R.; Gawley, R. E. *J. Am. Chem. Soc.* **2007**, *129*, 4126–4127.

(15) Mcgarrity, J. F.; Ogle, C. A.; Brich, Z.; Loosli, H.-R. *J. Am. Chem. Soc.* **1985**, *107*, 1810–1815.

(16) Mcgarrity, J. F. *Tetrahedron Lett.* **1982**, *23*, 417–420.

(17) Plessel, K. N.; Jones, A. C.; Wherritt, D. J.; Maksymowicz, R. M.; Poweleit, E.; Reich, H. J. *Org. Lett.* **2015**, *17*, 2310–2313.

(18) Sudmeier, J. L.; Pesek, J. J. *Inorg. Chem.* **1971**, *10*, 860–863.

(19) Grimaldi, J. J.; Sykes, B. D. *Rev. Sci. Instrum.* **1975**, *46*, 1201–1205.

(20) Fyfe, C. A.; Cocivera, M.; Damji, S. W. H. *Acc. Chem. Res.* **1978**, *11*, 277–282.

(21) McGee, W. A.; Parkhurst, L. J. *Anal. Biochem.* **1990**, *189*, 267–273.

(22) Frieden, C.; Hoeltzli, S. D.; Ropson, I. J. *Protein Sci.* **1993**, *2*, 2007–2014.

(23) Funahashi, S.; Ishihara, K.; Aizawa, S.; Sugata, T.; Ishii, M.; Inada, Y.; Tanaka, M. *Rev. Sci. Instrum.* **1993**, *64*, 130–134.

(24) Gomez-Hens, A.; Perez-Bendito, D. *Anal. Chim. Acta* **1991**, *242*, 147–177.

(25) Hore, P. J.; Winder, S. L.; Roberts, C. H.; Dobson, C. M. *J. Am. Chem. Soc.* **1997**, *119*, 5049–5050.

(26) Christianson, M. D.; Tan, E. H. P.; Landis, C. R. *J. Am. Chem. Soc.* **2010**, *132*, 11461–11463.

(27) Hoeltzli, S. D.; Ropson, I. J.; Frieden, C. In *Techniques in Protein Chemistry V*; Crabb, J. W., Ed.; Academic Press: San Diego, CA, 1994; p 455–465.

(28) Yushmanov, P. V.; Furó, I.; Stilbs, P. *Langmuir* **2006**, *22*, 2002–2004.

(29) Yushmanov, P. V.; Furó, I.; Stilbs, P. *Colloids Surfaces A Physicochem. Eng. Asp.* **2006**, *291*, 59–62.

(30) Ammann, C.; Meier, P.; Merbach, A. *J. Magn. Reson.* **1982**, *46*, 319–321.

(31) Culkin, D. A.; Jeong, W.; Csihony, S.; Gomez, E. D.; Balsara, N. P.; Hedrick, J. L.; Waymouth, R. M. *Angew. Chemie - Int. Ed.* **2007**, *46*, 2627–2630.

(32) Jeong, W.; Shin, E. J.; Culkin, D. A.; Hedrick, J. L.; Waymouth, R. M. *J. Am. Chem. Soc.* **2009**, *131*, 4884–4891.

(33) Bantreil, X.; Nolan, S. P. *Nat. Protoc.* **2011**, *6*, 69–77.

(34) Shreve, A. P.; Mulhaupt, R.; Fultz, W.; Calabrese, J.; Robbins, W.; Ittel, S. D. *Organometallics* **1988**, *7*, 409–416.

Chapter 4

Reaction Monitoring using Online vs Tube NMR Spectroscopy: Seriously Different Results

This work was carried out in conjunction with David Foley and Mark Zell (Pfizer).

This chapter was accepted to *Magnetic Resonance in Chemistry* for publication. DOI: 10.1002/mrc.4259

4.1. Introduction

Nuclear Magnetic Resonance (NMR) is an extremely powerful tool for the analysis of reaction mixtures. Not only can NMR be used as a quantitative method of monitoring reaction processes, it also has the advantage of providing detailed structural information about reaction components in solution. These two characteristics give NMR a distinct advantage over other analytical techniques typically used for reaction monitoring purposes. Some of these techniques (i.e. infared or Raman) can identify functional groups of the molecules being analyzed; however, they lack the comprehensive characterization that NMR can provide.

There are four common approaches to conducting NMR reaction monitoring: (i) static, in standard NMR tubes, (ii) online monitoring, (iii) stopped-flow, and (iv) rapid injection NMR. Static NMR tube monitoring (i) is the simplest and therefore most extensively used of these techniques, and involves placing reagents into a standard NMR tube, then monitoring reaction progress of the static solution within the spectrometer.[1] This approach requires no specialized equipment beyond that normally used to run NMR samples and can be practically conducted in deuterated solvent because of the small volume required. This has been shown to be an effective method for probing mechanistic details of reactions.[2] An alternative method is to remove aliquots from a reaction vessel (sometimes followed by a quench step) and transfer the sample to an NMR tube for offline analysis.[3] This could equally be conducted in protonated solvents using proton gradient shimming for efficient shimming without the presence of a deuterium source.[4]

The second approach, online NMR (ii), transfers a flowing stream of the reaction mixture from a reaction vessel to the NMR probe where the analysis is conducted. The speed of flow is optimized to allow enough residence time of the magnetized sample for acquisition.[5] The reaction mixture can then be returned to the reaction vessel or directed to a waste container,

depending on the requirements of the experiment. Online NMR requires special probes or custom NMR tubes, however it does facilitate online sampling, obviating the need for operator input once the experiment is running. Monitoring an online sample from a reaction vessel allows replication of reaction conditions while allowing for analysis in an essentially unperturbed state. There are examples of online NMR reaction monitoring being applied at both high and low fields.[6]

The third method, stopped-flow NMR (iii), is typically used for the detection of rapid kinetics (within 2.5–100 ms of reagents mixing), a feature that both NMR tube and online reaction monitoring cannot provide due to the time required to mix and get reagents to the detection region.[7] Stopped-flow NMR typically employs custom probes designed to flow reagents first into a mixing region and then into the detection region of the spectrometer with extremely high flow rates to minimize dead time. Prior to acquisition, the flow must be stopped due to the short residence times of magnetized sample at the high flow rates. The flow system allows for multiple time points to be easily taken by flowing more unreacted starting material into the mixing, then detection regions with different delay values in the pulse sequence. The stopped-flow NMR technique has allowed detection of short-lived intermediates, study of complex protein-folding mechanisms,[8] and insights into the effects of fast kinetics on NMR lineshape.[9]

The fourth approach, rapid injection NMR (iv), allows acquisition typically 40 ms – 1 s after reagents have mixed. Rapid injection NMR often utilizes custom probes or probe inserts that allow for quick insertion of reagents into the NMR tube and sometimes include a mechanical mixing period along with injection.[10] Rapid injection NMR techniques have allowed direct observation of multiple reactive intermediate species, providing valuable mechanistic

information.[11] However, the lack of a flow system means that subsequent measurements may only be taken after replacement or cleaning of parts of the system.

In the last few decades, there have been numerous reports on the analysis of reaction mixtures using NMR. The majority use standard NMR tube reaction monitoring.[12] While there is little doubt that monitoring a static NMR tube gives excellent mechanistic information, there is a lack of proof of how kinetic information gathered from this type of experiment is representative of how a reaction process proceeds under standard laboratory-scale synthetic chemistry conditions. We evaluated the validity of the following NMR reaction monitoring techniques from a kinetic standpoint: online NMR, standard NMR tubes, and NMR tubes with periodic inversion. The results that we present here demonstrate that reaction monitoring techniques have a significant influence on the kinetic understanding of a reaction.[13]

4.2. Results and Discussion

This study was undertaken to evaluate how basic NMR tube monitoring techniques compare with following the progress of a reaction using an online NMR system such as the one developed in our laboratory.[14] While numerous reports of kinetic and mechanistic studies using both standard NMR tube and online approaches have appeared in the literature, none have undertaken a systematic comparison of NMR reaction monitoring techniques. This investigation was designed to look at both homogeneous and heterogeneous reactions, to provide evidence that the NMR monitoring technique can influence the kinetic results for a wide variety of reactions.

Three modes of NMR spectroscopy reaction monitoring were investigated; online NMR spectroscopy, NMR tube reaction monitoring with and without periodic agitation of the reaction mixture. The online NMR method, using our custom reaction monitoring system, was directly compared with the basic method of reaction monitoring in an NMR tube.[15] A third method was

also used involving periodic inversion by inverting a standard NMR tube three times during the interval between each NMR spectrum acquisition. Periodic inversion gave insight into an intermediate mixing regime between constant mixing (online NMR) and a static sample (NMR tube).

Three reaction types were evaluated in this study. The *L*-proline catalyzed self-condensation of propionaldehyde was examined to compare different NMR methods of observing heterogeneous reaction progression. The homogenous coupling reaction of aniline and 4-fluorobenzaldehyde was also analyzed using the same three reaction monitoring methods (online, tube, and periodic inversion). Finally, the acid-catalyzed transesterification of isopropanol and acetic anhydride was also studied to show that the results obtained are not limited to only very slow reactions.

Heterogeneous reaction

The *L*-proline-catalyzed self-condensation of propionaldehyde **1** was chosen for the kinetic comparison study because of the well-established mechanism and the ability to observe many intermediate species via NMR spectroscopy.[16] In 2011, Zeitler and Gschwind reported an elegant mechanistic study of the *L*-proline catalyzed self-condensation of propionaldehyde **1**. The conclusions of their study, which involved observing reaction progression in an NMR tube, indicated that the aldol addition pathway to **2a**/**2b** is competitive with aldol condensation to **3** (Scheme 4.1A) and the mechanism is a double-activation Mannich-type mechanism involving two catalyst molecules (Scheme 4.1B). According to their results, the mechanism involves simultaneous activation with proline (**Pro**) of the donor aldehyde to form **4a** and the acceptor aldehyde to form **4d**. The interconversion between **4a** and **4d** goes through **4b**/**4c**. The C-C bond

formation step was indicated to be the rate determining step and could be monitored by observing the species **4b** – the maximum concentration of **4b** was determined to correspond with the fastest formation rate of **3**.

Mechanistic observations from this study were consistent with those reported by Zeitler and Gschwind, so all chemical assignments used in this study are in agreement with their published chemical shifts.

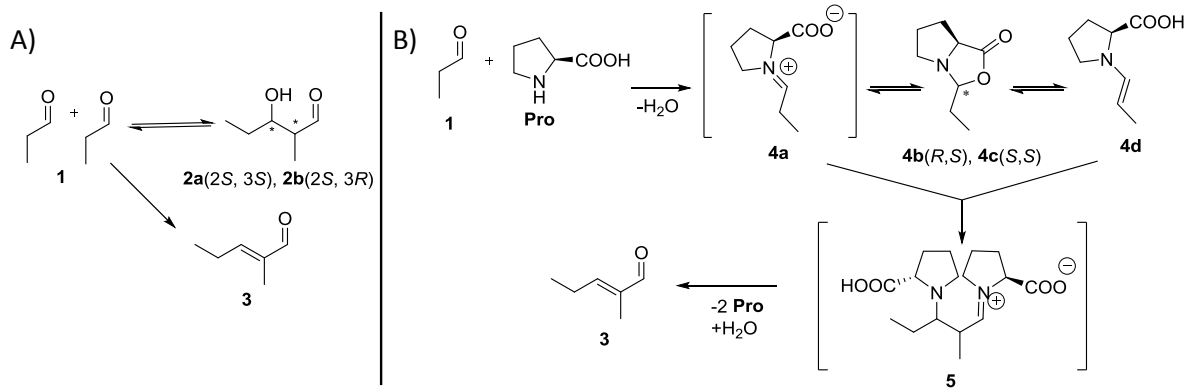

Scheme 4.1. (A) Aldol addition to form **2a**/**2b** indicated a competitive process with the desired aldol condensation to **3**. (B) Double-activation Mannich-type pathway indicated in the mechanistic study by Zeitler and Gschwind. Species in brackets could not be directly detected by NMR.

The progress of the *L*-proline catalyzed aldol condensation was monitored by ^{1}H NMR by three methods; (i) online NMR, (ii) periodic inversion, and (iii) a static NMR tube. This heterogeneous reaction clearly displays the effect of efficient mixing on reaction progression. All three experiments were conducted at the same concentration (50 mM). The results of these experiments are displayed in Figure 4.1. Characteristic resonances outlined by Gschwind *et al.* were also tracked as reaction monitoring handles.[16a] Because of overlap of the aldehyde protons related to **1** and **2a** at δ_H 9.65 ppm, these two components were tracked together. Intermediate **4b** was monitored using the resonance at δ_H 5.06 ppm and the aldol condensation product **3** at δ_H 9.34 ppm. It can be clearly seen from the reaction profiles that the time to reaction completion is

very different when adequate mixing is applied. Intermediate **4b**, which was correlated with the rate determining step in Zeitler and Gschwind's study, forms at a much faster rate when agitation is applied (Figure 4.1A and B). When the reaction is diffusion controlled, as for the static NMR tube (Figure 4.1C), there is much less **4b** observed, corresponding to the much slower rate of product **3** formation. Mol% was calculated by setting all propionaldehyde methyl signals and the methylene signal from the one intermediate without a distinct methyl (**4d**) from the first spectrum to 100%.

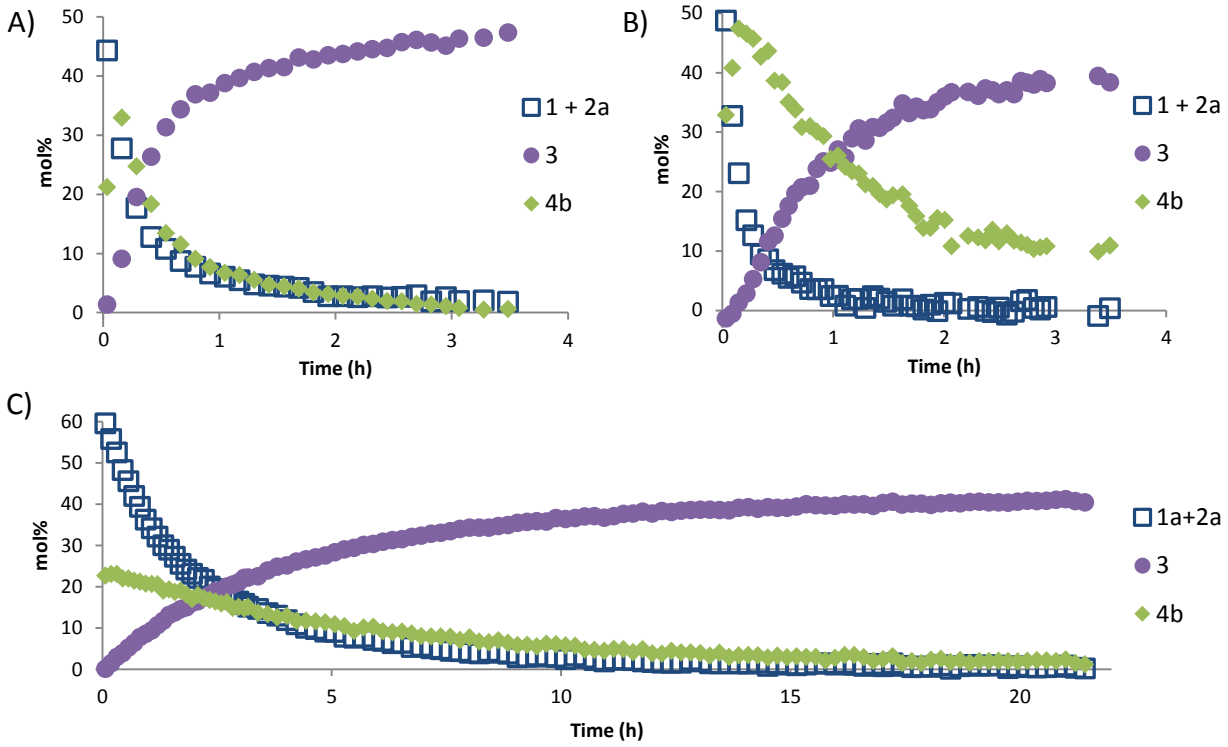

Figure 4.1. Study of the *L*-proline catalyzed self-condensation of propionaldehyde **1** in dimethyl sulfoxide at 27 °C as observed by (A) online NMR (B) NMR tube with periodic inversion (C) static NMR tube. All methods have initial **1** and **Pro** concentrations of 50.0 mM.

Figure 4.2 displays an overlay of the rate of product formation from all three methods (online NMR, static NMR tube, and periodic inversion) on a single plot, demonstrating clearly that formation of product is dependent on amount of mixing. For clarity, minor components

involved in the reaction mechanism (i.e. **2b**, **4b**, **4c**, and **4d**) are not shown; however, these were included in the mass balance calculation and conversion to mol%. The method with continuous mixing, online NMR, has the fastest growth of product. The method with an intermediate amount of mixing, periodic inversion – where there are some periods of mixing and some periods of no mixing – shows an intermediate rate of product growth. The NMR tube reaction, which is entirely under diffusion control, displays by far the slowest rate of product growth, clearly demonstrating that any kinetics derived from the reaction conditions are highly dependent upon the amount of mixing in the system and do not necessarily display the true kinetics of the reaction under investigation. In addition, variability in the rates derived from the NMR tube monitoring was observed, likely due to the inability to control how much catalyst stuck to the walls of the NMR tube upon the initial mixing of reagents.

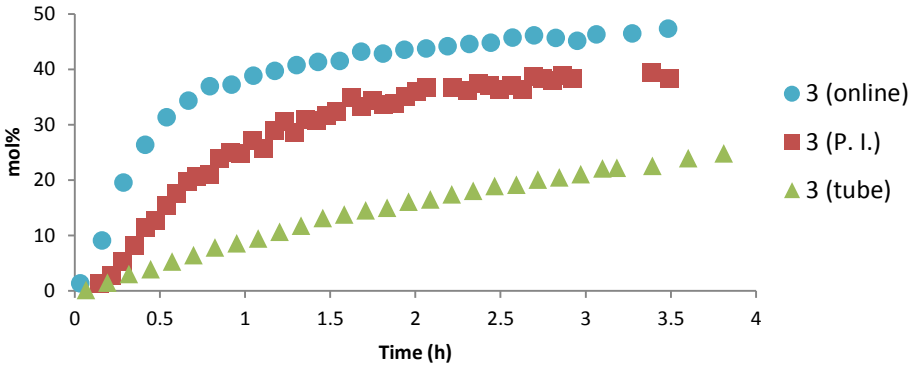

Figure 4.2. Overlay of product formation profiles for all methods used to study the *L*-proline catalyzed self-condensation of propionaldehyde **1** to form **3** in dimethyl sulfoxide at 27 °C.

Homogeneous reaction

The second reaction investigated was the homogeneous coupling reaction of aniline **6** and 4-flurobenzaldehyde **7** to produce the corresponding imine at 25 °C (Scheme 4.2). This reaction

was chosen for the investigation as a comparative study to the heterogeneous case, outlined in the previous section. The reaction kinetics were found to be relatively slow, and ^{19}F NMR spectroscopy could be used to monitor the progress of the reaction.

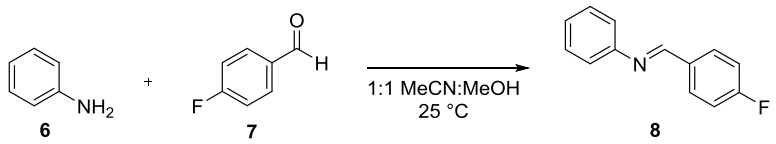

Scheme 4.2. The coupling reaction of aniline **6** and 4-fluorobenzaldehyde **7** to form imine **8** in 1:1 methanol: acetonitrile at 25 °C.

The results from this experiment are outlined in Figure 4.3. There is a less pronounced difference between the kinetic results obtained (online vs tube) when monitoring the homogeneous reaction as compared to the heterogeneous reaction. Mol% was calculated by setting the total amount of 4-fluorobenzaldehyde **7** and imine **8** detected by ^{19}F NMR at each time point to 100% (at -105.2 ppm and -110.2 ppm, respectively). The method with the most mixing (online NMR) has decidedly the quickest conversion to product. Periodic inversion of the NMR tube does not increase the rate of reaction as compared to the static NMR tube, showing that for this homogenous reaction, inversion every 6-7 minutes is not enough to show improvement upon diffusion-limited mixing. Regardless, it is clear that any kinetic rates derived from the static NMR tube would reflect more upon being diffusion controlled than the actual rates of reaction.

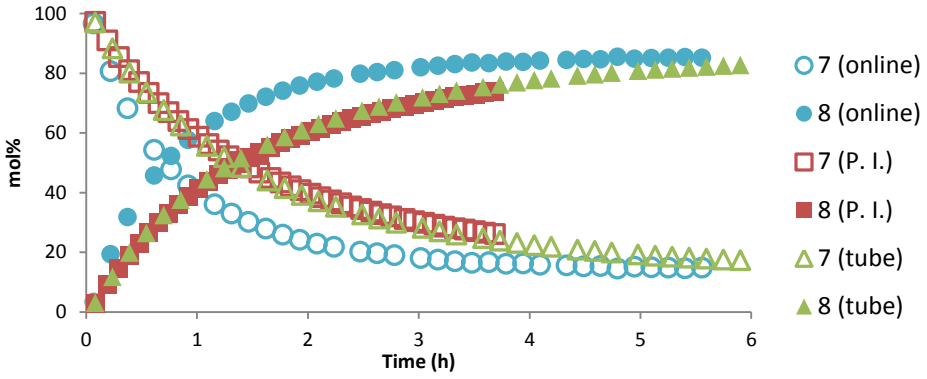

Figure 4.3. A summary of all methods used to study the aniline **6** and 4-fluorobenzaldehyde **7** coupling reaction to form the imine **8** in 1:1 methanol: acetonitrile at 25 °C. Online NMR initial concentrations were 64 mM each of **6** and **7**. Periodic inversion and NMR tube reactions initial concentrations were 69 mM each of **6** and **7**.

Homogeneous reactions, fast kinetics

In order to test the effect of mixing on reactions with shorter half-lives (i.e. on the order of a few minutes), the transesterification of acetic anhydride **9** and isopropanol **10** to produce acetic acid **11** and isopropyl acetate **12** at 25 °C in acetonitrile was studied (Scheme 4.3).

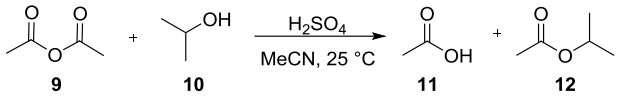

Scheme 4.3. The sulfuric acid-catalyzed transesterification reaction of acetic anhydride **9** and isopropanol **10** in acetonitrile at 25 °C.

Figure 4.4 shows that even for reactions with half-lives on the order of minutes, mixing is still crucial to obtaining accurate rate values. The periodic inversion results for the transesterification reaction are not presented due to the reaction completion being too fast to obtain an appropriate number of data points. Mol% was calculated by setting the total integration of isopropanol **10** methine (3.9 ppm) and isopropyl acetate **12** methine (4.9 ppm) detected at each time point to 100%.

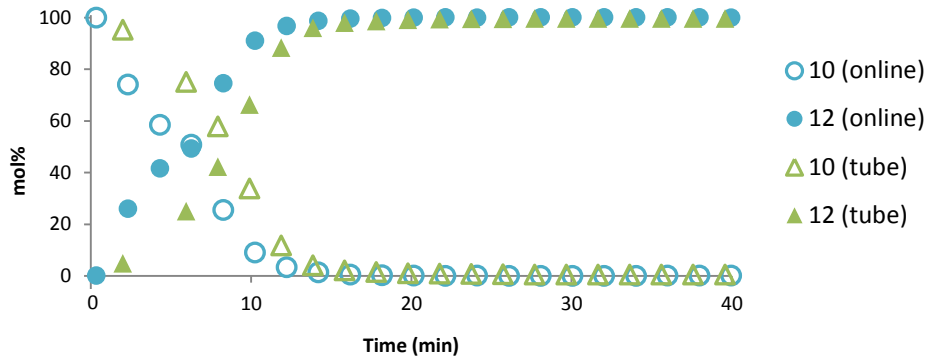

Figure 4.4. A summary of the methods used to study the transesterification reaction of acetic anhydride **9** and isopropanol **10** in acetonitrile at 25°C. Online NMR initial concentrations were 2.5 M each of **9** and **10** and 44 mM H_2SO_4. Tube initial concentrations were 2.3 M each of **9** and **10** and 46 mM H_2SO_4.

Because of the residence time characteristics of the online system used, the early portion of the online data (< 3.2 min) cannot be used for kinetic calculations; however, there is still a clear difference in the reaction completion time between the two experiments. This difference is again due to the mixing effects, efficient stirring is applied in the reaction vessel in the case of the experiment monitored by online NMR spectroscopy, while diffusion-controlled kinetics have a greater effect on the result obtained from the static NMR tube experiment.

There are positive and negative aspects to each reaction monitoring technique that must be evaluated when designing an experimental procedure. Table 4.1 summarizes some of these considerations. Online NMR monitoring allows the closest replication to a non-monitored experiment, achieving control over parameters such as temperature, rate of mixing, and rate of addition of reagents, which is key to developing a chemical reaction process. There are some limitations associated with monitoring a reaction online because of the distance between the reaction vessel and the detection cell, which can influence sample transfer time and temperature gradients. Details of the online NMR spectroscopy system used in this study have been published

previously,[14] and a number of reports of the characteristics of online NMR systems have provided in-depth analysis of the considerations when conducting this type of analysis.[5,6b,17] Online NMR also allows for the introduction of other analytical instruments in-line, but requires specialized equipment that may not be available to all users.

Conducting a reaction in an NMR tube requires only basic equipment, but at the cost of sacrificing efficient mixing during the reaction. Temperature gradients are likely between the top and bottom of the NMR tube, especially at elevated temperatures, also evaporation and condensation of volatile solvents could be experienced, which could result in concentration gradients or changes because of solvent loss. These effects will influence the kinetic results obtained.

The periodic inversion method also requires only basic equipment; however, it has the major drawback of the operator having to physically invert the NMR tube between each spectrum for the entirety of the reaction. Acquiring data points in this way can also lead to brief loss of temperature control of the sample, which can affect the results obtained. Taking aliquots from a stirred reaction vessel should give similar results to a non-monitored experiment, but again requires the operator to be present at each time point. Aliquots of the *L*-proline catalyzed aldol condensation were also taken, but upon diluting the reaction mixture with deuterated solvent to lock, the sample was far too dilute to get meaningful results. Also, taking aliquots causes brief loss of temperature control as well as loss of material.

One must also consider the larger purpose of the NMR monitoring study when deciding upon a monitoring method. If the data from the monitoring study is to be used in the development of a chemical process for scale-up, it would be wise to use a monitoring method that facilitates similar reaction conditions to the large-scale reaction, such as that provided by

online NMR.[18] Online NMR is particularly amenable to tracking flow chemistry processes, where the output stream can be readily monitored in real-time, allowing quick optimization of experimental conditions. Offline sampling will not produce accurate results for a flow chemistry process as a result of averaged response due to pooling of the sample stream in the detection cell before detection. Accurate results would require the use of a flow-through NMR cell, rather than the online NMR tube system used to monitor the reactions described in the current study, due to similar pooling effects.

Conditions	Online NMR	NMR Tube	Periodic Inversion
Automated Sampling	✓	✓	✗
Temperature Control	✓	✓	✗
Efficient Mixing	✓	✗	✗
Standard Equipment	✗	✓	✓
Deuterated Solvent	✗	✓	✓
Scalability	✓	✗	✗

Table 4.1. Summary of some important considerations when choosing an NMR monitoring method.

4.3. Conclusion

In conclusion, we present evidence that mixing has a large effect on the rate of reaction determined by NMR spectroscopy for three different types of reactions [heterogeneous, homogeneous with long (> 1 h) reaction times, and homogeneous with short (< 1 h) reaction times]. All three reactions studied show conclusive evidence that the NMR monitoring technique can have a significant effect on reaction rates, providing support for the application of continuous flow online NMR methods for kinetic studies when the most accurate results are

required. Studies in static NMR tubes can provide good mechanistic and structural information particularly for labile or reactive intermediates. However, as the results from this work demonstrate, caution should be applied when relying on kinetic data acquired from systems lacking adequate mixing.

4.4. Experimental

General procedure for online NMR

The online NMR setup was used as previously described with removal of the needle splitting valve.[15] Temperature control was achieved by setting reaction vessel, sample loop and spectrometer to the specified temperature. The flow rate was set to 4 mL/min.[14] Spectra were acquired on the flowing sample on a Bruker 400 MHz Avance III NMR (Billerica, MA, USA) equipped with broad band fluorine observation (BBFO) probe. ^{1}H NMR spectra were acquired with 4 scans, a 30° pulse angle and a 10 s relaxation delay, unless otherwise noted. If applicable, ^{19}F{^{1}H} spectra were acquired with 8 scans, 90° pulse angle, and 30 s relaxation delay.

General procedure for static NMR tube reactions

Reagents were added to a 5 mm NMR tube, inverted three times and inserted into spectrometer that began taking spectra immediately. Spectra were acquired on a Bruker 400 MHz Avance III NMR equipped with BBFO probe. The temperature of the sample was controlled using the variable temperature heater of the probe. ^{1}H NMR spectra were acquired with 4 scans, a 30° pulse angle, and a 10 s relaxation delay, unless otherwise noted. If applicable, ^{19}F{^{1}H} spectra were acquired with 8 scans, a 90° pulse angle, and a 30 s relaxation delay.

General procedure for NMR tube reactions with periodic inversion

Reagents were added to an NMR tube, inverted 3 times and inserted into spectrometer where initial spectrum was acquired. Prior to each subsequent spectrum, the NMR tube was removed from the spectrometer and inverted three times before inserting back into the spectrometer. Spectra were acquired on a Bruker 400 MHz Avance III with BBFO probe. The temperature of the sample was controlled by the variable temperature heater of the probe. ^{1}H NMR spectra were acquired with 4 scans, 30° pulse angle, and 10 s relaxation delay, unless otherwise noted. If applicable, ^{19}F{^{1}H} spectra were acquired with 8 scans, 90° pulse angle, and 30 s relaxation delay.

L-proline catalyzed aldol self-condensation of propionaldehyde at 27 °C

Online NMR. *L*-proline (**Pro)**, (Amresco) (208.9 mg, 1.8 mmol) was suspended in 36 mL protio dimethyl sulfoxide (DMSO) in a 50 mL reactor and propionaldehyde **1** (Sigma-Aldrich) (0.13 mL, 1.8 mmol) was added in one portion via syringe. ^{1}H NMR spectra were acquired at intervals of 5 min until 200 min, then at 10 min intervals with a 90° pulse angle and a 15 s relaxation delay. The DMSO singlet was suppressed using the water suppression enhanced through T1 effects (WET) solvent suppression pulse sequence.[19]

Static NMR tube reaction: L-proline (**Pro**) (3.7 mg, 0.03 mmol) was suspended in 0.6 mL DMSO-d6 in an NMR tube. Propionaldehyde **1** (2.2 µL, 0.03 mmol) was added in one portion via micropipette and the tube was inverted 3 times. ^{1}H NMR spectra were initially acquired at 5 min intervals, then at 10 min intervals. All spectra were acquired with 8 scans and a 15 s relaxation delay.

NMR tube with periodic inversion: L-proline (**Pro**) (3.7 mg, 0.03 mmol) was suspended in 0.6 mL DMSO-d3 in an NMR tube. Propionaldehyde **1** (2.2 µL, 0.03 mmol) was added in one portion via micropipette. ^{1}H NMR spectra were acquired with 8 scans.

Aniline and 4-fluorobenzaldehyde coupling at 25 °C

Online NMR: 4-Fluorobenzaldehyde **7** (Sigma-Aldrich) (0.28 mL, 2.6 mmol) was added to 20 mL protio acetonitrile and 20 mL protio methanol in a 50 mL reaction vessel. Aniline **6** (Sigma-Aldrich) (0.24 mL, 2.6 mmol) was added in one portion via micropipette. ^{19}F{^{1}H} and ^{1}H NMR spectra were acquired at 5 min intervals.

Static NMR tube reaction: 4-Fluorobenzaldehyde **7** (7 µL, 0.07 mmol) was added to an NMR tube with 0.5 mL methanol-d4 and 0.5 mL acetonitrile-d3 via micropipette. Aniline **6** (6 µL, 0.07 mmol) was added in one portion via micropipette and the NMR tube was inverted three times. ^{19}F{^{1}H} spectra were acquired at 5 min intervals. ^{1}H NMR spectra were also acquired but not used for analysis.

NMR tube with periodic inversion: 4-Fluorobenzaldehyde **7** (7 µL, 0.07 mmol) was added to an NMR tube with 0.5 mL methanol-d4 and 0.5 mL acetonitrile-d3 via micropipette. Aniline **6** (6 µL, 0.07 mmol) was added in one portion via micropipette. ^{19}F{^{1}H} spectra were acquired for analysis.

Isopropanol and acetic anhydride transesterification at 25 °C

Online NMR: Acetic anhydride **9** (Sigma-Aldrich) (10 mL, 106 mmol) and isopropanol **10** (Sigma-Aldrich) (8.1 mL, 106 mmol) were dissolved in 25 mL protio acetonitrile in a 50 mL

reaction vessel. Conc. sulfuric acid (J.T. Baker) (100 µL, 1.9 mmol) was added in one portion via syringe. ^{1}H NMR spectra were acquired in 60 s intervals.

Static NMR tube reaction: Acetic anhydride **9** (0.2 mL, 2 mmol), isopropanol **10** (0.16 mL, 2 mmol), and acetonitrile-d3 (0.5 mL) were added to an NMR tube. Conc. sulfuric acid (2 µL, 0.04 mmol) was added in one portion via syringe. ^{1}H NMR spectra were acquired at 60 s intervals.

4.5. References

1. F. Susanne, D.S. Smith, and A. Codina, *Org. Process Res. Dev.*, **2012**, *16*, 61-64.
2. Y. Yokoyama, M. Nakakoshi, H. Okuno, Y. Sakamoto, and S. Sakurai, *Magn. Reson. Chem.*, **2010**, *48*, 811-817.
3. T. Bartik, B. Bartik, B.E. Hanson, T. Glass, and W. Bebout, *Inorg. Chem.*, **1992**, *31*, 2667-2670.
4. T.R. Hoye, B.M. Eklov, T.D. Ryba, M. Voloshin, and L.J. Yao, *Org. Lett.*, **2004**, *6*, 953-956.
5. M. Maiwald, H.H. Fischer, Y.-K. Kim, K. Albert, and H. Hasse, *J. Magn. Reson.*, **2004**, *166*, 135-146.
6. (a) M. Maiwald, H.H. Fischer, Y.-K. Kim, and H. Hasse, *Anal. Bioanal. Chem.*, **2003**, *375*, 1111-1115;

   (b) F. Dalitz, M. Cudaj, M. Maiwald, and G. Guthausen, *Prog. Nucl. Magn. Reson. Spectrosc.*, **2012**, *60*, 52-70;

   (c) F. Dalitz, L. Kreckel, M. Maiwald, and G. Guthausen, *Appl. Magn. Reson.*, **2014**, *45*, 411-425;

(d) A.C. Barrios Sosa, R.T. Williamson, R. Conway, A. Shankar, R. Sumpter, and T. Cleary, *Org. Process Res. Dev.*, **2011**, *15*, 449-454;

(e) D.A. Foley, C.W. Doecke, J.Y. Buser, J.M. Merritt, L. Murphy, M. Kissane, S.G. Collins, A.R. Maguire, and A. Kaerner, *J. Org. Chem.*, **2011**, *76*, 9630-9640;

(f) M.A. Bernstein, M. Stefinovic, and C.J. Sleigh, *Magn. Reson. Chem.*, **2007**, *45*, 564-571.

7. (a) P.V. Yushmanov and I. Furo, *J. Magn. Reson.*, **2005**, *175*, 264-270;

(b) M.D. Christianson, E.H.P. Tan, and C.R. Landis, *J. Am. Chem. Soc.*, **2010**, *132*, 11461-11463.

8. C. Frieden, S.D. Hoeltzli, and I.J. Ropson, *Protein Sci.*, **1993**, *2*, 2007-2014.

9. (a) M.D. Christianson and C.R. Landis, *Concepts Magn. Reson., Part A*, **2007**, *30A*, 165-183;

(b) W.A. McGee and L.J. Parkhurst, *Anal. Biochem.*, **1990**, *189*, 267-273;

(c) R.O. Kuehne, T. Schaffhauser, A. Wokaun, and R.R. Ernst, *J. Magn. Reson.*, **1979**, *35*, 39-67.

10. S.E. Denmark, B.J. Williams, B.M. Eklov, S.M. Pham, and G.L. Beutner, *J. Org. Chem.*, **2010**, *75*, 5558-5572.

11. (a) A.C. Jones, A.W. Sanders, W.H. Sikorski, K.L. Jansen, and H.J. Reich, *J. Am. Chem. Soc.*, **2008**, *130*, 6060-6061;

(b) A.C. Jones, A.W. Sanders, M.J. Bevan, and H.J. Reich *J. Am. Chem. Soc.*, **2007**, *129*, 3492-3493;

(c) J.F. McGarrity and J. Prodolliet, *J. Org. Chem.*, **1984**, *49*, 4465-4470;

(d) J.F. McGarrity, J. Prodolliet, and T. Smyth, *Org. Magn. Reson.*, **1981**, *17*, 59-65.

12. (a) N.M. Do, M.A. Olivier, J.J. Salisbury, and C.B. Wager, *Anal. Chem.*, **2011**, *83*, 8766-8771;

(b) D.H. Pieper, K. Pollmann, P. Nikodem, B. Gonzalez, and V. Wray, *J. Bacteriol.*, **2002**, *184*, 1466-1470;

c) J. Bures, A. Armstrong, and D.G. Blackmond, *J. Am. Chem. Soc.*, **2011**, *133*, 8822-8825;

(d) I.M. Clegg, C.M. Gordon, D.S. Smith, R. Alzaga, and A. Codina, *Anal. Methods*, **2012**, *4*, 1498-1506;

(e) C.J. Morten, J.A. Byers, and T.F. Jamison, *J. Am. Chem. Soc.*, **2011**, *133*, 1902-1908.

13. D.G. Blackmond, *Angew. Chem., Int. Ed.*, **2005**, *44*, 4302-4320.

14. D. A. Foley, E. Bez, A. Codina, K. L. Colson, M. Fey, R. Krull, D. Piroli, M. T. Zell, B. L. Marquez. *Anal. Chem.* **2014**, *86*, 12008-12013.

15. D.A. Foley, J. Wang, B. Maranzano, M.T. Zell, B.L. Marquez, Y. Xiang, and G.L. Reid, *Anal. Chem.*, **2013**, *85*, 8928-8932.

16. (a) M.B. Schmid, K. Zeitler, and R.M. Gschwind, *J. Org. Chem.*, **2011**, *76*, 3005-3015;

(b) M.B. Schmid, K. Zeitler, and R.M. Gschwind, *Angew. Chem., Int. Ed.*, **2010**, *49*, 4997-5003.

17. F. Dalitz, M. Maiwald, G. Guthausen. *Chem. Eng. Sci.* **2012**, *75*, 318-326.

18. (a) J.M. Merritt, J.Y. Buser, A.N. Campbell, J.W. Fennell, N.J. Kallman, T.M. Koenig, H. Moursy, M.A. Pietz, N. Scully, and U.K. Singh, *Org. Process Res. Dev.*, **2014**, *18*, 246-256;

(b) A. C. Barrios Sosa, R. Conway, R. T. Williamson, J. P. Suchy, W. Edwards, T. Cleary. *Org. Process Res. Dev.* **2011**, *15*, 1458-1463.

19. S.H. Smallcombe, S.L. Patt, and P.A. Keifer, *J. Magn. Reson., Ser. A*, **1995**, *117*, 295-303.

Chapter 5

A Detailed Mechanistic Investigation into the Reaction of 3-Methylpentanoic Acid with Meldrum's Acid utilizing Online NMR Spectroscopy

This work was a collaboration with Pfizer and Bruker. NMR spectra figures processed with Bruker Dynamics Center were contributed by Anna Codina (Bruker UK Limited). David Foley (Pfizer) contributed to the writing of the manuscript, data interpretation, and some NMR experiments. Brian Marquez (Bruker Biospin) and Mark Zell (Pfizer) also provided helpful insight.

This chapter was accepted into *Magnetic Resonance in Chemistry* for publication.

5.1. Introduction

Process analytical technology (PAT) is routinely used to monitor chemical reactions; however, most monitoring methods require some type of calibration step to normalize the output to relate concentration versus time.[1] Many of these instruments may not readily reveal which species in the reaction matrix are responsible for a given change in analytical response, due to their lack of structural information. NMR spectroscopy overcomes these limitations as it inherently provides a quantitative signal response based on the number of nuclei, and it is the primary structural elucidation tool for small molecule characterization, making it a powerful investigational tool for reaction understanding.[2]

Online NMR spectroscopy typically involves transfer of a reaction mixture from a reaction vessel to the active region of the NMR probe for measurement on the flowing sample without the need for discrete sampling or exposure to the external atmosphere. Multiple designs of online systems have been reported which take advantage of the ability to track reaction progression in real-time with minimal disturbance to the reaction matrix.[3] The application of online NMR has been used to probe reaction processes and monitor the progress of reactions in various fields.[4]

As part of the development of an active pharmaceutical ingredient,[5] a study of one of the steps in the synthetic route was undertaken by Clegg *et al.* (Scheme 5.1).[6] The reaction analysis was conducted by NMR spectroscopy, as other analytical techniques such as UV (ultraviolet) spectroscopy and GC-MS (gas chromatography mass spectrometry) were not amenable to track reaction progression. Clegg's investigation revealed a mechanistic pathway involving pivalic anhydride **5** and mixed anhydride **6a** intermediates and their structures were assigned based on 2D NMR spectroscopy, GC-EI-MS and IR (infrared) spectroscopy data. However, additional

peaks observed in the ^{1}H NMR spectrum suggested additional intermediate species were present in the reaction mixture. The authors also hypothesized that other intermediates could be chemically possible, such as 3-methylhexanoic anhydride **7a**, but no empirical evidence for their existence was noted during their study.

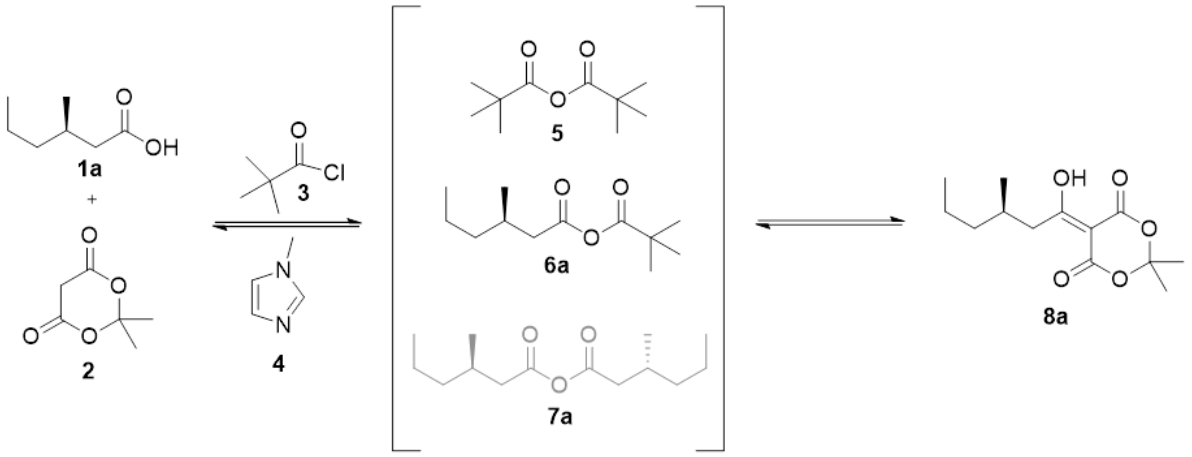

Scheme 5.1. Summary of the finding from the NMR study by Clegg e*t al.* on the formation of **8a**, an intermediate in the synthesis of Imagabalin. The grey structure **7a** represents an intermediate which was hypothesized but not substantiated by evidence.

In the current work we examine the analogous reaction using a shorter chain carboxylic acid **1b** (Scheme 5.2) and demonstrate the use of online NMR spectroscopy for reaction monitoring and mechanistic characterization of the transformation. All reactive intermediates are characterized by ^{1}H and ^{13}C NMR spectroscopy and their mechanistic pathways elucidated.

5.2. Results and Discussion

Online NMR reaction profiling

In the original NMR study by Clegg *et al.*, the disadvantage of monitoring the progress of the reaction in an NMR tube was highlighted. Initiation of the reaction by dropwise addition of

pivaloyl chloride **3** outside of the spectrometer, in addition to operations such as locking and shimming caused the initial part of the reaction to be unobservable by NMR.

In the current study, the reaction displayed in Scheme 5.2 was analyzed using online NMR spectroscopy to assist in capturing the onset of reaction, providing a more complete reaction profile. Offline characterization of the unknown components within the reaction matrix was also conducted, allowing definitive mechanistic elucidation.

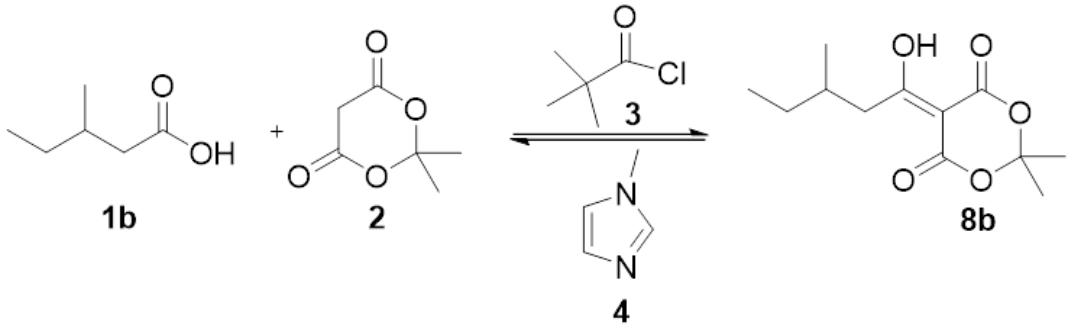

Scheme 5.2. Reaction scheme of the transformation studied using online NMR spectroscopy.

The online NMR spectroscopy experimental set-up has been described previously and was designed to allow the chemistry to be conducted following the conditions under which the reaction would occur in the absence of NMR analysis.[3c, 7] Therefore, reaction parameters such as agitation, dosing, temperature and atmosphere were easily replicated. These features provide distinct advantages over offline sampling or conducting the reaction in a standard NMR tube. 3-Methylpentanoic acid **1b**, Meldrum's acid **2** and 1-methylimidazole **4** were dissolved in acetonitrile in a 50 mL reaction vessel. The reaction solution was circulated throughout the system to achieve equilibration of concentration and temperature (25 °C). Pivaloyl chloride **3** was then added using a dosing syringe over the course of 10 minutes while the online system was circulating at a rate of 3 mL/min. ^{1}H NMR spectra were obtained on the flowing reaction

mixture at 2 minute intervals for the first 20 spectra, at 6 minute intervals until the reaction time reached 185 minutes, and then at 16 minute intervals until reaction completion. A ^{1}H NMR spectra stacked plot of the aliphatic region of the initial 300 minutes after reaction initiation is displayed in Figure 5.1a. The bottom spectrum in the stacked plot was recorded as the dosing of pivaloyl chloride into the reaction vessel began, but appearance of intermediates does not occur until the third spectrum (3.9 minutes reaction time) due to the transfer time from the reaction vessel to the NMR detection region and time delay between experiments.

A number of components were involved in the reaction and key resonances that represent these components are displayed in Figure 5.1b (a single ^{1}H NMR spectrum extracted from the stacked plot at 13.7 minutes after reaction initiation). The reaction profile is plotted in Figure 5.1c, showing the change in reaction species concentration over the course of the reaction.

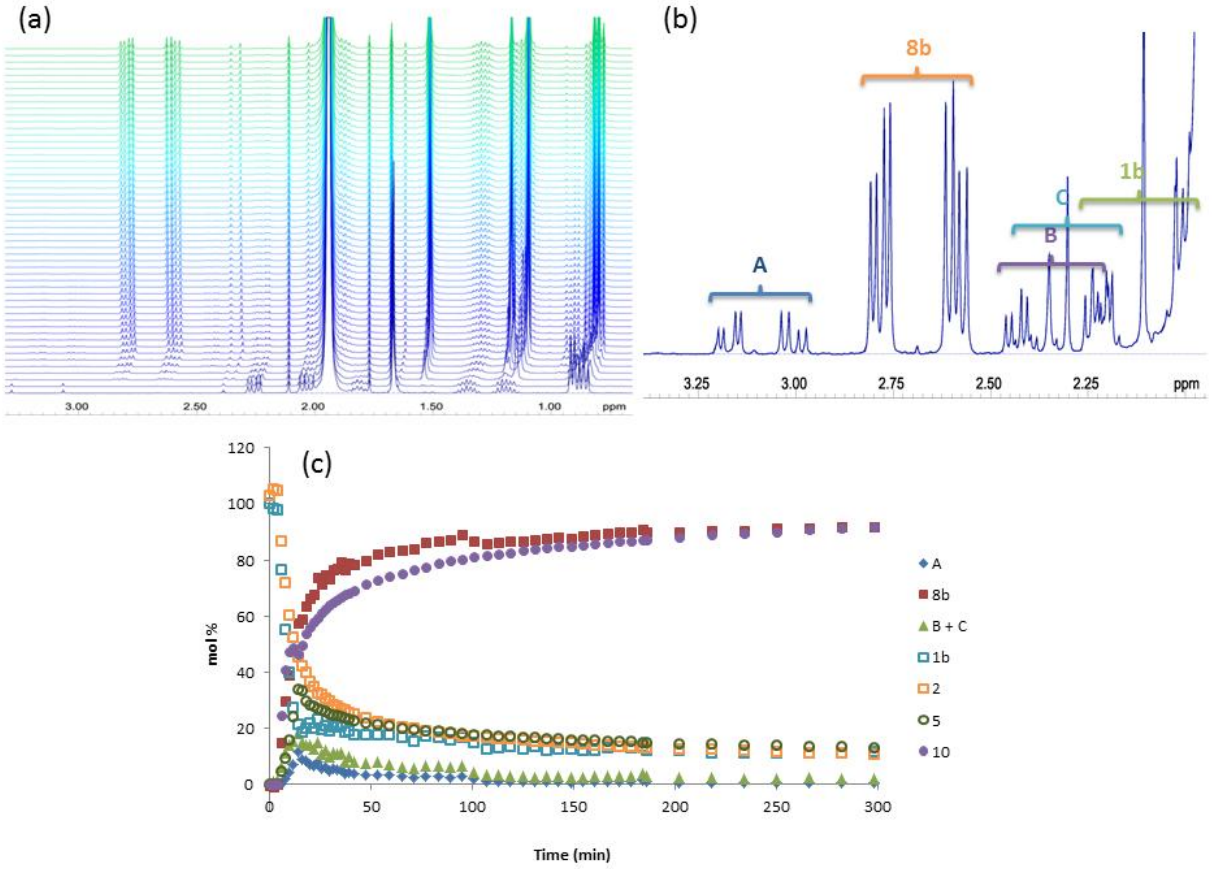

Figure 5.1. (a) ^{1}H NMR stack plot of the aliphatic region showing reaction progression (Scheme 2) with respect to time. The bottom spectrum is at time zero, with each subsequent spectrum spaced approximately 2 min (first 20 spectra) or 6 minutes apart (additional spectra). **(b)** 2.0–3.5 ppm region of the ^{1}H NMR spectrum recorded at 13.7 minutes reaction time. Characteristic ^{1}H NMR resonances of reaction components are highlighted. **(c)** Reaction profile for the reaction of 3-methylpentanoic acid with Meldrum's acid.

Intermediate characterization experiments

A number of species (labeled **A**, **B** and **C,** Figure 5.1) were observed in the reaction matrix, and their structural identification was desired. While parallels with the 3-methylhexanoic acid **1a** reaction studied previously were likely, definitive proof of structure of the components observed in our experiment was desired. To elucidate these reaction components, a number of experiments were conducted to prove the structure of these unknown species. The design of

these experiments was assisted by the knowledge gained in the investigation by Clegg *et al*. In their NMR tube study, resonances in the methyl region were used as characteristic signals for tracking the reaction components. The authors did not focus on the region between 2.0 and 3.5 ppm, which in our investigation was observed to contain a number of signals beneficial to reaction monitoring (Figure 5.1b). To provide structural characterization of intermediate species **A**, **B** and **C**, experiments were conducted in deuterated acetonitrile in 5 mm NMR tubes. These experiments were designed to maximize the formation of possible intermediates to allow chemical shift and structure assignment.

Identification of anhydride **7b** and acyl chloride **9**

The first of these structural characterization experiments was carried out to verify that the dimeric anhydride, analogous to **7a** postulated by Clegg, *et al.* was present as an intermediate in the process. A sample of the dimeric anhydride **7b** was synthesized and characterized *in situ* in order to determine if this component was present and to identify which of the signals (**A**, **B** or **C**) it represented. The reference sample of the dimeric anhydride **7b** was generated in a stepwise manner via reaction of 3-methylpentanoic acid **1b** with oxalyl chloride in a 5 mm NMR tube to activate the carboxylic acid by conversion to the corresponding acyl chloride **9**. This was then reacted with a second mole of 3-methylpentanoic acid **1b**, furnishing the dimeric anhydride **7b**. 3-Methylpentanoic acid **1b** and *N*,*N*-dimethylformamide (DMF) are shown in Figure 5.2 spectrum (a), confirming that the signals at 2.08 and 2.29 ppm belong to the starting material **1b**. Figure 5.2 spectrum (b) presents the ^{1}H NMR spectrum of the reaction mixture obtained following addition of oxalyl chloride to 3-methylpentanoic acid **1b** in the presence of a catalytic

amount of DMF, allowing for the identification of the signals at 2.77 and 2.98 ppm as 3-methylpentanoyl chloride **9**.

Comparison of spectrum (b) in Figure 5.2 to the spectra recorded for online process monitoring revealed the acyl chloride **9** to be intermediate species **A** (Figure 5.1b). This proved to be a valuable experiment in forming a reference sample for characterization of the pentanoyl chloride **9**, which was not previously indicated as being involved in the reaction mechanism in the case of the longer chain carboxylic acid (Scheme 5.1). With characterization of the pentanoyl chloride **9** complete, an additional 1.5 equivalents of 3-methylpentanoic acid and triethylamine (TEA) were added to this sample. This resulted in formation of the dimeric anhydride **7b**, evident from a set of diastereotopic methylene protons at 2.25 and 2.46 ppm in the ^{1}H NMR spectrum shown in Figure 5.2 spectrum (c). This independent synthesis of a reference sample of dimeric anhydride **7b**, and observance of the same peaks in the reaction monitored by online NMR provided evidence that the dimeric anhydride **7b** was in fact an intermediate in the reaction (species **C,** Figure 5.1b), lending evidence to the hypothesis proposed by Clegg, *et al*.

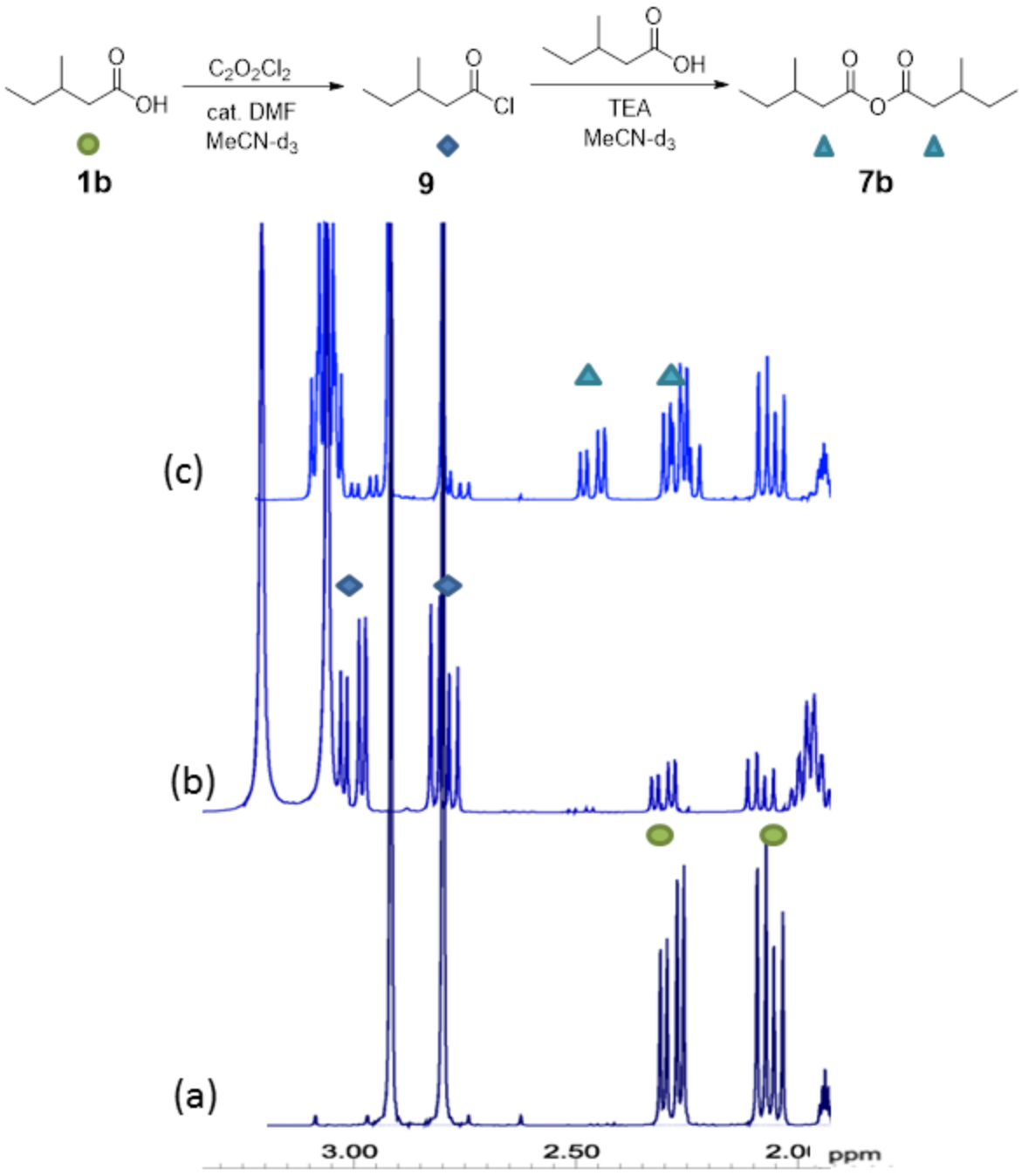

Figure 5.2. ^{1}H NMR spectral overlay of the two step process to form the dimeric anhydride **7b** in acetonitrile-d_3. **(a)** ^{1}H NMR spectrum of 3-Methylpentanoic acid **1b** and catalytic DMF; **(b)** ^{1}H NMR spectrum following the addition of one equivalent oxalyl chloride to the reaction mixture; **(c)** ^{1}H NMR spectrum following the addition of 1.5 additional equivalents **1b** and TEA to the reaction mixture.

Identification of mixed anhydride **6b**

Clegg, *et al*. identified the mixed anhydride species **6a** in their study of the reaction with 3-methylhexanoic acid **1a**. Therefore it was expected that the mixed anhydride species **6b** (Figure 5.3) would also exist in the analogous reaction with **1b**.

The previous experiment demonstrated that **7b** was formed in the reaction mixture. If mixed anhydride **6b** was also present in the reaction mixture it was expected that it would have similar methylene proton chemical shift to symmetrical anhydride. Therefore an experiment was designed to generate a reference sample of **7b.** To achieve this, pivalic acid **10** was added to the sample of **1b**, **9** and **7b** that was generated in the previous experiment. This reaction generated a sample of the mixed anhydride **6b** and resulting spectra are in Figure 5.3. During the reaction, growth of signals at 2.25 and 2.46 ppm were observed, and 2D NMR spectroscopy experiments were used to confirm that these resonances were consistent with the mixed anhydride structure **6b**. Finally the ^{1}H NMR spectrum was compared to that generated during the online NMR experiment, which correlated the mixed anhydride species **6b** with species **B** in the reaction profile shown in Figure 5.1.

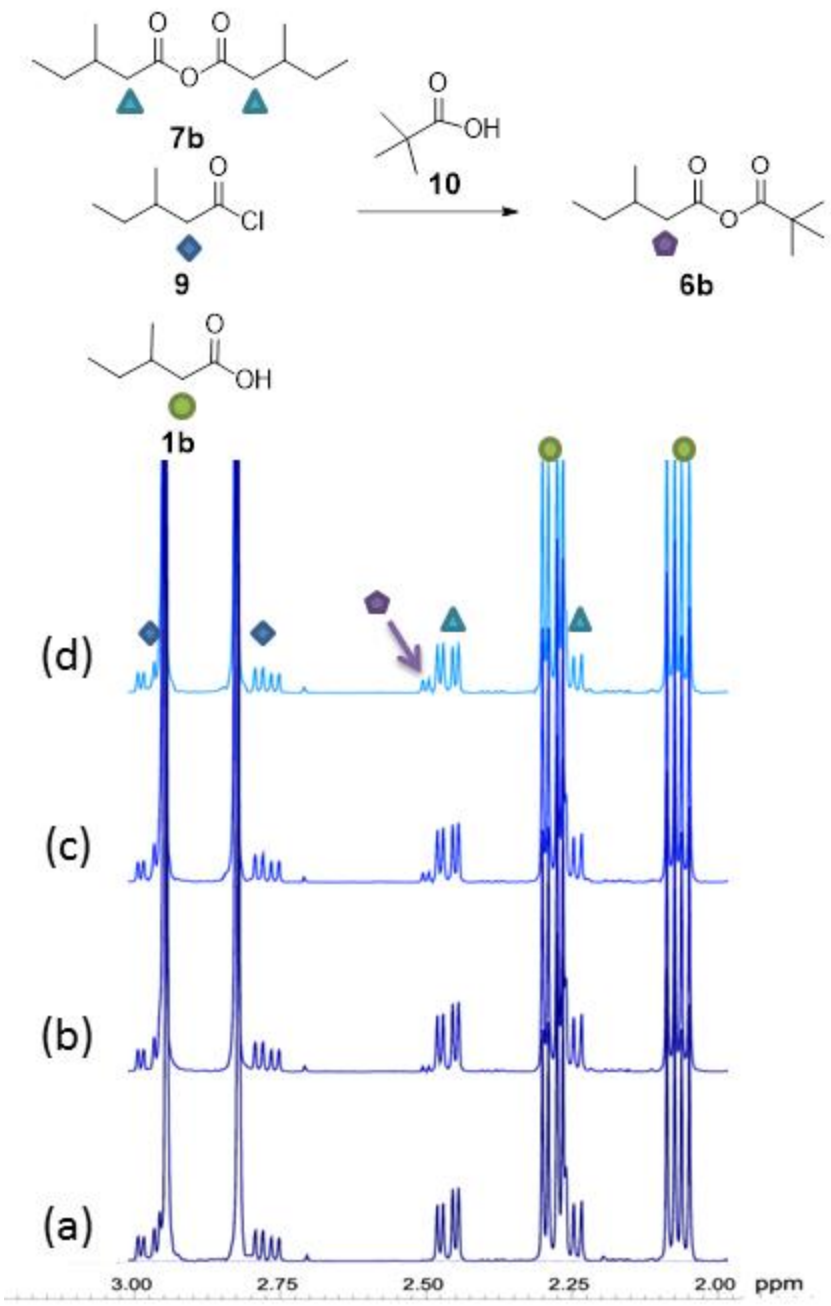

Figure 5.3. Expansion of the aliphatic region of the ^{1}H NMR spectra in acetonitrile-d_3: **(a)** 1 min., **(b)** 15 min. **(c)** 44 min. and **(d)** 111 min. after addition of pivalic acid **10** to the mixture from Figure 2 spectrum (c). Peaks corresponding to species **1b**, **7b** and **9** are highlighted.

Figure 5.4 provides a summary of the diagnostic chemical shifts which were used to identify each species at 25 °C in acetonitrile-d_3. Many of these species have chemical shifts

which are dependent upon reaction conditions, so the assignment displayed may vary slightly under actual reaction conditions.

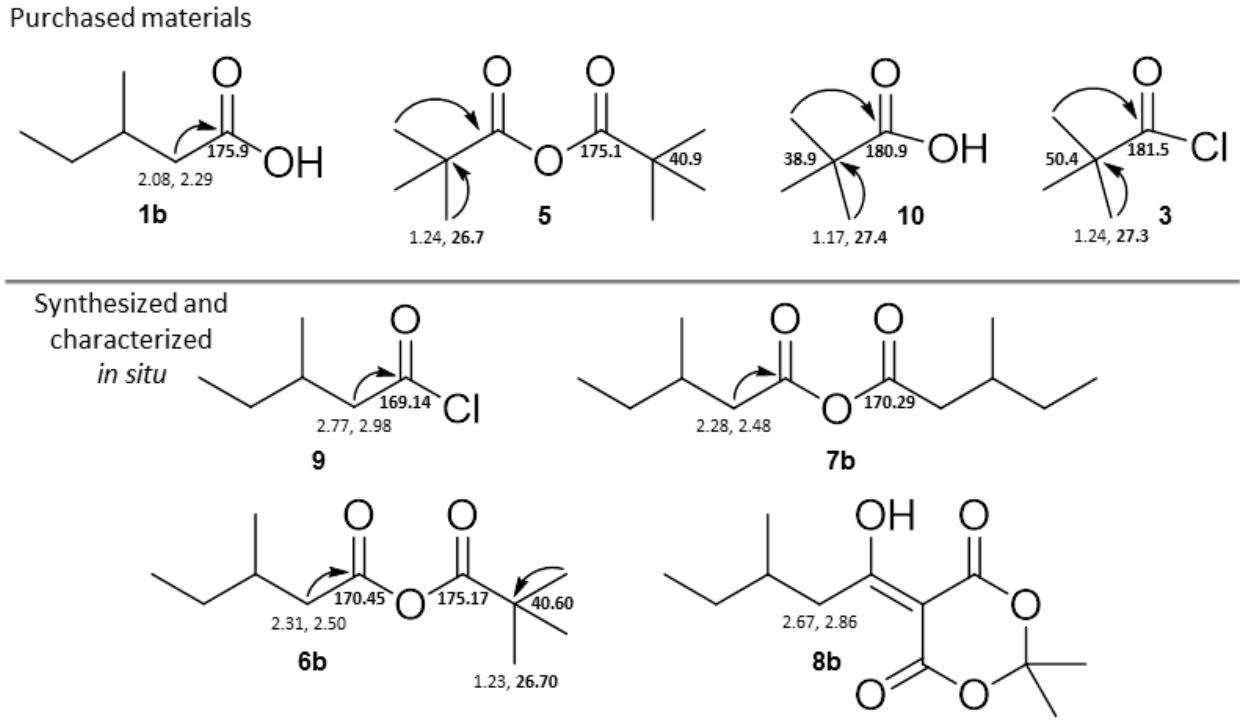

Figure 5.4. Summary of diagnostic chemical shifts in acetonitrile-d_3 at 25 °C for major species observed in this work. ^{1}H NMR assignments are in regular text, ^{13}C NMR assignments in bold. Curved arrows indicate ^{1}H-^{13}C HMBC correlations.

A number of control experiments were also conducted to observe reactions between pivaloyl chloride and Meldrum's acid or *N*-methylimidazole. However in both cases no significant reaction was observed in the control experiments or in the complete reaction shown in Scheme 5.2.

Investigation into productive mechanistic pathways

After identification of each reactive intermediate, mechanistic investigations were performed to investigate which intermediates are on productive pathways. Since 3-

methylpentanoyl chloride **9** was not previously identified in the mechanism, an experiment was designed to confirm if **9** reacts to form product **8b**. The chloride **9** was synthesized as previously described and added to Meldrum's acid **2** in the presence of excess 1-methylimidazole **4**. The reaction was monitored at 25 °C by ^{1}H NMR and immediate growth of product **8b** occurred upon addition of **2** (Figure 5.5). In this reaction the anhydride species **6b** and **7b** could not form (which would have characteristic resonances at 2.25 and 2.46 ppm), therefore acyl chloride **9** was the only productive intermediate to generate **8b**. This result indicated that **9** is present on a productive mechanistic pathway, and does not merely exist as an intermediate to an anhydride.

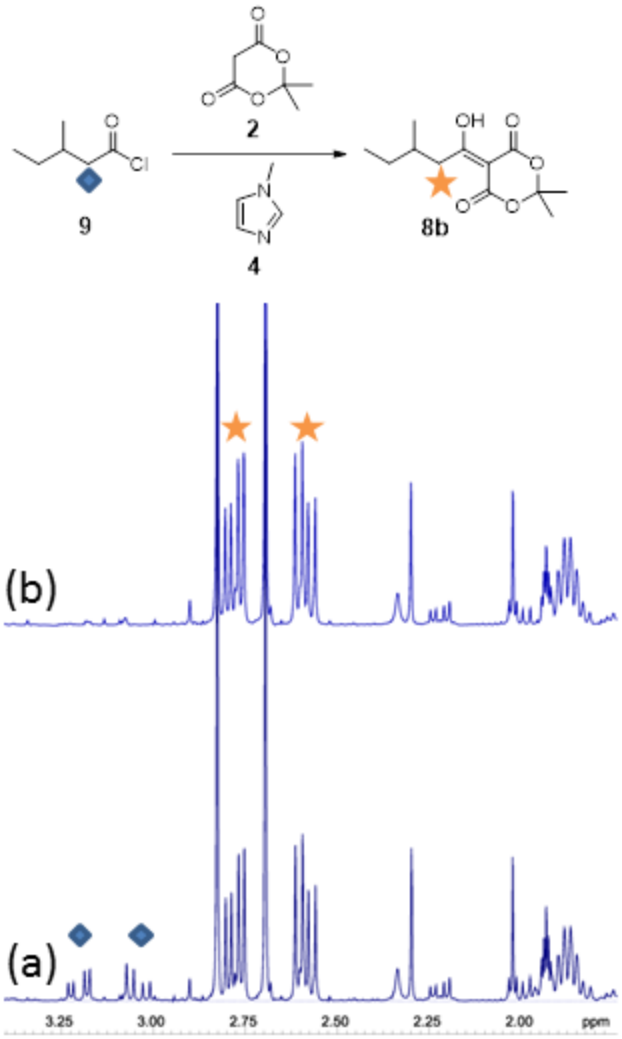

Figure 5.5. Expansion of the aliphatic region of the ^{1}H NMR spectra of the reaction between acyl chloride **9** and Meldrum's acid **2** in acetonitrile d_3 after **(a)** 1 and **(b)** 13 minutes.

In order to determine if the anhydride species **6b** and **7b** were also on a productive pathway, a mixture of the mixed anhydride **6b**, dimer anhydride **7b**, and 3-methylpentanoic acid **1b** was generated by reacting **1b** with pivalic anhydride **5** under basic conditions.[8] Meldrum's acid **2** was then added to this mixture and growth of product was immediately observed [Figure 5.6 spectrum (b)]. Under these reaction conditions there was no chloride source present,

therefore **9** could not form. This experiment clearly demonstrated that the intermediate anhydride species **6b** and **7b** are also productive intermediates on the mechanistic pathway.

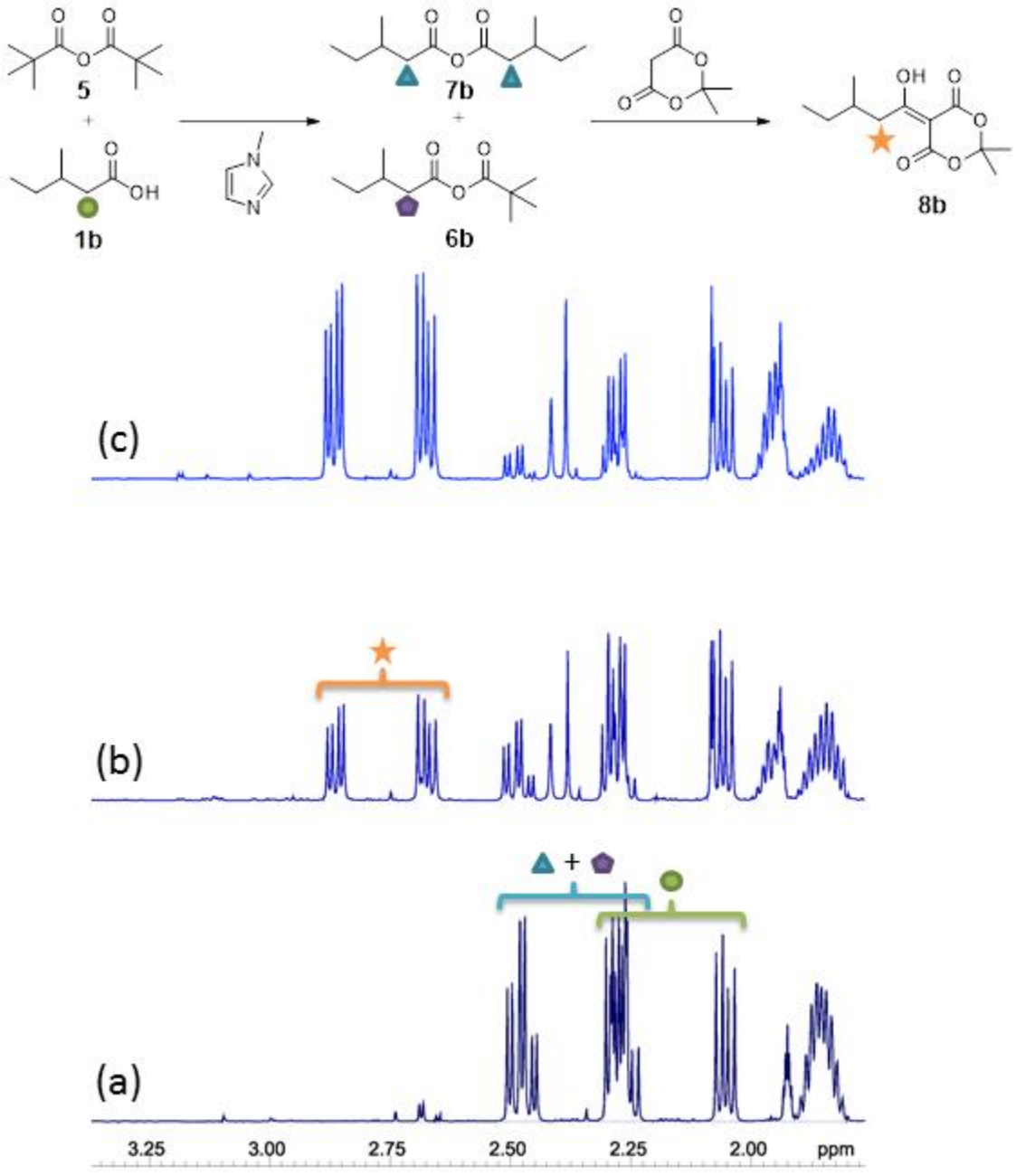

Figure 5.6. (a) Expansion of the aliphatic region of the ^{1}H NMR spectrum in acetonitrile d_3 obtained after reacting **1b** with **5; (b)** 3.5 min and **(c)** 63 min after the addition of Meldrum's acid **2.**

Clegg, *et al.* indicated that pivalic anhydride **5** was an intermediate species for the reaction with **1a**. In that transformation **5** could be have been generated by the reaction of pivalic acid **10** (a byproduct of the reaction) with **6a** or **3**. In order to observe if **5** was also an intermediate in the current study using starting material **1b**, the full reaction (Scheme 5.2) was monitored in an NMR tube at 0 °C with alternating proton and ^{1}H-^{13}C HMBC spectra. Pivalic anhydride **5** and pivaloyl chloride **3** display the same ^{1}H chemical shift for the *t*-butyl methyl, but their quaternary carbon chemical shifts are distinctive at 40.9 ppm and 50.4 ppm, respectively. ^{1}H-^{13}C HMBC data recorded fifteen minutes after reaction initiation showed ^{1}H-^{13}C HMBC correlations from the *t*-butyl methyl ^{1}H signals at 1.2 ppm to a quaternary ^{13}C signal at 40.9 ppm. This ^{13}C chemical shift correlation was consistent with those from a commercially available sample of **5**, indicating that **5** was formed during the reaction.

Acyl chloride formation

The source of the formation of the acyl chloride **9**, was thought to be reaction of chloride anion with anhydrides **6b** and **7b**. The only source of chlorine in the reaction mixture is pivaloyl chloride which reacts with carboxylic acid species resulting in HCl, and forms *N*-methylimidazole hydrochloride. In order to demonstrate that the acyl chloride is formed via reaction of chloride anion with the anhydrides **6b** and **7b**, a sample of these components was generated and *N*-methyl imidazole hydrochloride was added. The proton NMR spectrum of this mixture showed the appearance of resonances that were previously demonstrated to be related to acyl chloride **9**. This result supported the hypothesis that the chloride anion could react with the anhydrides **6b** and **7b** to form the acyl chloride **9** as shown in Figure 5.7.

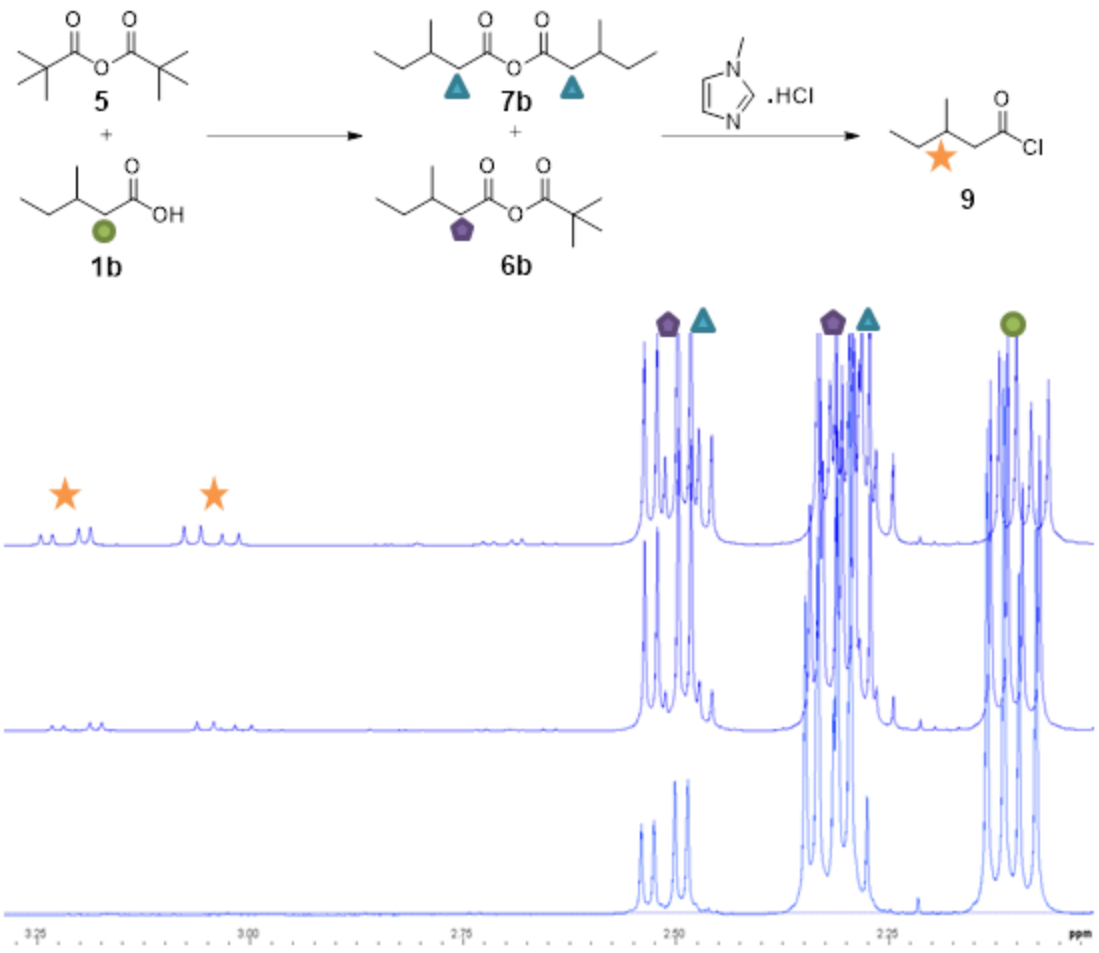

Figure 5.7. Formation of acyl chloride **9** by reaction of N-methylimidazole hydrochloride with anhydrides **6b** and **7b**. (Experiment performed by D. A. Foley)

Completion of reactive intermediate characterization revealed the full mechanism of this reaction and is summarized in Scheme 5.3. The starting material **1b** reacts with pivaloyl chloride **3** in order to produce the mixed anhydride species **6b** and the chloride salt of the base. Mixed anhydride **6b** can react with the chloride anion to produce the acyl chloride **9** and pivalic acid **10,** or can also react with another equivalent of **1b** to produce the dimer anhydride **7b** and pivalic acid **10**. Mixed anhydride **6b** can also react with **10** to produce pivalic anhydride **5**. Reaction of pivalic acid **10** with pivalyl chloride **3** can also result in the formation of **5**. The mixed

anhydride **6b**, dimer anhydride **7b** and acyl chloride **9** can each react with Meldrum's acid **2** to produce **8b**. A ^{1}H 2D ROESY experiment was performed on the reaction mixture to confirm the equilibrium between the intermediates involved (Figure 5.8). Exchange cross peaks were observed between acyl chloride **9**, mixed **6b** and symmetric anhydrides **7b**.

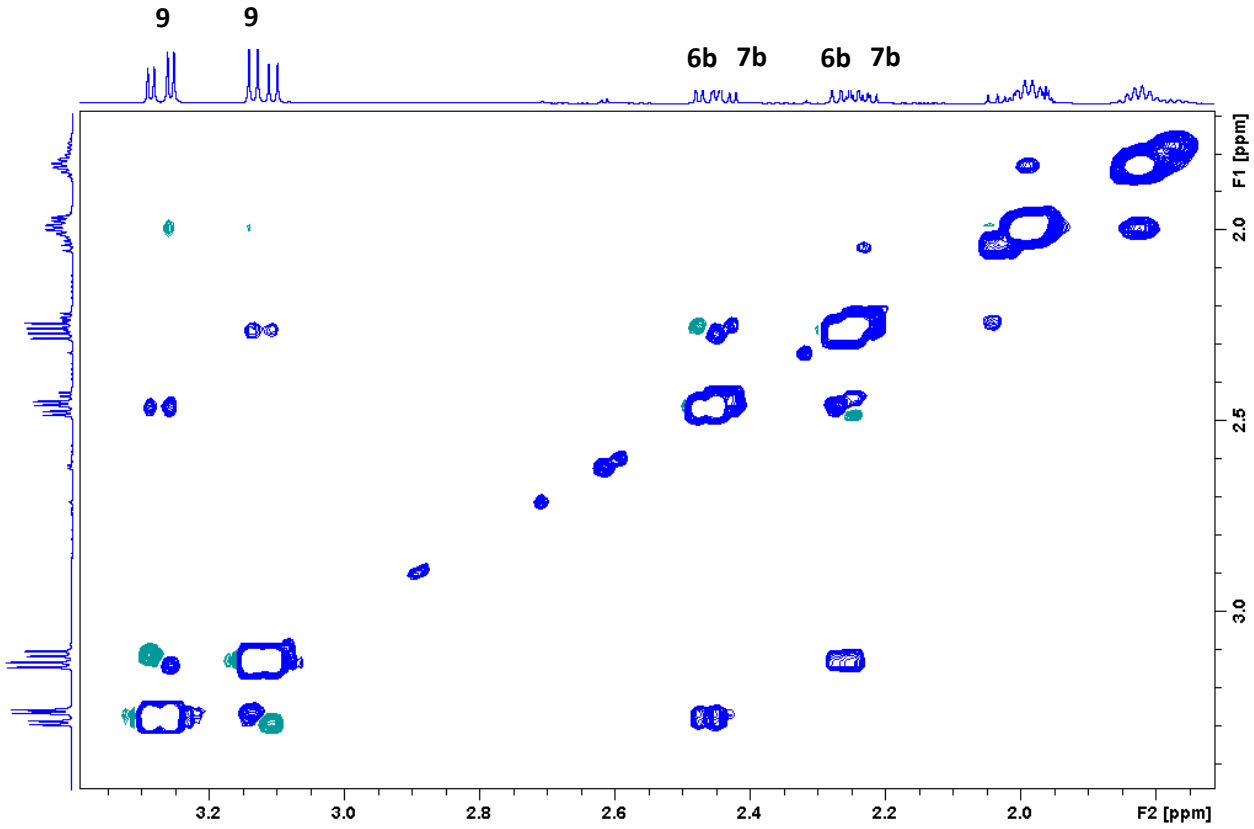

Figure 5.8. ^{1}H-^{1}H ROESY of reaction mixture showing exchange correlations between acyl chloride **9**, mixed **6b** and symmetric anhydrides **7b**. Parameter set used: ^{1}H 2D Tr-ROESY with 350 ms mixing time with 4.3 kHz spin lock field. (Performed by D. A. Foley)

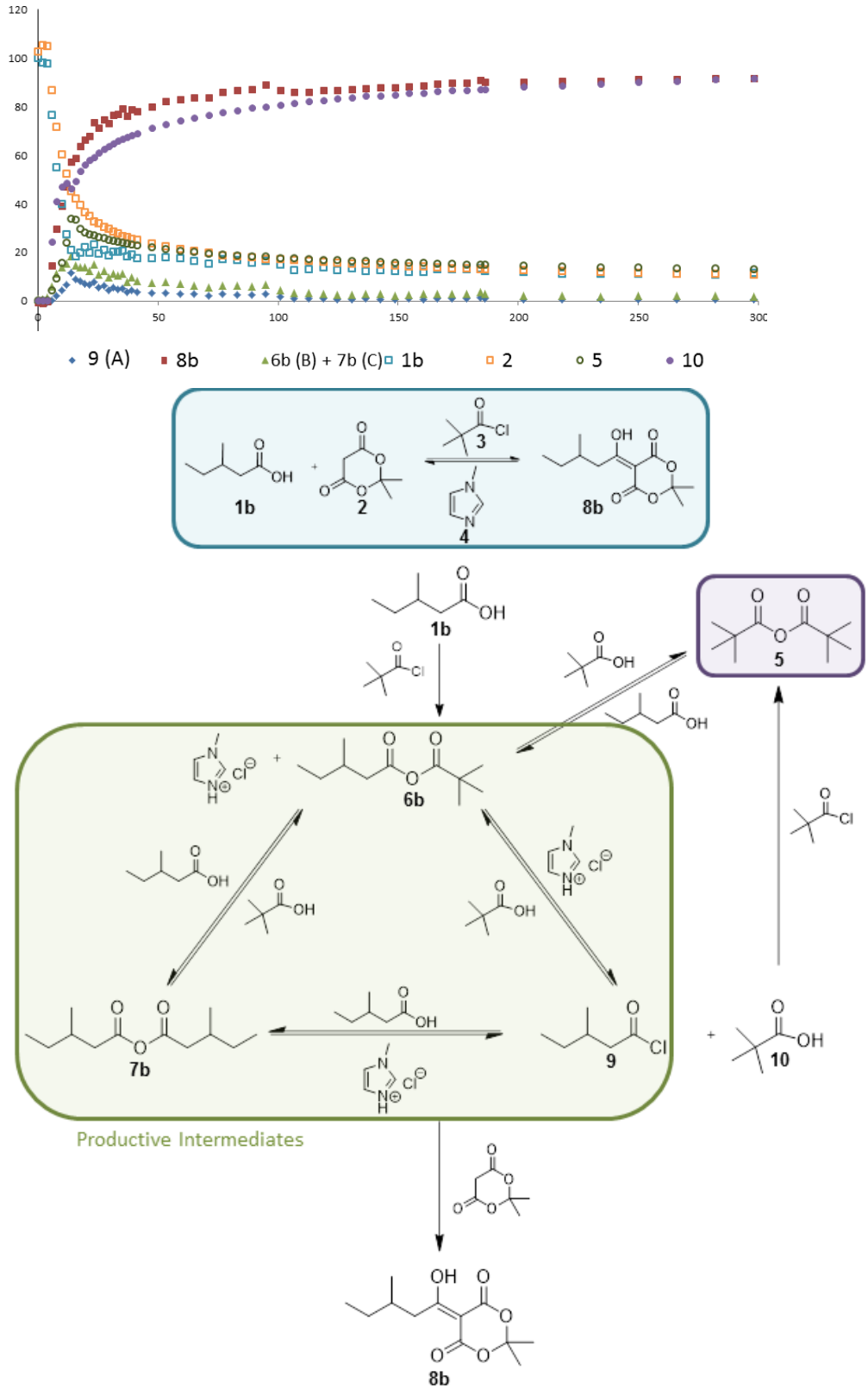

Scheme 5.3. Summary of the key steps in the mechanistic pathway of the reaction.

5.3. Conclusions

Online NMR was utilized to monitor the reaction of 3-methylpentanoic acid **1b** with Meldrum's acid **2** and a detailed investigation into the reaction mechanism was undertaken. A combination of the online NMR experiment and a number of offline characterization experiments uncovered new details about this synthetic transformation which had not been identified previously. Conclusive evidence is presented for the previously hypothesized dimer anhydride intermediate species. In addition, the presence of an acyl chloride intermediate species, 3-methylpentanoyl chloride **9**, was discovered. The 3-methylpentanoic acid analogue **1b** is shown to have similar behavior under these reaction conditions as 3-methylhexanoic acid **1a**. Online NMR is capable of providing a full reaction profile which assisted in identification of new reactive intermediates in this synthetic transformation. This coupled with offline characterization of these intermediates yielded a detailed mechanistic picture of the synthetic step, building on the original work by Clegg *et al*. These results demonstrate how online NMR spectroscopy facilitates analysis of the constantly changing reaction system while also allowing standard unit operations such as reagent addition to be conducted effectively.

5.4. Experimental

General Considerations:

NMR spectra were acquired on either a Bruker 400 MHz AVANCE III NMR equipped with a BBFO probe or a Bruker 600 MHz AVANCE III NMR with a TXO probe. ^{1}H NMR spectra were processed with Bruker TopSpin 3.2.pl6 and analyzed with Dynamics Center 2.2.4 (Bruker BioSpin).[9] Spectra were referenced to acetonitrile at δ_H 1.94 ppm. All reagents were purchased from Sigma-Aldrich and used without further purification. Acetonitrile-d_3 was

purchased from Cambridge Isotope Laboratories in 0.75 mL ampules and was used without further purification.

Online NMR spectroscopy:

The online NMR system was used as previously described with the needle splitting valve removed.[7] The reaction vessel (Mettler Toledo Easymax), sample loop and spectrometer were all temperature controlled to 25 °C using a heating circulator (Julabo FP-50-HE) with Syltherm XLT temperature regulation fluid. The flow rate through the system was 3 mL/min regulated by a dual piston pump (Lab Alliance Prep 100), and spectra were acquired on the flowing solution on a 400 MHz spectrometer. ^{1}H NMR spectra were acquired with 4 scans, 30° pulse angle and 10 s relaxation delay. 3-methylpentanoic acid **1b** (3.5 mL, 28 mmol), 1-methylimidazole **4** (7.4 mL, 92 mmol) and Meldrum's acid **2** (4.5 g, 31 mmol) were added to 30 mL anhydrous acetonitrile in a reaction vessel under an atmosphere of N_2. Reagents were circulated through system to achieve temperature (25 °C) and concentration equilibration. Pivaloyl chloride **3** (4.1 mL, 34 mmol) was added to reaction vessel over the course of 10 minutes via dosing syringe. ^{1}H NMR spectra were obtained on the flowing sample at 2 minute intervals for the first 20 spectra, 6 minute intervals until reaction time reached 185 minutes, and then every 16 minutes until reaction completion was observed.

Offline NMR tube Characterization:

*Synthesis of 3-methylpentanoyl chloride **9**:*

3-methylpentanoic acid **1b** (60 µL, 0.48 mmol) and 3 drops DMF were added to 0.75 mL acetonitrile-d_3. Oxalyl chloride (42 µL, 0.48 mmol) was added *via* micropipette in two portions

over 15 min at room temperature. ^{1}H, ^{13}C, HSQC and HMBC data were recorded for characterization of the reaction components.

*Synthesis of 3-methylpentanoic anhydride **7b**:*

To crude reaction mixture of synthesized 3-methylpentanoyl chloride **9** in an NMR tube, 3-methylpentanoic acid **1b** (50 µL, 0.40 mmol) and triethylamine (50 µL, 0.36 mmol) were added *via* micropipette. ^{1}H, ^{13}C, HSQC and HMBC data were recorded for characterization of the reaction components.

*Synthesis of 3-methylpentanoic pivalic anhydride **6b**:*

To a crude reaction mixture of 3-methylpentanoic anhydride **6b**, 3-methylpentanoyl chloride **9** and 3-methylpentanoic acid **1b**, added 5 mg pivalic acid **10** in an NMR tube at room temperature. The reaction was monitored at 25 °C with ^{1}H NMR.

*Synthesis of 3-methylpentanoic pivalic anhydride **6b** and 3-methylpentanoic anhydride **7b**:*

3-methylpentanoic acid **1b** (62 µL, 0.5 mmol), pivalic anhydride **5** (102 µL, 0.5 mmol) and 1-methylimidazole **4** (131 µL, 1.65 mmol) were added to 0.75 mL acetonitrile-d_3 in an NMR tube at room temperature. ^{1}H, ^{13}C, HSQC and HMBC data were recorded for characterization of the reaction components.

*Reaction of 3-methylpentanoyl chloride **9** with Meldrum's acid **2** to produce 5-(1-hydroxy-3-methylpentylidene)-2,2-dimethyl-1,3-dioxane-4,6-dione **8b**:*

3-Methylpentanoyl chloride **9** (0.24 mmol) in 0.75 mL acetonitrile-d_3 was synthesized as described previously. A large excess of 1-methylimidazole **4** (2.5 mmol) was added to the solution of **9**. A bright yellow solid formed immediately upon addition and was filtered off. Meldrum's acid **2** was added to the filtrate *via* micropipette at room temperature (36 mg, 0.24 mmol). The reaction was monitored at 25 °C with ^{1}H NMR.

*Reaction of 3-methylpentanoic pivalic anhydride **6b** and 3-methylpentanoic anhydride **7b** with Meldrum's acid **2** to produce 5-(1-hydroxy-3-methylpentylidene)-2,2-dimethyl-1,3-dioxane-4,6-dione **8b**:*

Meldrum's acid **2** (72 mg, 0.5 mmol) was added to the crude reaction mixture of 3-methylpentanoic acid **1b**, 3-methylpentanoic anhydride **7b**, and 3-methylpentanoic pivalic anhydride **6b** in an NMR tube at room temperature. The reaction was monitored at 25 °C with ^{1}H NMR.

5.5. References

1. (a) A. Chanda, A.M. Daly, D.A. Foley, M.A. LaPack, S. Mukherjee, J.D. Orr, G.L. Reid, D.R. Thompson, and H.W. Ward, *Org. Process Res. Dev.*, **2015**, *19*, 63-83;
(b) A.S. Rathore, R. Bhambure, and V. Ghare, *Anal. Bioanal. Chem.*, **2010**, *398*, 137 - 154;
(c) D.J. Ertl, S.E. Barnes, B.E. Cooley, and C.A. Goss, *American Pharmaceutical Review*, **2009**, *12*.
2. U. Holzgrabe, *Prog. Nucl. Magn. Reson. Spectrosc.*, **2010**, *57*, 229 - 240.

3. (a) M. Maiwald, H.H. Fischer, Y.-K. Kim, K. Albert, and H. Hasse, *J. Magn. Reson.*, **2004**, *166*, 135-146;

(b) M.A. Bernstein, M. Stefinovic, and C.J. Sleigh, *Magn. Reson. Chem.*, **2007**, *45*, 564 - 571;

(c) D.A. Foley, E. Bez, A. Codina, K.L. Colson, M. Fey, R. Krull, D. Piroli, M.T. Zell, and B.L. Marquez, *Anal. Chem.*, **2014**, *86*, 12008-12013.

4. (a) M. Maiwald, H.H. Fischer, Y.-K. Kim, and H. Hasse, *Anal. Bioanal. Chem.*, **2003**, *375*, 1111-1115;

(b) F. Dalitz, M. Cudaj, M. Maiwald, and G. Guthausen, *Progr. Nucl. Magn. Reson. Spectrosc.*, **2012**, *60*, 52 - 70;

(c) A.C. Barrios Sosa, R.T. Williamson, R. Conway, A. Shankar, R. Sumpter, and T. Cleary, *Org. Process Res. Dev.*, **2011**, *15*, 449-454;

(d) D.A. Foley, C.W. Doecke, J.Y. Buser, J.M. Merritt, L. Murphy, M. Kissane, S.G. Collins, A.R. Maguire, and A. Kaerner, *J. Org. Chem.*, **2011**, *76*, 9630 - 9640;

(e) J.Y. Buser and A.D. McFarland, *Chem. Comm.*, **2014**, *50*, 4234 - 4237;

(f) N. Zientek, C. Laurain, K. Meyer, M. Kraume, G. Guthausen, and M. Maiwald, *J. Magn. Reson.*, **2014**, *249*, 53-62.

5. M. Birch, S. Challenger, J.-P. Crochard, D. Fradet, H. Jackman, A. Luan, E. Madigan, J.S. Mathew, N. McDowall, K. Meldrum, C.M. Gordon, P. Peach, and S. Yeo, *Org. Process Res. Dev.*, **2011**, *15*, 1358-1364.

6. I.M. Clegg, C.M. Gordon, D.S. Smith, R. Alzaga, and A. Codina, *Anal. Methods*, **2012**, *4*, 1498-1506.

7. D.A. Foley, J. Wang, B. Maranzano, M.T. Zell, B.L. Marquez, Y. Xiang, and G.L. Reid, *Anal. Chem.*, **2013**, *85*, 8928-8932.

8. Y. Oikawa, K. Sugano, and O. Yonemitsu, *J. Org. Chem.*, **1978**, *43*, 2087-2088.

9. *http://www.bruker.com/products/mr/nmr/nmr-software/software/dynamics-center/overview.html* 30 Nov 14.

Chapter 6

Mechanistic and Kinetic Insights into Lactide Polymerization Utilizing Stopped-Flow NMR Spectroscopy and Kinetic Modeling of the Molecular Weight Distribution

Meso-lactide by SF NMR was first observed by Dr. Emily Tan. Dr. Bernie Anding provided the band broadening figure and provided assistance with initial MWD modeling.

6.1. Introduction

Polylactide (PLA) is a biodegradable, non-toxic polymer with good performance characteristics that is derived from lactide, the cyclic diester of lactic acid. Renewable resources such as corn or sugar beets provide lactide. Biodegradation characteristics of PLA make it an attractive polymer for use in environmental and medical applications such as biodegradable consumer plastic products and heart stents. Polylactide degrades on the time scale of six months to two years to biologically nontoxic lactic acid, while polystyrene or polyethylene can take 500 to 1000 years to degrade.[1–3] PLA can be made as cyclic or linear (or non-cyclic) polymer. Commonly the linear form is produced with catalysts such as simple metal (Li, Na, K) alkoxides, aluminum porphyrin alkoxides, lanthanide (La, Sm, Y, Yb) oxo isopropoxides, and Zn(II), Mg(II) and Sn(II) alkoxide complexes.[4] Metal-free synthesis of PLA is desirable for use in semiconductor coatings and other materials that would be sensitive to metallic impurities.

In 2007, Waymouth, *et al.* demonstrated that the *N*-heterocyclic carbene 1,3-dimesitylimidazol-2-ylidene (IMes) catalyzes lactide polymerization to produce cyclic PLA (Scheme 6.1).[5,6] The IMes catalyzed production of PLA displays complicated kinetics and produces high molecular weights with a polydispersity index (PDI) of less than 1.4, except for at high conversions. They note that the PDI sharply increases to 1.6 for polymers with more than 90% monomer conversion. The Waymouth group examined the time course of lactide polymerization by quenching the reaction at different time points and analyzing monomer concentration, number average molecular weight (M_n) of the polymer, and polymer PDI with time and fitting these three pieces of data to kinetic models. The best fit to the data was obtained using a kinetic model with slow initiation, quick propagation, depropagation (where backbiting on the propagating species occurs such that one lactide unit is removed from the propagating

chain), and slow termination. Due to the inherent nature of the experimentation, they were unable to observe any events that occur in the first few seconds of the reaction, particularly because the polymerization is complete within minutes at room temperature.

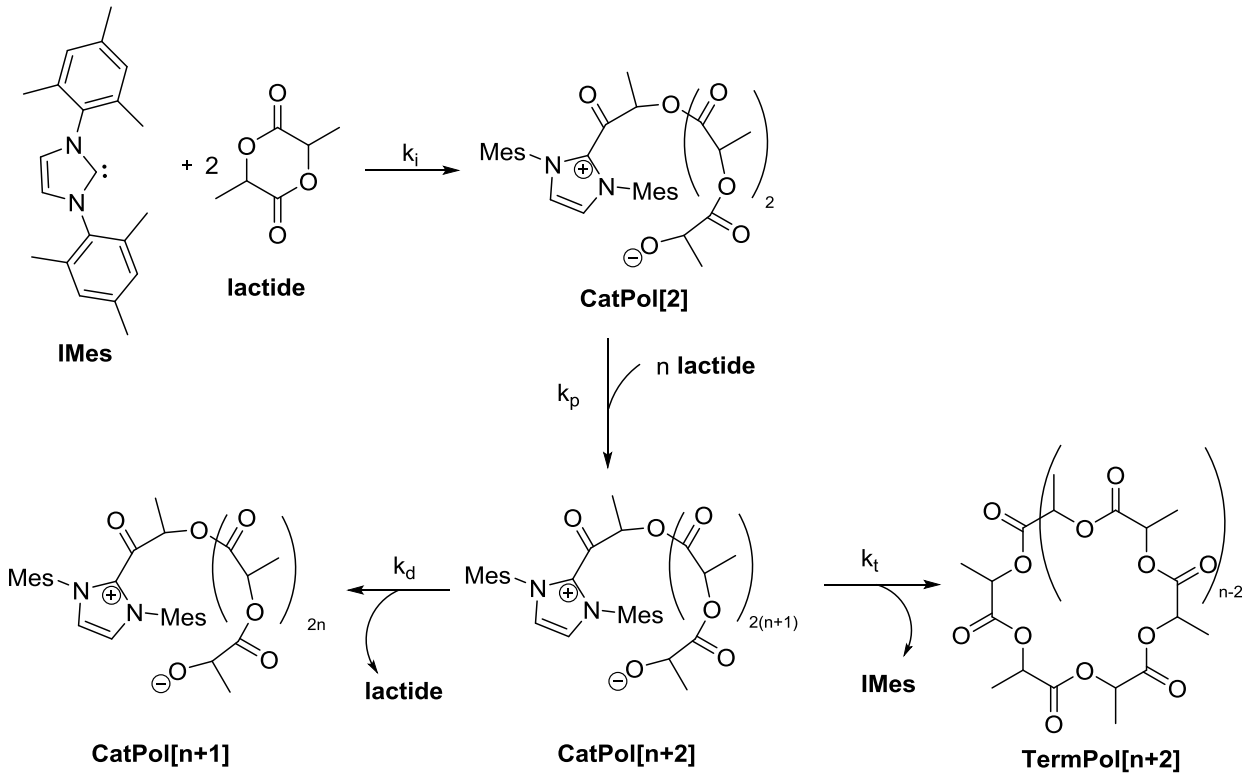

Scheme 6.1. Waymouth kinetic model of lactide polymerization as catalyzed by IMes.[6] Propagating species are designated CatPol and terminated species are designated TermPol. The number in brackets represents how many lactide monomers were inserted. The rate constants are as follows: k_i = initiation, k_p = propagation, k_d = depropagation, k_t = termination.

One way to probe reaction mechanisms and kinetics is to follow the appearance and disappearance of reactants, intermediates, and products by nuclear magnetic resonance (NMR) spectroscopy. However, the most common technique for reaction monitoring using NMR spectroscopy, by which reagents are mixed in an NMR tube that is then inserted into the spectrometer, is limited to slow reactions (half-lives less than *ca.* 30 seconds) due to the dead time between initiation of the reaction and the collection of the first NMR experiment. Currently the most common ways to monitor fast reactions via NMR are to use low temperature (thus,

slowing the reaction) and rapid injection techniques. Low temperature NMR is limited to the temperature capabilities of the probe, restricts the choice of solvent, and moves the study of the reaction out of the regime in which it is commonly practiced. Rapid injection techniques allow for one run at a time, only, as the NMR tube must be cleaned or replaced before the procedure may be repeated.[7–15]

Stopped-flow (SF) NMR spectroscopy is a flow technique that enables measurement of kinetics of reactions with short half-lives (longer than *ca.* 100 ms) in real time at room temperature by rapidly pushing two solutions through a mixer and the detection region of the NMR spectrometer.[16–23] Upon stopping the flow the detection region is filled with freshly mixed reagents. Landis and coworkers developed a stopped-flow NMR probe that utilizes a four-jet mixer and effects complete mixing of solutions directly above the NMR detection region. The effectiveness of this device was demonstrated by kinetic study of [*rac*-(C_2H_4(1-indenyl)$_2$)ZrMe][MeB(C_6F_5)$_3$]-catalyzed polymerization of 1-hexene.[24]

The polymerization of lactide as catalyzed by IMes is complete within minutes at room temperature, making this reaction challenging to study with traditional NMR spectroscopy. Utilization of the stopped-flow NMR technique to observe lactide polymerization could provide insight into this fast reaction mechanism and improve the existing kinetic model. We describe two experimental approaches to the study of IMes-catalyzed lactide polymerization. One approach is stopped-flow NMR spectroscopy, which uniquely provides insight into the early steps of the reaction. The second approach concerns determination of the time evolution of the molecular weight distribution of PLA. These data are then subjected to kinetic modeling.

6.2. Study of Lactide Epimerization with SF and ^{13}C NMR Spectroscopy

SF NMR Spectroscopy

The polymerization of pure *L*-lactide was monitored with stopped-flow NMR spectroscopy (Figure 6.1). Figure 6.1a displays the disappearance of the methine signal of *L*- (or *rac*-) lactide and the growth of the methine signal of PLA as a function of time. Somewhat surprisingly the growth and disappearance of *meso*-lactide, also, is observed in the first few seconds of the reaction. (Note: Dr. Emily Tan was the first person to perform SF NMR for the lactide polymerization system and was the first to note the appearance of *meso*-lactide.) Thus the apparent half-life of epimerization is less than 5 s. These studies were conducted in toluene to avoid NMR chemical shift overlap noted in THF.

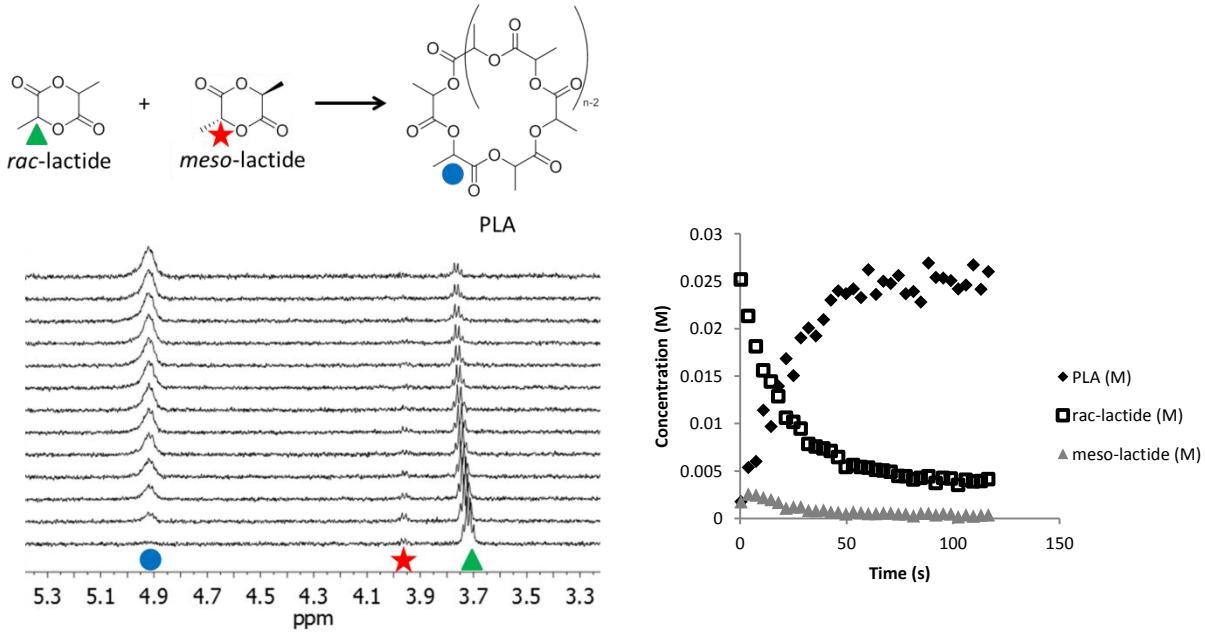

Figure 6.1. a) Direct, *in situ* observation of *meso*-lactide growth and disappearance during time course of reaction in toluene at room temperature. The bottom spectrum is at reaction time 1 s, with each subsequent spectrum 9 s later. b) Concentrations plotted with reaction time, clearly showing initial growth of *meso*-lactide and its subsequent disappearance. Initial concentrations: 30 mM *L*-lactide; 6 mM IMes. All concentrations are calculated from integration of an unreactive internal standard, *bis*-trimethylsilylbenzene (BTMSB).

Stereoerrors during lactide polymerization can arise from poor control of tacticity during insertion events or from epimerization of the lactide monomer. Waymouth, *et al.* noted the apparent partial epimerization of lactide monomer prior to insertion for polymerizations catalyzed by strong bases, such as cyclohexyldimethylamine.[25] However, issues such as the rate of monomer epimerization were not explored. When using traditional NMR spectroscopy to observe the polymerization of *L*- or *rac*-lactide, the *meso*- monomer grows in and becomes indistinguishable from baseline before the first spectrum can be acquired. Stopped-flow NMR spectroscopy enables the direct observation and quantification of lactide epimerization during polymerization (Figure 6.1). With initial concentrations of 30 mM lactide and 6 mM IMes, *rac*-/*meso*-lactide equilibrium appears to be reached by the time of the second data point (4 s) and then both monomers disappear as they are incorporated into the polymer. These data require addition of an IMes-dependent lactide epimerization step to the existing mechanistic scheme (Scheme 6.2). Epimerization of lactide monomer increases the number of stereoerrors expected in PLA.

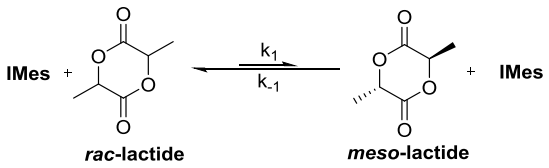

Scheme 6.2. Epimerization of lactide monomer as catalyzed by IMes.

The *rac-meso* epimerization proceeds through either a ring-opened mechanism with IMes acting as a nucleophile or a ring-closed mechanism with IMes acting as a base (Scheme 6.3). The pKa of lactide and IMes are *ca.* 25 and 24 in DMSO, respectively.[26] Therefore, it is difficult to predict the prevalent epimerization mechanism without further experimental evidence.

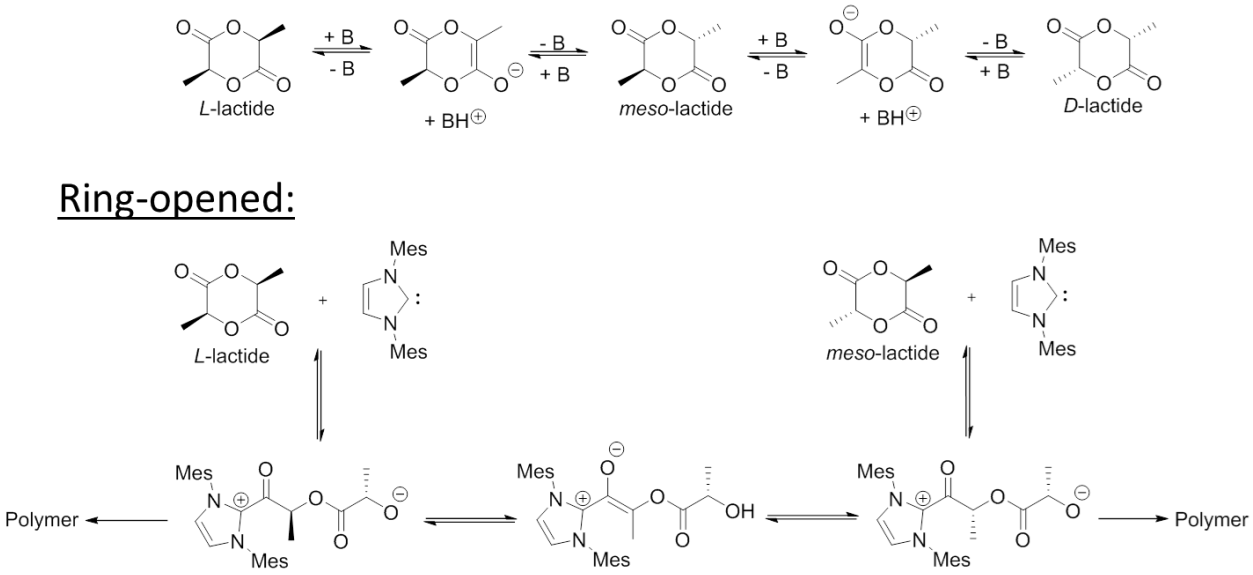

Scheme 6.3. Two possible mechanisms for epimerization: ring-closed base-catalyzed enolization (top), and ring-opened zwitterionic enolization (bottom).

A simple model to examine epimerization was optimized using the modeling software Copasi[27] (Scheme 6.4). Using this kinetic model, good fits of the concentrations of *rac*-, *meso*- and polylactide were achieved when $k_{epim} = 0.104 \pm 0.017\ s^{-1}$, $K_{eq} = 8.16 \pm 0.20$, $k_{prop} = 0.0330 \pm 0.0006\ M^{-1}s^{-1}$, and $[rac\text{-lactide}]_0 = 0.0270 \pm 0.0003$ M (Figure 6.2). All errors reported are the standard deviations.

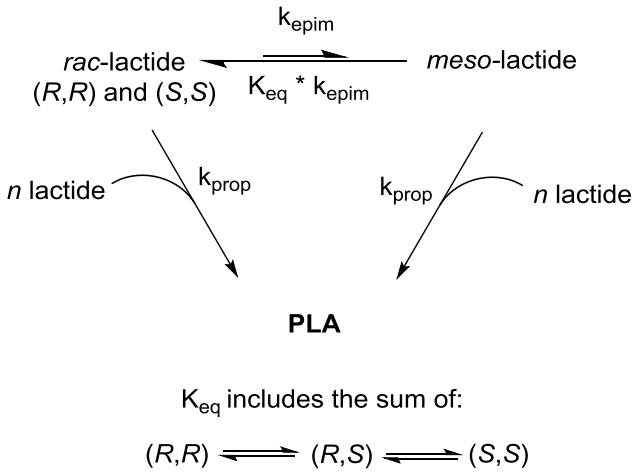

Scheme 6.4. The simple model used to examine monomer epimerization and propagation. It was assumed that propagation of both *rac*- and *meso*-lactide would proceed at the same rate.

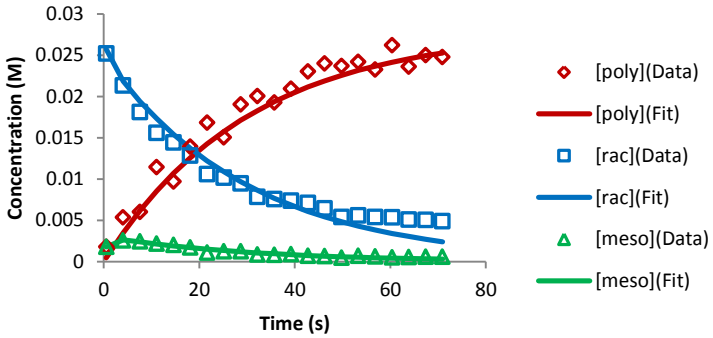

Figure 6.2. The fit (solid lines) of the model in Scheme 6.4 to the SF NMR data at room temperature (points). The initial concentrations were 30 mM lactide and 6 mM IMes.

^{13}C NMR Spectra Hexad Analysis

To further probe the origins of stereoerrors in lactide polymerization, we performed hexad analysis of ^{13}C NMR spectra as previously described in the literature.[28,29] Polymerizations were performed to partial conversion using a) *L*-, b) *rac*-, and c) *meso*-enriched lactide (89% *meso*-, 11% *rac*-lactide) (Figure 6.3) as monomers. The carbonyl region of the ^{13}C NMR spectrum displays peaks based upon hexad tacticity (i = isotactic, s = syndiotactic). Band 1 of the carbonyl region includes the hexads iiiii, iiiis, siiii, siiis; band 2 includes the hexads iiisi,

iisis, iisii, sisii, sisis, isiii; band 3 is the isisi hexad.[29] A hexad labeling of iiiii indicates a block of six lactic acid units, each with the same absolute configuration; inversion of the last stereocenter in that hexad would result in the iiiis designation and so on.

As expected by the previously proposed chain-end stereocontrol mechanism,[30] *L*-lactide monomer results in a polymer with ^{13}C carbonyl resonances largely in the isotactic (Band 1) region. Conversely, *meso*-enriched monomer yields largely syndiotactic polymer (Bands 2 and 3) (Table 6.1). *Rac*-lactide results in a polymer which is much more isotactic than the calculated distribution obtained by assuming random integration of stereocenters. The fact that *L*-lactide does not result in a completely isotactic polymer lends further support for the observation of the epimerization to *meso*-lactide which is then incorporated into PLA by the proposed chain end control mechanism.

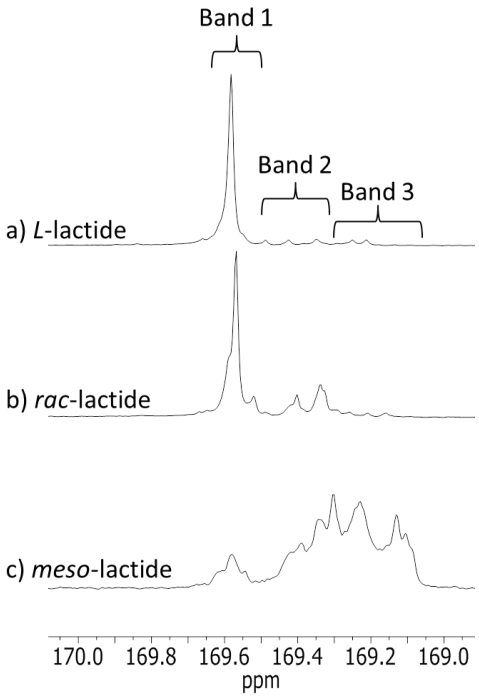

Figure 6.3. Carbonyl region of ^{13}C NMR spectra in toluene-d_8 of polymers obtained from the following monomers: a) *L*-lactide, b) *rac*-lactide, c) *meso*-enriched lactide (89% *meso*-, 11% *rac*-lactide). The band regions are labeled as according to Zhao, *et. al*.[29] Polymers were precipitated out from dichloromethane with hexanes and water.

Table 6.1. Hexad distribution from integration of carbonyl region of ^{13}C NMR spectra.

Monomer	**Yield***	**Band 1**	**Band 2**	**Band 3**
L-lactide	25%	86%	9%	5%
rac-lactide (theoretical†)	54%	69% (36%)	28% (50%)	3% (14%)
meso-enriched lactide	33%	11%	67%	22%

*Yield of PLA

†Theoretical distribution calculated by assuming random integration of stereocenters

Quenched Polymerization Reactions

There have been several reports indicating that *meso*- and *rac*-lactide may polymerize at different rates, depending on the nature of the catalysts.[30,31] However, *rac*- and *meso*-lactide polymerize at similar rates using the combination of IMes and an alcohol initiator.[30] Under our quenched polymerization conditions, which include *rac*-lactide monomer with IMes catalyst and no alcohol initiator, the percentage of lactide present as *meso* isomer rapidly grows from 0% to a maximum value of *ca.* 14-17%; the maximum percentage of *meso* isomer is reached by *ca.* 10-20% conversion of total lactide. Therefore, even if *rac* and *meso* isomers polymerize with slightly different rate constants in our system, the contribution from the *meso* isomer is much smaller than that of the *rac* isomer. In order to simplify our model, we will assume that both *rac*- and *meso*-lactide polymerize with the same rate constants. Polymerizations quenched at several different reaction times with different initial monomer and catalyst concentrations are displayed in Figure 6.4.

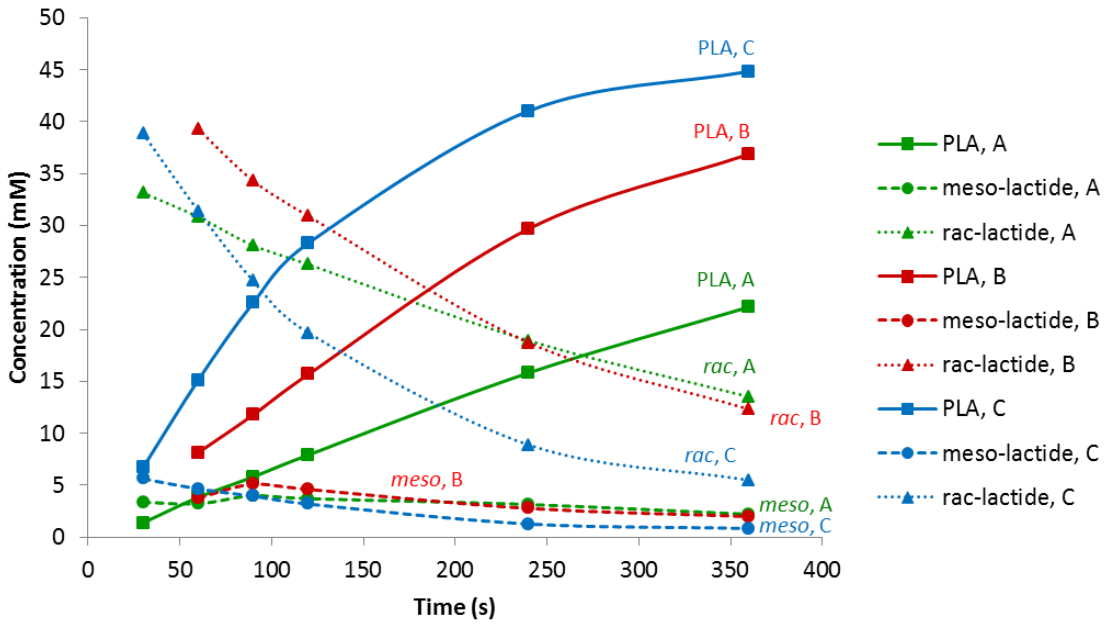

Figure 6.4. The polymerization quench studies used in the modeling described herein. Condition A: [*rac*-lactide]$_0$ = 37.9 mM, [IMes]$_0$ = 1.0 mM; Condition B: [*rac*-lactide]$_0$ = 51.2 mM, [IMes]$_0$ = 1.0 mM; Condition C: [*rac*-lactide]$_0$ = 51.2 mM, [IMes]$_0$ = 1.83 mM. Each data point is the average of two runs.

6.3. Kinetic Modeling of Polylactide Molecular Weight Distributions

Further kinetic information about IMes-catalyzed polymerization of lactide can be obtained by modeling the shapes of the molecular weight distribution (MWD) as a function of time. As discussed by Abu-Omar, modeling the MWD obtained from gel permeation chromatography (GPC) instead of just the M_n allows access to an even greater amount of kinetic information.[32] For our modeling simulations we utilize the kinetic modeling software Copasi.[27]

Background

The RI signal at each *n* monomer insertion is calculated in the following manner:

$$RI_n = \frac{dn}{dc} * K_{detector} * MW_n * conc_n \quad (1)$$

Where dn/dc = refractive index increment of polylactide (mL/g), MW_n = molecular weight of polymer at *n* insertions (mol/L), and $conc_n$ = concentration of propagating and terminated polymer of *n* monomer length (g/mol).

$K_{detector}$, the detector constant, is defined by equation (2)[33]

$$K_{detector} = \frac{RI\ Area}{dn/_{dc*conc}} \tag{2}$$

Since GPC analysis of polymerization reactions is performed using an approximately 1 mg/mL solution of product PLA from the quench reactions, it is necessary to (a) account for the true concentration and resulting RI signal of PLA at different percent conversions and (b) account for error in precise PLA concentration of the GPC sample. A fractional conversion scalar is used and the RI area of the sample is normalized to the RI area of an exactly 1 mg/mL PLA solution, as displayed in equation (3):

$$RI_n = \frac{dn}{dc} * K_{detector} * MW_n \ * conc_n * fractional\ conversion * \left(\frac{RI\ Area_{1\ mg/mL}}{RI\ Area_{\ sample}}\right) \tag{3}$$

Using equation (2), the RI area of a 1 mg/mL sample is:

$$RI\ Area_{1\ mg/mL} = K_{detector} * \frac{dn}{dc} * 1 \tag{4}$$

Substituting equation (4) into equation (3) and combining variables gives:

$$RI_n = K_{detector}^2 * \left(\frac{dn}{dc}\right)^2 * MW_n \ * conc_n * fractional\ conversion * \frac{1}{RI\ Area_{sample}} \tag{5}$$

Since $K_{detector}$ and dn/dc are both constants for our system, we can combine them into one constant value, a scaling factor (sf):

$$RI_n = sf * MW_n \ * conc_n * fractional\ conversion * \frac{1}{RI\ Area_{sample}} \tag{6}$$

Broadening of the signals on the GPC column, called GPC band broadening, must be accounted for in order to accurately simulate the experimental GPC traces. If there were no experimental GPC band broadening, each polymer would elute from the column at a discrete

retention volume with the larger polymers (lower retention volumes) eluting much closer together than the lower molecular weight polymers due to retention volume being a function of the log of the molecular weight of the polymer (Figure 6.5a). However, each polymer species will not elute as a discrete point due to Eddy diffusion, longitudinal diffusion, and mass transfer.[34] This broadening is represented in Figure 6.5b as a Gaussian distribution on each signal from 6.5a. Upon summing each Gaussian function (Figure 6.5c), the overall, band-broadened signal is significantly amplified at lower retention volumes due to the larger amount of overlap of higher molecular weight polymers.

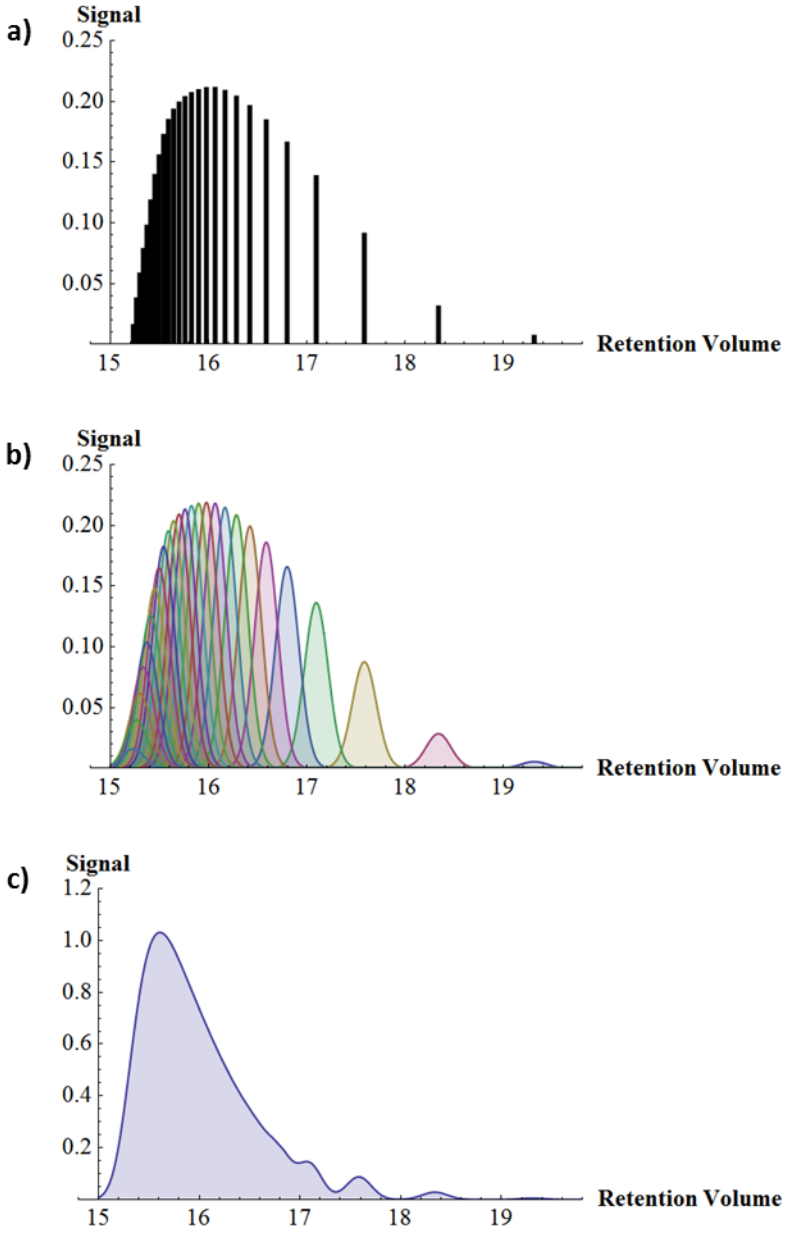

Figure 6.5. GPC band broadening. a) Each polymer eluting at a discrete retention volume; b) Gaussian broadening due to diffusion and mass transfer; c) the band broadened signal which is a sum of the Gaussians in b. (Figure provided by Dr. Bernie Anding)

Because band broadening affects the observed intensities in the high molecular weight range much more than the lower molecular weights, a simple correction for GPC band broadening is to multiply the calculated RI signal by an additional molecular weight term.[35]

Applying the band broadening correction to equation (6) gives equation (7) to calculate the RI signal at each *n* monomer insertion value.

$$RI_n = sf * MW_n^2 * conc_n * fractional\ conversion * \frac{1}{RI\ Area_{sample}} \quad (7)$$

Some simplifications were necessary in order to converge on meaningful rate constants due to the lack of observable species (only polymer and monomer are observed by NMR). The initiation process is modeled as two sequential lactide insertions, as proposed by Waymouth, *et al.* (Scheme 6.5). Assuming a steady state condition of the single insertion species and that k_{-1} is greater than k_2[lactide], the initiation rate constant (k_i) is expressed as the combination of rate constants in equation 8.

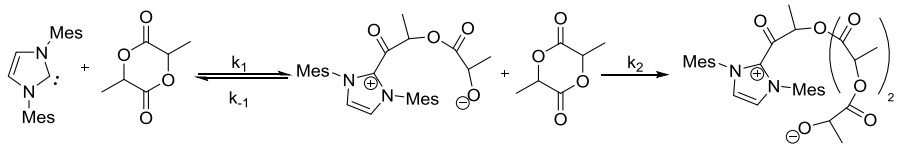

Scheme 6.5. Two-step initiation as proposed by Waymouth, *et. al.*[6]

$$k_i = \frac{k_1 k_2}{k_{-1}} \quad (8)$$

Efforts to evaluate all three rate constants (k_1, k_2, and k_{-1}), assuming the steady-state approximation of the single insertion species, converged to $k_{-1} >> k_2$[lactide]. This is evidence that use of the single initiation rate constant k_i suffices.

Parameter (i.e. rate constant) estimations were performed in Copasi using the Levenberg-Marquardt algorithm. The rate constants of initiation (k_i), propagation (k_p), depropagation (k_d), termination (k_t), and ring-opening of the terminated polymer by IMes to reform propagating species (k_{-t}) were optimized to obtain the best fit between the observed timecourses for monomer

consumption and evolution of the molecular weight distributions (Scheme 6.6). A reversible termination step was added due to observations that the PDI increases once monomer conversion surpasses 90%.[5] Modeled data was limited to the first 70% conversion of lactide to PLA in order to avoid modeling redistribution equilibria at the end of the reaction.

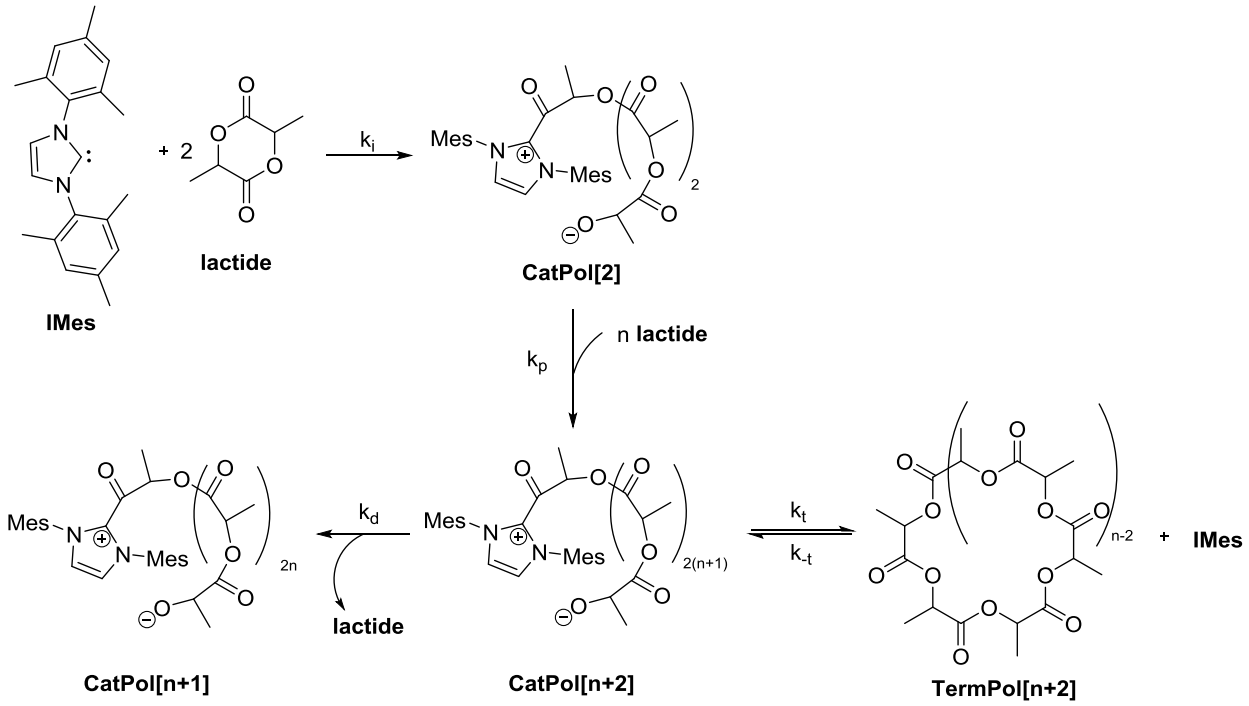

Scheme 6.6. The kinetic model used in the simulation of lactide as catalyzed by IMes.

An important consideration in kinetic modeling concerns weighting of the input data especially when the data are heterogeneous, such as monomer concentrations and molecular weight distributions. When fitting data, the sum of squared deviations (SSD) between the model and the data is minimized. Therefore, data with higher absolute values will tend to be larger contributors to the SSD. Inherently the optimization process is biased to best fit the data that contributes most to the goodness-of-fit metric, at the expense of data that contribute less. The input files include two types of data, monomer concentration (M) with time and the RI signals as

a function of retention volume for different reaction times, with absolute values that differ by a factor of 10. To effectively fit both types of data, a weighting scheme must be assumed. However, a suitable weighting scheme is not always obvious. The approach that is typically used is to weight the contributions of various datasets according to the inverse of the variance ($1/\sigma^2$) of each data set. This weighting scheme assumes that the inverse of the variance measures the certainty in the data.

Weighting Model 1: Monomer consumption and MWD data weighted as $1/\sigma^2$

With the data weighted as $1/\sigma^2$, the model converged to the following rate constant values: k_i = 1.05 ± 0.08 $M^{-2}s^{-1}$, k_p = 47.2 ± 0.9 $M^{-1}s^{-1}$, k_t = 0.012 ± 0.001 s^{-1}, k_{-t} = 0 ± 6.64E-06 $M^{-1}s^{-1}$, k_d = 0 ± 3.13E-05 s^{-1}, sf = 0.00165 ± 0.0001. The unweighted SSD of the fit is 12.37. The fit of monomer consumption to the monomer consumption data is displayed in Figure 6.6.

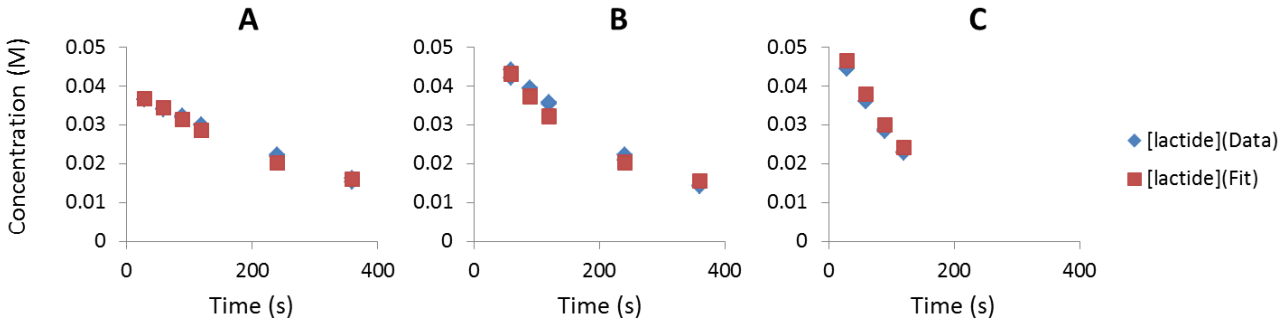

Figure 6.6. Monomer consumption with time as predicted by Weighting Model 1 as compared to experimental data. Condition **A**: [*rac*-lactide]$_0$ = 37.9 mM, [IMes]$_0$ = 1.0 mM; Condition **B**: [*rac*-lactide]$_0$ = 51.2 mM, [IMes]$_0$ = 1.0 mM; Condition **C**: [*rac*-lactide]$_0$ = 51.2 mM, [IMes]$_0$ = 1.83 mM. Two runs are displayed for each experimental time point.

Although the monomer consumption timecourses are fit well, the molecular weight distributions are not. The fit of the MWD for each of the 3 experimental conditions (**A**, **B**, **C**) is displayed in Figure 6.7. The experimental data (two independent runs) is plotted as solid lines, and the computed fit from the model is displayed as dotted lines.

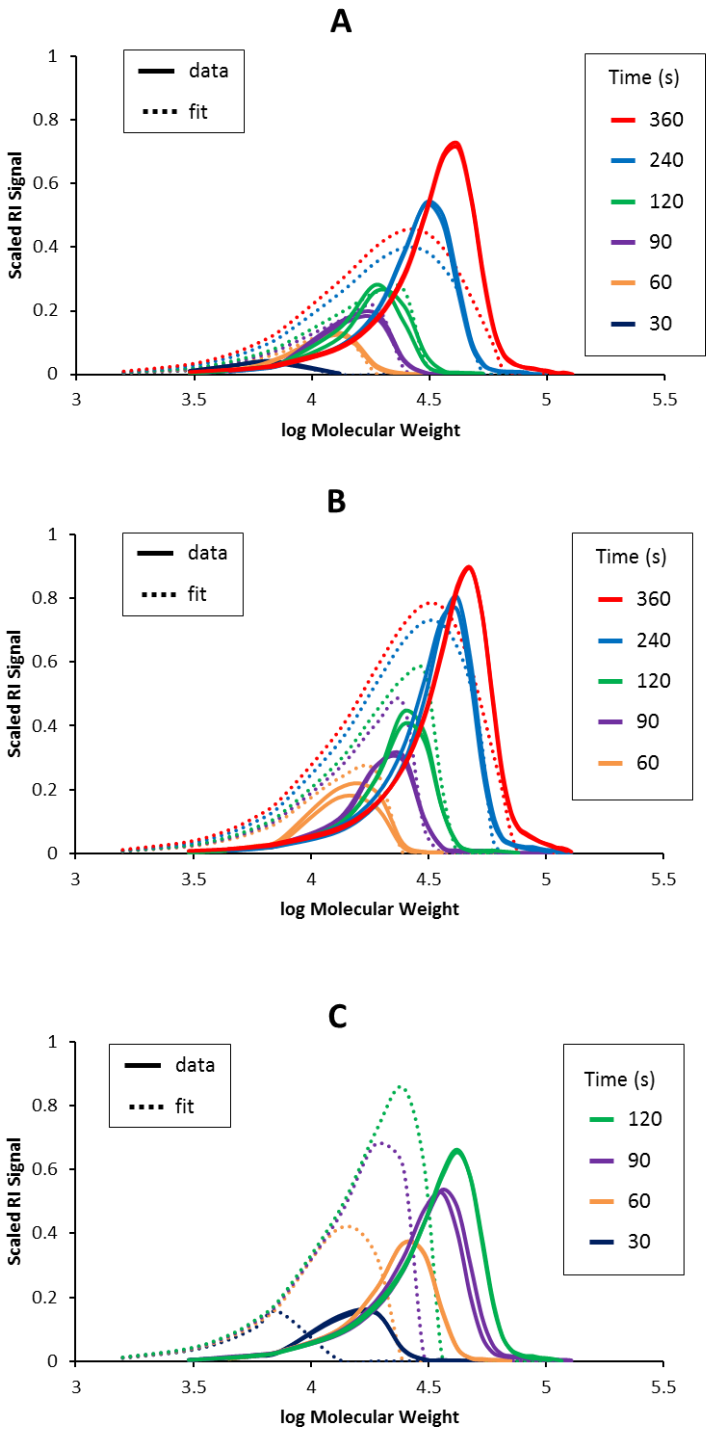

Figure 6.7. Display of the data (solid) and Weighting Model 1 (dotted) MWD for each experimental condition. Condition **A**: [*rac*-lactide]$_0$ = 37.9 mM, [IMes]$_0$ = 1.0 mM; Condition **B**: [*rac*-lactide]$_0$ = 51.2 mM, [IMes]$_0$ = 1.0 mM; Condition **C**: [*rac*-lactide]$_0$ = 51.2 mM, [IMes]$_0$ = 1.83 mM. Two runs are displayed for each experimental time point.

The concentration of active catalyst (equal to the sum of all CatPol[n+2] concentrations) with time was calculated for each of the three experimental conditions **A**, **B**, and **C** using the rate constants obtained from Model 1 (Figure 6.8). As predicted for an initiation step that is second order in lactide concentration, the experimental conditions with higher lactide concentration (**B**, **C**) show higher maximum concentrations of active catalyst vs. time than the condition with lowest lactide concentration (**A**).

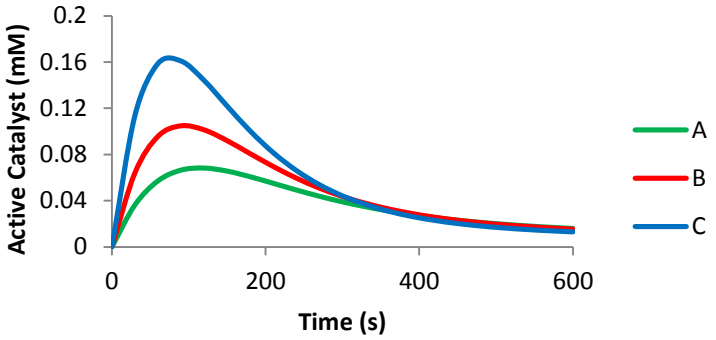

Figure 6.8. Active catalyst with time predicted for each experimental condition with Weighting Model 1. Condition **A**: [*rac*-lactide]$_0$ = 37.9 mM, [IMes]$_0$ = 1.0 mM; Condition **B**: [*rac*-lactide]$_0$ = 51.2 mM, [IMes]$_0$ = 1.0 mM; Condition **C**: [*rac*-lactide]$_0$ = 51.2 mM, [IMes]$_0$ = 1.83 mM.

The biggest failures of the kinetic model at this stage are its inability to accurately model the polymer molecular weight distributions at all reaction times and accurately predicting MWDs with higher catalyst loadings (condition **C**). At shorter reaction times for condition **A** (120 s and below), the experimental and modeled MWDs appear similar but the fits deteriorate at longer reaction times. A second set of data weighting factors (Weighting Model 2) was attempted in order to improve the fits of the MWD at longer reaction times.

*Weighting Model 2: Increased weighting of MWDs for longer reaction times under condition **A** and decreased weighting of monomer consumption*

Weighting Model 1 gave good fits for monomer consumption and the early time point MWD for condition **A**, so condition **A** was used to optimize the fitted rate constants used in Weighting Model 2. In order to force the model to overcome an apparent local minimum that yields a poor fit to MWDs at longer reaction times, the weighting was skewed to emphasize the last two time points. To accomplish this emphasis, the weighting of the MWDs for the first three time points was set to $1/(80\sigma^2)$. The fourth time point MWD (120 s) was weighted as $1/(40\sigma^2)$. Also, the monomer consumption data was weighted as $1/(6\sigma^2)$.

Once the rate constants were optimized by fitting exclusively condition **A**, those rate constants were applied to all three reaction conditions, resulting in an unweighted SSD of 8.76, indicating that Weighting Model 2 is a better fit for the system than Model 1. The rate constants obtained were: $k_i = 0.68 \pm 0.04\ M^{-2}s^{-1}$, $k_p = 66.6 \pm 2.1\ M^{-1}s^{-1}$, $k_t = 0.0039 \pm 0.0005\ s^{-1}$, $k_{-t} = 1.01 \pm 1.63\ M^{-1}s^{-1}$, $k_d = 0.75 \pm 0.10\ s^{-1}$, sf = 0.0014 ± 0.0001. The fit of Weighting Model 2 to the experimental monomer consumption data is displayed in Figure 6.9.

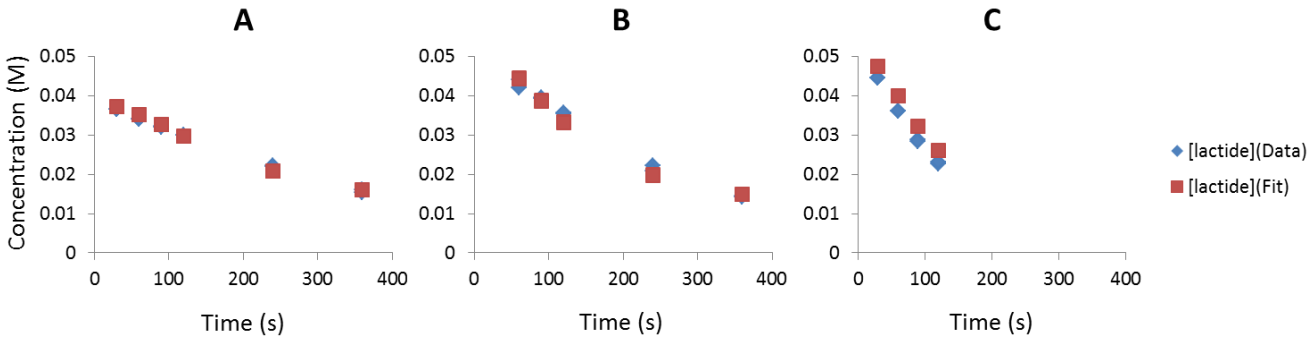

Figure 6.9. Monomer consumption as predicted by Weighting Model 2 compared to experimental data. Condition **A**: [*rac*-lactide]$_0$ = 37.9 mM, [IMes]$_0$ = 1.0 mM; Condition **B**: [*rac*-lactide]$_0$ = 51.2 mM, [IMes]$_0$ = 1.0 mM; Condition **C**: [*rac*-lactide]$_0$ = 51.2 mM, [IMes]$_0$ = 1.83 mM. Two runs are displayed for each experimental time point.

The fit (dotted) of each experimental MWD (solid) for each of the experimental conditions is displayed in Figure 6.10.

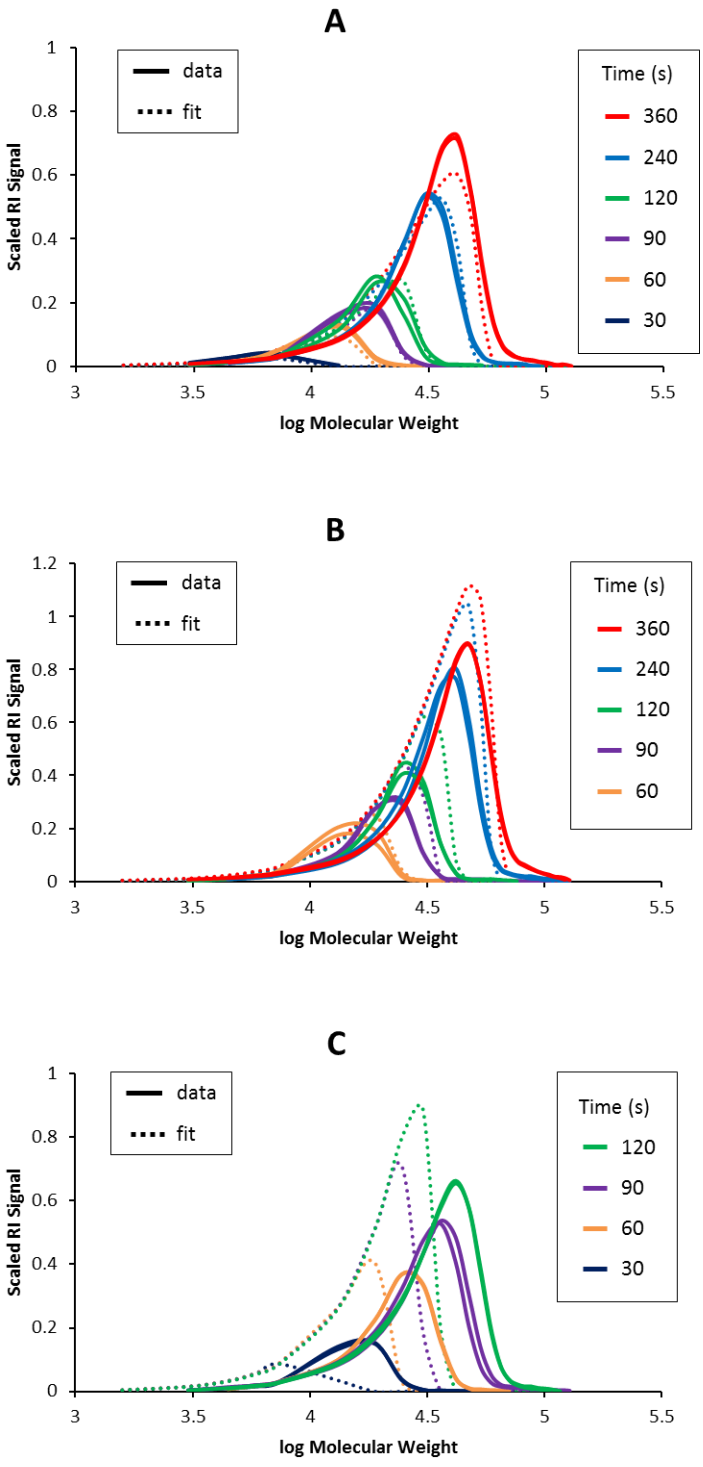

Figure 6.10. Display of the data (solid) and Weighting Model 2 (dotted) MWD for each experimental condition. Condition **A**: [*rac*-lactide]$_0$ = 37.9 mM, [IMes]$_0$ = 1.0 mM; Condition **B**: [*rac*-lactide]$_0$ = 51.2 mM, [IMes]$_0$ = 1.0 mM; Condition **C**: [*rac*-lactide]$_0$ = 51.2 mM, [IMes]$_0$ = 1.83 mM. Two runs are displayed for each experimental time point.

The concentration of active catalyst with respect to time was computed using the rate constants obtained from Weighting Model 2 (Figure 6.11). Again, the conditions with a higher lactide concentration (**B**, **C**) have more active catalyst than condition **A**.

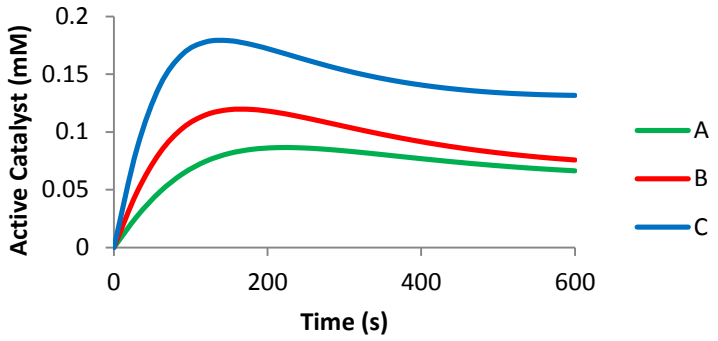

Figure 6.11. The active catalyst concentration with time for the rate constants obtained with Weighting Model 2. Condition **A**: [*rac*-lactide]$_0$ = 37.9 mM, [IMes]$_0$ = 1.0 mM; Condition **B**: [*rac*-lactide]$_0$ = 51.2 mM, [IMes]$_0$ = 1.0 mM; Condition **C**: [*rac*-lactide]$_0$ = 51.2 mM, [IMes]$_0$ = 1.83 mM.

Weighting Model 2 displays improved MWD fits than Weighting Model 1, particularly for the two reaction conditions with lower catalyst concentration (**A**, **B**). In addition, the unweighted SSD for Weighting Model 2 is less than Weighting Model 1, indicating a better fit to the data. However, Weighting Model 2 is unable to accurately predict the MWD data for the condition with a higher catalyst loading, **C**, and predicts lower MW polymers than what is observed experimentally, although there is noticeable improvement over the fits for condition **C** with Weighting Model 1. Although our data indicate that the MWD is largely independent of the catalyst concentration, Weighting Models 1 and 2 do not exhibit that behavior.

Weighting Model 3: Monomer consumption and MWD data weighted equally

In order to increase the overall quality of the fit to experimental data (i.e., decrease the unweighted SSD) and to demonstrate the fit in the absence of any data weighting, Weighting

Model 3 was created. When all 3 experimental conditions are fit to Weighting Model 3, the unweighted SSD is 1.26, indicating a better fit than Weighting Models 1 and 2. The observation that a lower *unweighted* SSD is obtained using an unweighted fit suggests that the parameter fitting surface is complex and the fitting procedure is prone to stopping at local minima. Apparently the data weighting scheme of Weighting Model 3 enables the procedure to surpass these local minima. The rate constants obtained were: k_i = 0.77 ± 0.02 $M^{-2}s^{-1}$, k_p = 382.6 ± 40.5 $M^{-1}s^{-1}$, k_t = 1.22 ± 0.19 s^{-1}, k_{-t} = 161.5 ± 8.8 $M^{-1}s^{-1}$, k_d = 0 ± 1.24E-06 s^{-1}, sf = 0.00079 ± 0.00001. Although Weighting Models 1 and 2 displayed good fits of monomer consumption to the data, Weighting Model 3 does a poorer job of predicting monomer consumption (Figure 6.12). Note that due to long computational times, Weighting Model 3 was converged to a tolerance of 10^{-3}, while Weighting Models 1 and 2 converged to a tolerance of 10^{-5}. Therefore, the calculated errors are likely underestimated for Weighting Model 3 as compared to Weighting Models 1 and 2.

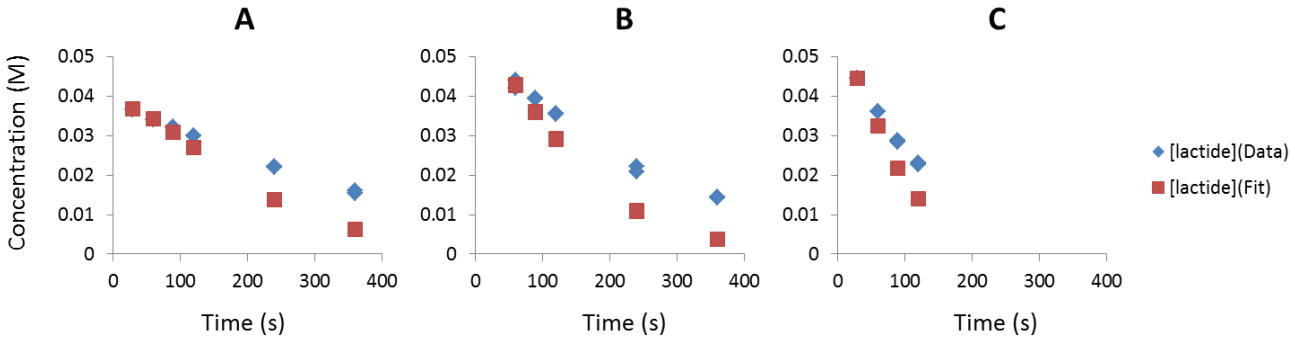

Figure 6.12. Monomer consumption as predicted by Weighting Model 3 compared to experimental data. Condition **A**: [*rac*-lactide]$_0$ = 37.9 mM, [IMes]$_0$ = 1.0 mM; Condition **B**: [*rac*-lactide]$_0$ = 51.2 mM, [IMes]$_0$ = 1.0 mM; Condition **C**: [*rac*-lactide]$_0$ = 51.2 mM, [IMes]$_0$ = 1.83 mM. Two runs are displayed for each experimental time point.

The fit of Weighting Model 3 (dotted) to the experimental data (solid) MWDs is displayed in Figure 6.13.

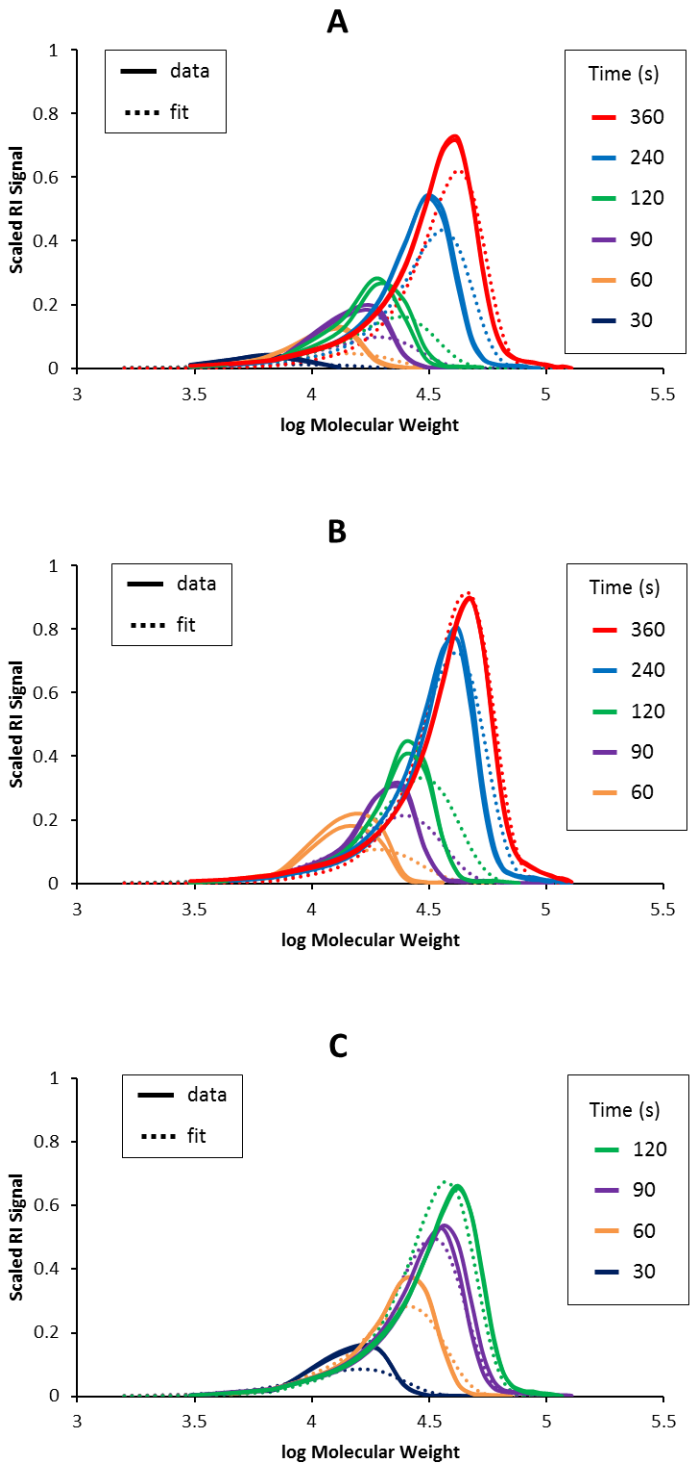

Figure 6.13. The data (solid) and predicted with Weighting Model 3 (dotted) MWD for each experimental condition. Condition **A**: [*rac*-lactide]$_0$ = 37.9 mM, [IMes]$_0$ = 1.0 mM; Condition **B**: [*rac*-lactide]$_0$ = 51.2 mM, [IMes]$_0$ = 1.0 mM; Condition **C**: [*rac*-lactide]$_0$ = 51.2 mM, [IMes]$_0$ = 1.83 mM. Two runs are displayed for each experimental time point.

The MWD fit is noticeably improved over the fits from Weighting Models 1 and 2, particularly for the higher catalyst concentration reaction condition **C**. The concentration of active catalyst with respect to time for each experimental condition calculated with Weighting Model 3 is displayed in Figure 6.14. The shape of the graph of active catalyst with time is noticeably different for Weighting Model 3 than Weighting Models 1 and 2. Weighting Model 3 predicts that the active catalyst will reach a maximum concentration that does not decline with time, as would be predicted if termination events were significant. In other words, Weighting Model 3 is a quasi-living polymerization model with slow initiation.

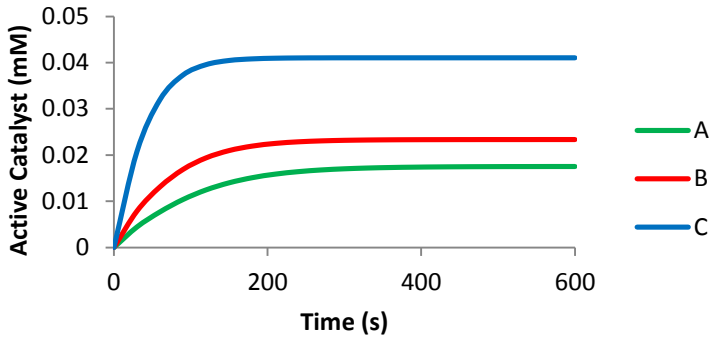

Figure 6.14. The active catalyst with time for the rate constants obtained with Weighting Model 3. Condition **A**: [*rac*-lactide]$_0$ = 37.9 mM, [IMes]$_0$ = 1.0 mM; Condition **B**: [*rac*-lactide]$_0$ = 51.2 mM, [IMes]$_0$ = 1.0 mM; Condition **C**: [*rac*-lactide]$_0$ = 51.2 mM, [IMes]$_0$ = 1.83 mM.

Summary of Weighting Models 1, 2, and 3

Table 6.2 displays the rate constants and their estimated standard deviations resulting from fits according to Weighting Models 1, 2, and 3. The correlation matrixes, which display the correlation of each computed rate constant, are given in Appendix E.

Table 6.2. The rate constants obtained for Weighting Models 1, 2, and 3 with computed standard deviations

Weighting Model	**Unweighted SSD**	**k_i ($M^{-2}s^{-1}$)**	**k_p ($M^{-1}s^{-1}$)**	**k_t (s^{-1})**	**k_{-t} ($M^{-1}s^{-1}$)**	**k_d (s^{-1})**	**sf**
1	12.37	1.05 ± 0.08	47.2 ± 0.9	0.012 ± 0.001	0 ± $7\cdot10^{-6}$	0 ± $3\cdot10^{-5}$	0.00165 ± 0.0001
2	8.76	0.68 ± 0.04	66.6 ± 2.1	0.0039 ± 0.0005	1.01 ± 1.63	0.75 ± 0.10	0.0014 ± 0.0001
3	1.26	0.77 ± 0.02	382.6 ± 40.5	1.22 ± 0.19	161.5 ± 8.8	0 ± $1\cdot10^{-6}$	0.00079 ± 0.00001

Waymouth Model for Lactide Polymerization by IMes in THF

The rate constants reported by Waymouth, *et al.*[6] for lactide polymerization with IMes in THF were used to simulate monomer consumption and MWD for experimental conditions **A**, **B**, and **C**. One should not expect the Waymouth model to simulate the results reported herein because Waymouth *et al.* obtained rate constants in THF solvent and our results used toluene as the solvent. The rate constants reported by Waymouth *et al.* are: $k_i = 0.274\ M^{-2}s^{-1}$, $k_p = 48.7\ M^{-1}s^{-1}$, $k_d = 0.208\ s^{-1}$, and $k_t = 0.0575\ s^{-1}$. Termination is irreversible in this model. The scaling factor, sf, was set to be 0.0014, the value determined in Weighting Model 2. The simulated monomer consumption for our experimental conditions is displayed in Figure 6.15. The Waymouth studies utilize an initial monomer concentration an order of magnitude larger than in our experimental conditions due to the increased solubility of lactide in THF as compared to toluene. Application of the Waymouth model to our experimental conditions yields very low conversions.

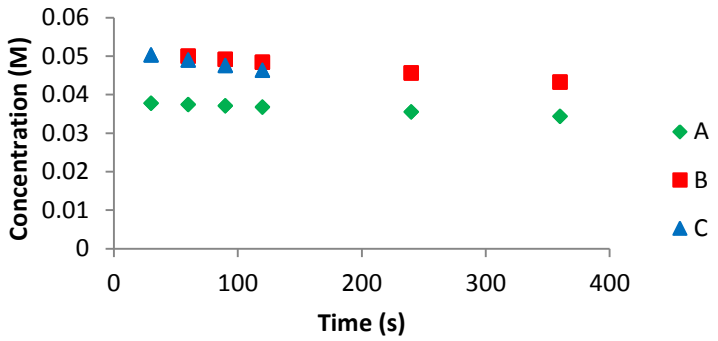

Figure 6.15. Monomer consumption as predicted by the Waymouth Model. Condition **A**: [*rac*-lactide]$_0$ = 37.9 mM, [IMes]$_0$ = 1.0 mM; Condition **B**: [*rac*-lactide]$_0$ = 51.2 mM, [IMes]$_0$ = 1.0 mM; Condition **C**: [*rac*-lactide]$_0$ = 51.2 mM, [IMes]$_0$ = 1.83 mM.

The MWDs as predicted by the Waymouth model are displayed in Figure 6.16.

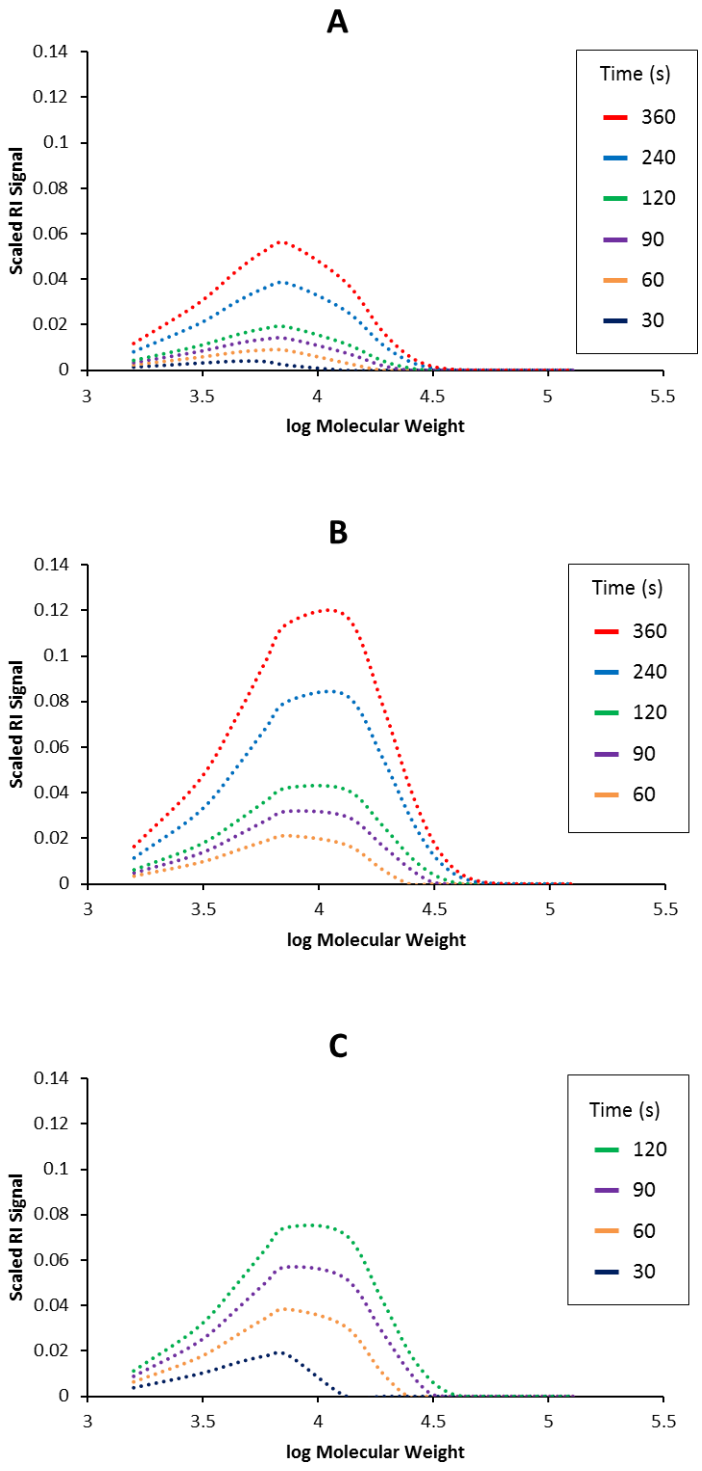

Figure 6.16. Simulated MWD for each experimental condition using the Waymouth Model. Condition **A**: [*rac*-lactide]$_0$ = 37.9 mM, [IMes]$_0$ = 1.0 mM; Condition **B**: [*rac*-lactide]$_0$ = 51.2 mM, [IMes]$_0$ = 1.0 mM; Condition **C**: [*rac*-lactide]$_0$ = 51.2 mM, [IMes]$_0$ = 1.83 mM.

The *centers* of the MWDs obtained with the Waymouth Model do not show increasing molecular weight with conversion. However the leading edge at the high MW end of the distribution does increase with monomer conversion. Such behavior is not unexpected for a slow initiating process during a time frame in which less than 15% of monomer conversion occurs. Chains that initiate early in the reaction continue to grow with time, forming the high MW leading edge. However, because the monomer concentration remains nearly constant in the first 15% of conversion, new chains continue to initiate at a constant rate. This causes the center of the mass distribution to remain nearly constant.

Three data points reported by Waymouth, *et al.* were used to simulate the monomer consumption and MWD at the concentrations used in their studies with the rate constants that they report. The reaction with 0.6 M initial lactide concentration and 0.006 M IMes concentration was simulated at 8, 16, and 24 s. The simulated monomer percent conversion is compared to the experimental percent conversion reported by Waymouth, *et al.* in Figure 6.17.

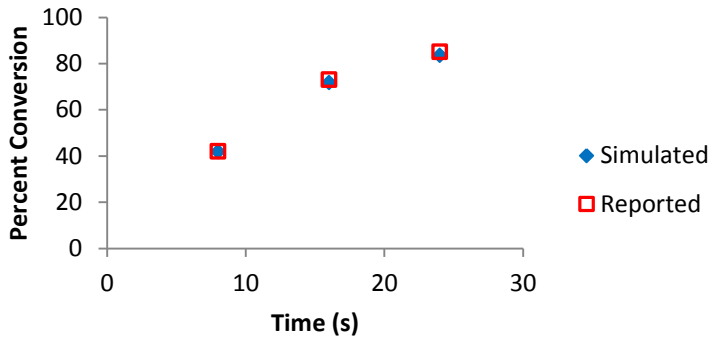

Figure 6.17. Simulated monomer percent conversion using the Waymouth rate constants with the reported percent conversions by Waymouth, *et al.*

The MWDs for these three time points is displayed in Figure 6.18.

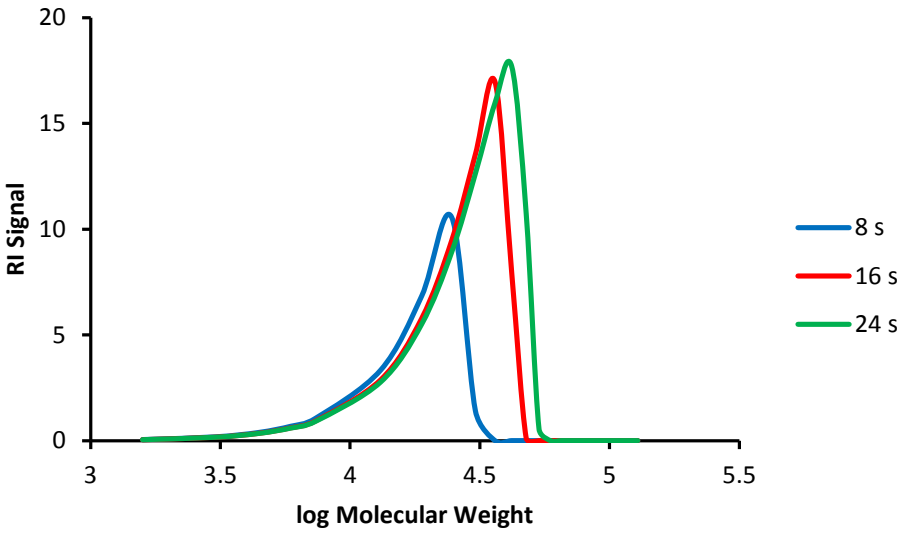

Figure 6.18. MWDs for the simulated Waymouth data utilizing the rate constants reported by Waymouth, *et al.*

The higher initial concentrations used by Waymouth, *et al.* in their studies lead to much higher conversions than the concentrations used in our studies. Simulated MWDs at higher conversions display evolution of MW with percent conversion as expected for the polymerization. However, the shapes of the MWD curves simulated using Waymouth's rate constants have a sharp high MW leading edge that is not replicated in experimental data. The shapes of the MWD curves simulated using Weighting Models 1-3 have leading edges that are much more consistent with the experimental data.

6.4. Conclusion

Stopped-flow NMR spectroscopy, which resolves the reaction progression in the first few seconds of reaction, enables the first direct, *in situ* observation of monomer epimerization during lactide polymerization. The monomer epimerization is successfully fit to a simple kinetic model that features a natural rate constant for the approach to equilibrium of 1 s^{-1} or a half-life of less

than 1 second at room temperature. ^{13}C NMR spectroscopy allows elucidation of polymer hexad tacticity and supports a chain-end stereocontrol mechanism. Polylactide MWDs and monomer consumption from quenched polymerization studies are fit to a kinetic model using three different weighting treatments. Good fits of either monomer consumption *or* MWD are obtained, but we are unable to successfully fit both types of data with a single weighting factor. Simulations of MWDs utilizing rate constants reported by Waymouth, *et al.* under the conditions used for this study do not predict the observed evolution of molecular weight with percent conversion. This is a result of the different solvents used in the Waymouth study and this work. Simulations of MWDs at higher conversions using rate constants reported by Waymouth, *et al.* display a sharp leading edge at high MW that is not replicated in the experimental data. However, Weighting Models 1-3 reported herein successfully predict the observed molecular weight evolution with conversion and simulate the leading edge of the MWD well. The modeling method reported herein displays the wealth of kinetic information that can be gained using data that is easily obtainable by GPC.

Future studies should focus on gaining a better understanding of the amount of active catalyst. The difference between the models that fit monomer consumption well (Weighting Models 1 and 2) and the model that fits MWD well (Weighting Model 3) is an order of magnitude difference in the predicted active IMes concentration. If the active IMes concentration could be experimentally determined with time, the model could be significantly improved. Appendix A describes my initial studies using a quench label to obtain accurate active site counts during lactide polymerization.

Additionally, the kinetic model simulated herein could be too simple to adequately fit all of the data. Likely, the depropagation step warrants further analysis. The kinetic model reported

used for all simulations in this manuscript does not allow for backbiting of the propagating chain beyond loss of two lactic acid units (one lactide). However, MALDI data displays both even and odd corporations of lactic acid units in the polymer, so backbiting must occur such that odd numbers of lactic acid units are removed from the propagating chain.[5] An approach would be to study the ratio of odd and even lactic acid incorporation with respect to reaction time.

6.5. Experimental

General Experimental Methods

Routine NMR spectra were performed on Bruker Avance 400 or 500 MHz spectrometers fitted with a SmartProbe and DCH cryoprobe, respectively. Stopped-Flow NMR spectroscopy was performed on Varian Inova 500 or 600 MHz spectrometers with a modified flowprobe.[24] Toluene, THF, and hexanes were each distilled under N_2 from sodium benzophenone and stored over molecular sieves. Toluene-d_8 and CS_2 were used as received from Sigma-Aldrich. IMes was synthesized according to literature procedure, except the deprotonation was performed by stirring with NaH overnight, and IMes was recrystallized with THF/hexanes.[36] *Rac*- and *L*-lactide were purchased from Sigma-Aldrich, dried over CaH_2 and sublimed twice to remove impurities. *Meso*-enriched lactide (89% *meso*-, 11% *rac*-lactide) was purchased from Natureworks LLC and dried over activated alumina. $Al(^{i}Bu)_2$(BHT) (BHT = 2,6 di-tert-butyl-4-methylphenol) was synthesized according to the literature procedure.[37] 1,4-bis(trimethylsilyl)benzene (BTMSB) was sublimed and stored in a N_2 glovebox. GPC analysis was performed with a Viscotek GPCmax/VE 2001 instrument fitted with PolyPore columns (2x, 300 x 7.5 mm, 5 μm particle size) from Polymer Laboratories that was calibrated with standard polystyrene samples. Samples eluted with THF at a flow rate of 1 mL/min at 40 °C and were

detected with a Viscotek Model 302-050 Tetra Detector Array. Omnisec software (Viscotek, Inc.) was utilized for data processing.

General Stopped-Flow Procedure

The stopped-flow procedure was previously described, and the procedure was followed as described except where noted.[24] Three syringes were prepared in an N_2 atmosphere glovebox: (a) *L*-lactide (48.6 mg, 0.34 mmol) and BTMSB (16.5 mg, 0.074 mmol) in 5 mL toluene, (b) IMes (22.3 mg, 0.073 mmol) in 5 mL toluene, (c) $Al(^{i}Bu)_2(BHT)$ (101.1 mg, 0.28 mmol) in 5 mL toluene. The syringes were sealed in plastic bags in the glovebox and transferred to a N_2-purged glovebag. The drive system and NMR probe were filled with toluene and each reagent line was injected with 2.5 mL of syringe (c) and allowed to stand for 30 minutes to remove trace water. 10 mL toluene was pushed through the system to remove $Al(^{i}Bu)_2(BHT)$ from the reactant lines. Syringes (a) and (b) were then simultaneously injected into the separate reagent lines. Each SF run used a push volume of 0.2 mL of each solution (0.4 mL total push volume).

General Polymerization Quench Procedure:

Under a purged N_2 glovebox atmosphere, stock solutions of rac-lactide (56.3 mM) and IMes (20.1 mM) were prepared in toluene. A half dram vial equipped with stir bar was charged with 1 mL lactide solution (8.11 mg, 0.056 mmol). Reaction was initiated by adding 0.1 mL IMes solution (0.61 mg, 2.0 μmol). At the indicated reaction time, 0.2 mL neat CS_2 (3.3 mmol) was added to quench, causing the solution to immediately turn red. The solvent was evaporated prior to NMR or GPC analysis.

6.6. References

(1) Drumright, R. E.; Gruber, P. R.; Henton, D. E. *Adv. Mater.* **2000**, *12*, 1841–1846.

(2) Garlotta, D. *J. Polym. Environ.* **2002**, *9*, 63–84.

(3) Suzuki, S. Ikada, Y. In *Poly(lactic acid): Synthesis, Structures, Properties, Processing, and Applications*; Auras, R. A., Ed.; John Wiley & Sons: New Jersey, 2010; pp 443–456.

(4) O'Keefe, B. J.; Hillmyer, M. A.; Tolman, W. B. *J. Chem. Soc. Dalt. Trans.* **2001**, No. 15, 2215–2224.

(5) Culkin, D. A.; Jeong, W.; Csihony, S.; Gomez, E. D.; Balsara, N. P.; Hedrick, J. L.; Waymouth, R. M. *Angew. Chemie - Int. Ed.* **2007**, *46* (15), 2627–2630.

(6) Jeong, W.; Shin, E. J.; Culkin, D. A.; Hedrick, J. L.; Waymouth, R. M. *J. Am. Chem. Soc.* **2009**, *131* (13), 4884–4891.

(7) McGarrity, J. F.; Prodolliet, J. *J. Org. Chem.* **1984**, No. 3, 4465–4470.

(8) Denmark, S. E.; Williams, B. J.; Eklov, B. M.; Pham, S. M.; Beutner, G. L. *J. Org. Chem.* **2010**, *75* (16), 5558–5572.

(9) Mok, K. H.; Nagashima, T.; Day, I. J.; Jones, J. A.; Jones, C. J. V.; Dobson, C. M.; Hore, P. J. *J. Am. Chem. Soc.* **2003**, *125* (41), 12484–12492.

(10) Jones, A. C.; Sanders, A. W.; Bevan, M. J.; Reich, H. J. *J. Am. Chem. Soc.* **2007**, *129* (12), 3492–3493.

(11) McGarrity, J. F.; Prodolliet, J.; Smyth, T. *Org. Magn. Reson.* **1981**, *17* (1), 59–65.

(12) Mcgarrity, J. F.; Ogle, C. A.; Brich, Z.; Loosli, H.-R. *J. Am. Chem. Soc.* **1985**, *107* (9), 1810–1815.

(13) Bertz, S. H.; Cope, S.; Murphy, M.; Ogle, C. A.; Taylor, B. J. *J. Am. Chem. Soc.* **2007**, *129*, 7208–7209.

(14) Bertz, S. H.; Carlin, C. M.; Deadwyler, D. A.; Murphy, M. D.; Ogle, C. A.; Seagle, P. H. *J. Am. Chem. Soc.* **2002**, *124* (46), 13650–13651.

(15) Plessel, K. N.; Jones, A. C.; Wherritt, D. J.; Maksymowicz, R. M.; Poweleit, E.; Reich, H. J. *Org. Lett.* **2015**, *17*, 2310–2313.

(16) Kühne, R. O.; Schaffhauser, T.; Wokaun, A.; Ernst, R. R. *J. Magn. Reson.* **1979**, *35* (1), 39–67.

(17) McGee, W. A.; Parkhurst, L. J. *Anal. Biochem.* **1990**, *189* (2), 267–273.

(18) Yushmanov, P. V.; Furó, I. *J. Magn. Reson.* **2005**, *175* (1), 264–270.

(19) Green, D. B.; Lane, J.; Wing, R. M. *Appl. Spectrosc.* **1987**, *41* (5), 847–851.

(20) Frieden, C.; Hoeltzli, S. D.; Ropson, I. J. *Protein Sci.* **1993**, *2* (12), 2007–2014.

(21) Sudmeier, J. L.; Pesek, J. J. *Inorg. Chem.* **1971**, *10* (4), 860–863.

(22) Fyfe, C. A.; Cocivera, M.; Damji, S. W. H. *Acc. Chem. Res.* **1978**, *11* (7), 277–282.

(23) Gomez-Hens, A.; Perez-Bendito, D. *Anal. Chim. Acta* **1991**, *242* (2), 147–177.

(24) Christianson, M. D.; Tan, E. H. P.; Landis, C. R. *J. Am. Chem. Soc.* **2010**, *132* (33), 11461–11463.

(25) Pratt, R. C.; Lohmeijer, B. G. G.; Long, D. A.; Lundberg, P. N. P.; Dove, A. P.; Li, H.; Wade, C. G.; Waymouth, R. M.; Hedrick, J. L. *Macromolecules* **2006**, *39* (23), 7863–7871.

(26) Bordwell, F. G. *Acc. Chem. Res* **1988**, *21* (10), 456–463.

(27) Hoops, S.; Sahle, S.; Gauges, R.; Lee, C.; Pahle, J.; Simus, N.; Singhal, M.; Xu, L.; Mendes, P.; Kummer, U. *Bioinforma.* **2006**, *22* (24), 3067–3074.

(28) Kasperczyk, J. *Macromolecules* **1996**, *28*, 3937–3939.

(29) Zhao, P.; Qin-Feng, W.; Zhong, Q.; Nai-Wen, Z.; Ren, J. *J. Appl. Polym. Sci.* **2010**, *115* (5), 2955–2961.

(30) Dove, A. P.; Li, H.; Pratt, R. C.; Lohmeijer, B. G. G.; Culkin, D. A.; Waymouth, R. M.; Hedrick, J. L. *Chem. Commun. (Camb).* **2006**, No. 27, 2881–2883.

(31) Buffet, J.-C.; Okuda, J. *Polym. Chem.* **2011**, *2* (12), 2758.

(32) Novstrup, K. A.; Travia, N. E.; Medvedev, G. A.; Stanciu, C.; Switzer, J. M.; Thomson, K. T.; Delgass, W. N.; Abu-Omar, M. M.; Caruthers, J. M. *J. Am. Chem. Soc.* **2010**, *132* (2), 558–566.

(33) Wen, J.; Arakawa, T.; Philo, J. S. *Anal. Biochem.* **1996**, *240* (2), 155–166.

(34) Van Deemter, J. J.; Zuiderweg, F. J.; Klinkenberg, A. *Chem. Eng. Sci.* **1956**, *5*, 271–289.

(35) *PL Caliber GPC Software Version 6.0 Manual*.

(36) Bantreil, X.; Nolan, S. P. *Nat. Protoc.* **2011**, *6* (1), 69–77.

(37) Shreve, A. P.; Mulhaupt, R.; Fultz, W.; Calabrese, J.; Robbins, W.; Ittel, S. D. *Organometallics* **1988**, *7*, 409–416.

Appendix A

Quench-labeling Studies of Lactide Polymerization

Introduction

The determination of accurate concentrations of active catalytic species by direct or indirect methods is essential for kinetic elucidation of any catalytic transformation.[1] Several methods have been reported for direct observation of polymerization intermediates by NMR including low temperature studies, stopped-flow, and hyperpolarized ^{13}C NMR.[2–4] Direct observation of intermediates provided valuable insight into the mechanisms studied; however, these techniques are limited by several requirements, including needing specialized equipment, high catalyst concentrations, and overall less authentic reaction conditions. The following studies expand upon a quench labeling approach with a chromophore developed in our group for active site counting in metal catalyzed olefin polymerization.[5,6] This chromophore quench labeling strategy will be applied to the NHC-catalyzed polymerization of lactide in order to elucidate active catalyst concentrations to better understand the kinetics of the reaction.

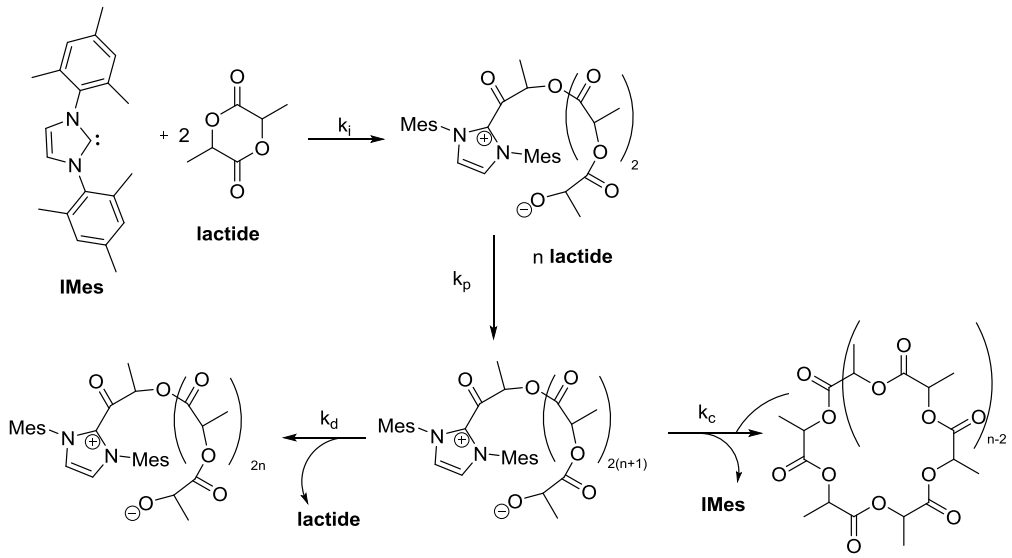

Scheme 1. A kinetic model proposed by Waymouth, *et al.* for the polymerization of lactide by 1,3-dimesitylimidazol-2-ylidene (IMes).[7]

The kinetics of lactide polymerization have proven to be complex (Scheme 1), and there have been no reports of experimental determination of the active site counts.[7,8] A pyrenyl

quench (λ_{max} = 344 nm, THF) will trap actively propagating polymeryl species, labeling them with the chromophore. This technique will be used in conjunction with UV-GPC in order to separate polymeryl species from low molecular weight species resulting from the use of excess quenching agent. Polymeryl species labeled with the chromophore are derived from actively propagating polymer chains and therefore active catalyst concentration can be quantitatively determined using this technique by careful integration of the resulting UV signal.

Results and Discussion

The proposed quenching mechanism is displayed in Scheme 2. Upon addition of the pyrenyl isocyanate to the reaction mixture, it is attacked by the propagating alkoxide species, adding a pyrenyl label to each actively propagating chain.

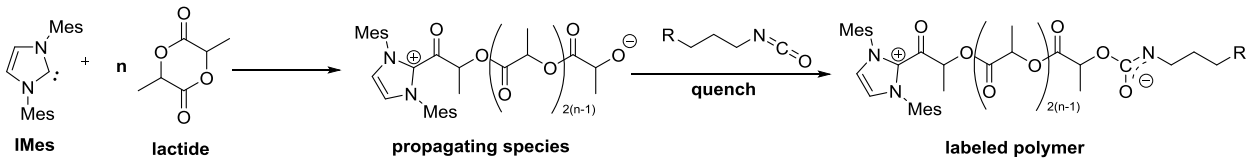

Scheme 2. Proposed quenching mechanism, where R = pyrene and Mes = mesityl

The concentration of propagating chains corresponds to the concentration of active IMes, meaning that the concentration of UV labeled polymeryl species is equal to the concentration of actively propagating IMes in the reaction. Additionally, any inactive (not propagating) IMes will react with the quench as indicated in Scheme 3 thus preventing new polymer chains from growing.

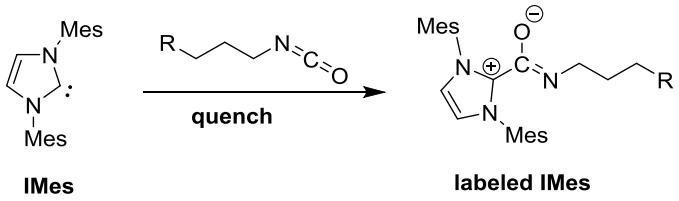

Scheme 3. Reaction of IMes with the pyrenyl isocyanate to form a labeled IMes species.

UV-GPC allows easy separation of the labeled polymer from any labeled small molecules, thus the integrated UV signal will correspond to only labeled polymer species. Unlabeled polymer species correspond to terminated species. Any pyrenyl-labeled polymeric species will show UV signals at the same retention volume as the polymer detected by RI, as displayed by Figure 1, where the RI (solid) and UV (dotted) signals are plotted with respect to retention volume.

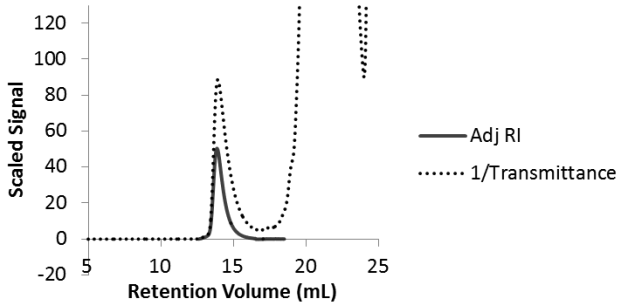

Figure 1. A quenched lactide polymerization displaying the RI and UV signals at the same retention volume. Retention volume was corrected for the distance between the RI and UV detectors. The instrument was calibrated to polystyrene standards. UV signal corresponding to low molecular weight species (after *ca.* 17 mL) are ignored. $[\text{lactide}]_0$ = 51.1 mM, $[\text{IMes}]_0$ = 1.0 mM, quenched with pyrenyl isocyanate at 4 minutes reaction time, 54% conversion.

The UV detector was calibrated to the concentration of pyrene (performed by Dr. Bernie Anding), so using the area of the UV-labeled polymer signal (dotted line, Figure 1) that corresponds to the polymer (in our case, typically between 12 and 16 mL retention volume) and

assuming one pyrene label per active catalyst and that each propagating chain is labeled, the percent active catalyst is calculated using the integration of the UV signal corresponding to polymer retention time. The shape of the UV signal is similar as that of the RI signal, indicating that we are not performing selective labeling for any specific molecular weight; we are achieving labeling over the entire range of the molecular weight distribution. Figure 2 displays the percent active catalyst with respect to percent conversion to polymer.

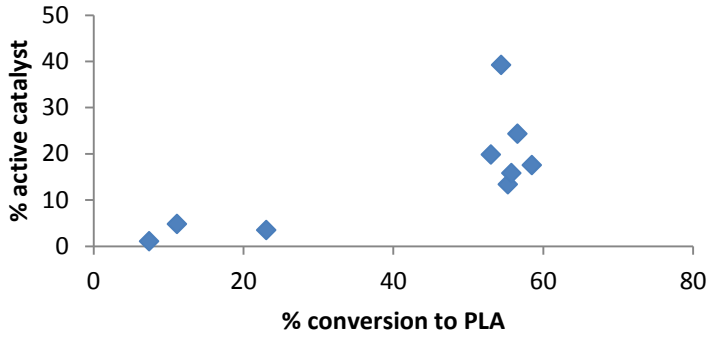

Figure 2. Percent active catalyst as a function of percent conversion to PLA. Note that the 40% active point may be an outlier and warrants repetition. For all reactions, $[\text{lactide}]_0$ = 51.1 mM, $[\text{IMes}]_0$ = 1.0 mM

The monomer consumption and active catalyst percentage did not significantly vary when the time between the primary (pyrenyl) and secondary (CS_2) quench was varied (Figure 3), particularly when considering that the 40% active catalyst data point is likely an outlier. This result indicates that the pyrenyl quench successfully stops polymerization.

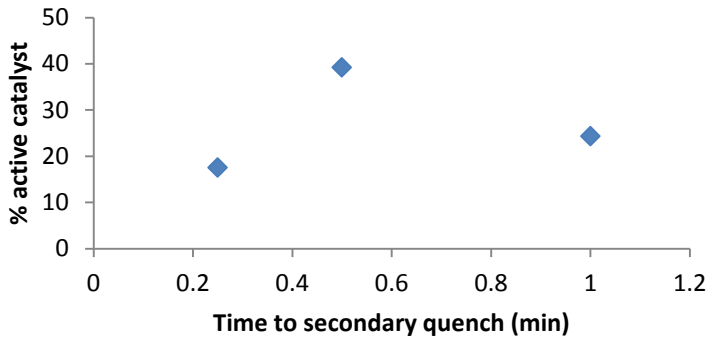

Figure 3. Percentage of active sites with a range of times between primary and secondary quench, showing no active site dependence with time of secondary quench. Each reaction was carried out to approximately 50% conversion. Note that the 40% active point may be an outlier and warrants repetition.

The percent active sites did not vary beyond reasonable experimental error when 4, 8, 16, or 24 equivalents (as compared to IMes) of pyrenyl isocyanate quench were used (Figure 4). If only a percentage of active sites were labeled by the pyrenyl isocyanate, the overall percent active sites should increase with increasing equivalents of quench. If impurities in the quench caused fewer active sites to be labeled, increasing equivalents of quench would result in decreasing percent active sites. Since the active site counts were independent of the amount of quench used, these results support that every actively propagating catalyst is labeled with the chromophore.

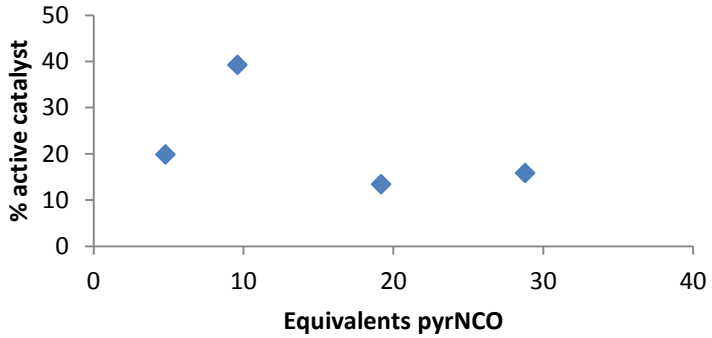

Figure 4. Display of independence of active site count to equivalents of pyrenyl isocyanate used to quench the reaction. Each reaction was carried out until approximately 50% conversion. Note that the 40% active point may be an outlier and warrants repetition.

A competition experiment was conducted between the pyrenyl isocyanate and IMes by mixing solutions of lactide and pyrenyl isocyanate, then adding IMes solution. No polylactide was observed by ^{1}H NMR, indicating that the pyrenyl isocyanate deactivates IMes (Scheme 3) at a faster rate than IMes polymerizes lactide.

IMes was reacted with the pyrenyl isocyanate (Scheme 3) and labeled IMes was observed quantitatively by ^{1}H NMR spectroscopy (Figure 5) and ESI-MS (Dr. Martha Vesting) at m/z 590.3. ^{13}C NMR spectra (Figure 6) displayed no carbene species (δ 218 ppm) in solution after addition of pyrenyl isocyanate. This result indicates that IMes deactivation occurs upon addition of pyrenyl isocyanate to the reaction mixture.

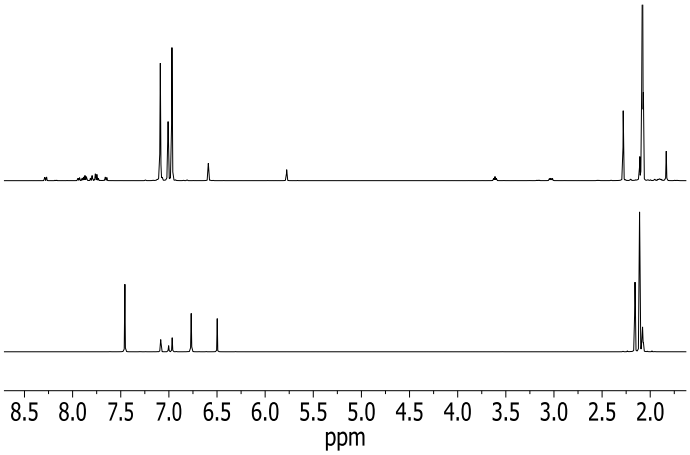

Figure 5. ^{1}H NMR spectra of IMes in toluene-d_8 (bottom) and IMes with pyrenyl isocyanate in toluene-d_8 (top) showing the difference in chemical shift between free IMes and labeled IMes.

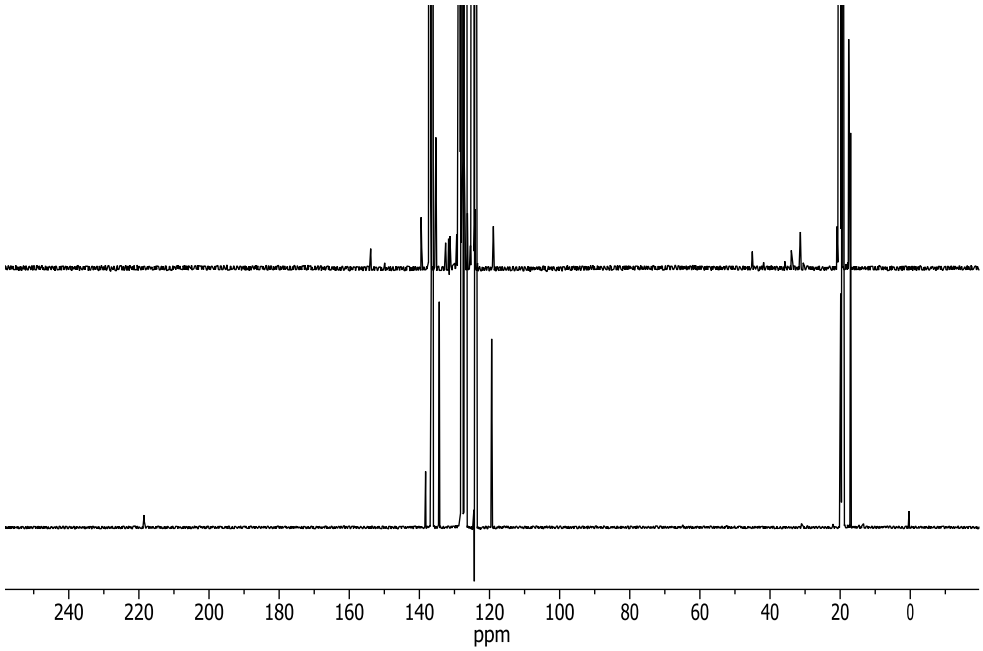

Figure 6. ^{13}C NMR spectra of IMes in toluene-d_8 (bottom) and IMes with pyrenyl isocyanate in toluene-d_8 (top) displaying the disappearance of the carbene peak at δ 218 ppm upon addition of pyrenyl isocyanate.

Conclusion

These initial studies indicate that a maximum of *ca.* 20% IMes is active during lactide polymerization, in contradiction with Waymouth's kinetic model, which predicted active site counts up to 65%.[7] However, the studies discussed herein assume quantitative labeling of each active species in solution. The modeling of lactide polymerization discussed in Chapter 6 suggests a maximum of *ca.* 10% active catalyst species during polymerization. If the quench labeling of IMes in the polymerization of lactide is a quanitative reaction, then adding the concentration of active catalyst with reaction time to the lactide polymerization model would likely result in better resolution of kinetic rates and the overall fit of the MWD, as discussed in Chapter 6.

One additional control still required for these studies is the observation of a quantitative reaction between an alkoxide (which will serve as a model for the propagating polymeryl) and

the isocyanate quench. If a quantitative reaction is observed it will further support quantitative labeling of active polymeryl species with the pyrenyl isocyanate quench.

Experimental

General Considerations

All reactions and polymerizations were carried out in an N_2 glovebox. ^{1}H and ^{13}C NMR spectra were recorded on 400 or 500 MHz Bruker NMR spectrometers. GPC was performed with a Viscotek GPCmax/VE 2001 instrument fitted with PolyPore columns (2x, 300 x 7.5 mm, 5 μm particle size) from Polymer Laboratories in THF at a flow rate of 1.0 mL/min at 40 °C. A Viscotek Model 302-050 Tetra Detector Array and Omnisec software (Viscotek, Inc.) was utilized for detection and data processing, respectively. Calibration was performed with polystyrene standards on a weekly basis. All solvents were degassed and dried over activated alumnia and molecular sieves. Lactide was purchased from Sigma, dried over CaH_2, and was purified by two air-free sublimations. IMes was synthesized via literature procedure,[9] with the exception that the deprotonation step was performed with NaH overnight, and was recrystallized from THF and hexanes. CS_2 was used as received. The pyrenyl isocyanate was synthesized by Dr. Luke Nelsen, Julie Sawicki, and Dr. Bernie Anding and the synthesis will be described in a future publication.

Representative Polymerization Procedure

In a purged N_2 glovebox atmosphere, stock solutions of *meso*-enriched lactide stock solution (89% *meso*-, 11% *rac*-lactide) (56.2 mM), IMes (10.9 mM) and pyrenyl isocyanate (49.0 mM) were prepared. An oven-dried half dram vial equipped with a stir bar was charged

with 1 mL lactide solution (56.2 mmol). Reaction was initiated by adding 100 μL IMes stock solution (1.1 μmol) via gastight syringe. At the desired quench time, 200 μL of a pyrenyl isocyanate stock solution (9.9 μmol) was added to the reaction vial. Neat CS_2 (100-200 μL, 1.66-3.32 mmol) was added as a secondary quench.

References

(1) Busico, V. *Dalton Trans.* **2009**, No. 41, 8794.

(2) Christianson, M. D.; Tan, E. H. P.; Landis, C. R. *J. Am. Chem. Soc.* **2010**, *132* (33), 11461.

(3) Landis, C. R.; Rosaaen, K. a.; Sillars, D. R. *J. Am. Chem. Soc.* **2003**, *125* (7), 1710.

(4) Chen, C.-H.; Shih, W.-C.; Hilty, C. *J. Am. Chem. Soc.* **2015**, *4*, 150522164041004.

(5) Moscato, B. M.; Zhu, B.; Landis, C. R. *Organometallics* **2012**, *31* (5), 2097.

(6) Moscato, B. M.; Zhu, B.; Landis, C. R. *J. Am. Chem. Soc.* **2010**, *132* (41), 14352.

(7) Jeong, W.; Shin, E. J.; Culkin, D. a.; Hedrick, J. L.; Waymouth, R. M. *J. Am. Chem. Soc.* **2009**, *131* (13), 4884.

(8) Culkin, D. a.; Jeong, W.; Csihony, S.; Gomez, E. D.; Balsara, N. P.; Hedrick, J. L.; Waymouth, R. M. *Angew. Chemie - Int. Ed.* **2007**, *46* (15), 2627.

(9) Bantreil, X.; Nolan, S. P. *Nat. Protoc.* **2011**, *6* (1), 69.

Appendix B

Fluorine-Tagged IMes to Observe Propagating Zwitterion

Introduction

As discussed in Chapter 2, proteins are often labeled with ^{19}F probes to simplify spectra in stopped-flow NMR studies.[1–3] Fluorine is used as a label in these systems because the ^{1}H NMR spectra are too complicated, with too many unassignable peaks. In addition to the only ^{19}F signals belonging to the labels, ^{19}F is a 100% NMR-active nucleus with a much larger possible dispersion of chemical shifts, decreasing probably of peak overlap as compared to ^{1}H NMR spectra.

In studies of IMes-catalyzed lactide polymerization (Figure 1), observation of catalyst speciation would give direct evidence of active site counts (how much catalyst participates in the reaction at any given time). When IMes attacks a lactide molecule and forms a zwitterion, the resulting positive charge on IMes should cause downfield shifts of the IMes protons. However, we were unable to differentiate between free IMes carbene peaks and zwitterionic IMes species by ^{1}H NMR spectroscopy. This is likely due to one or both of the following reasons: (i) the difference in chemical shift between the carbene and zwitterionic species is too small to give two separate peaks by ^{1}H NMR spectroscopy, or (ii) the amount of catalyst that is active (is initiated to form a zwitterion) is too low in concentration to detect by NMR spectroscopy.

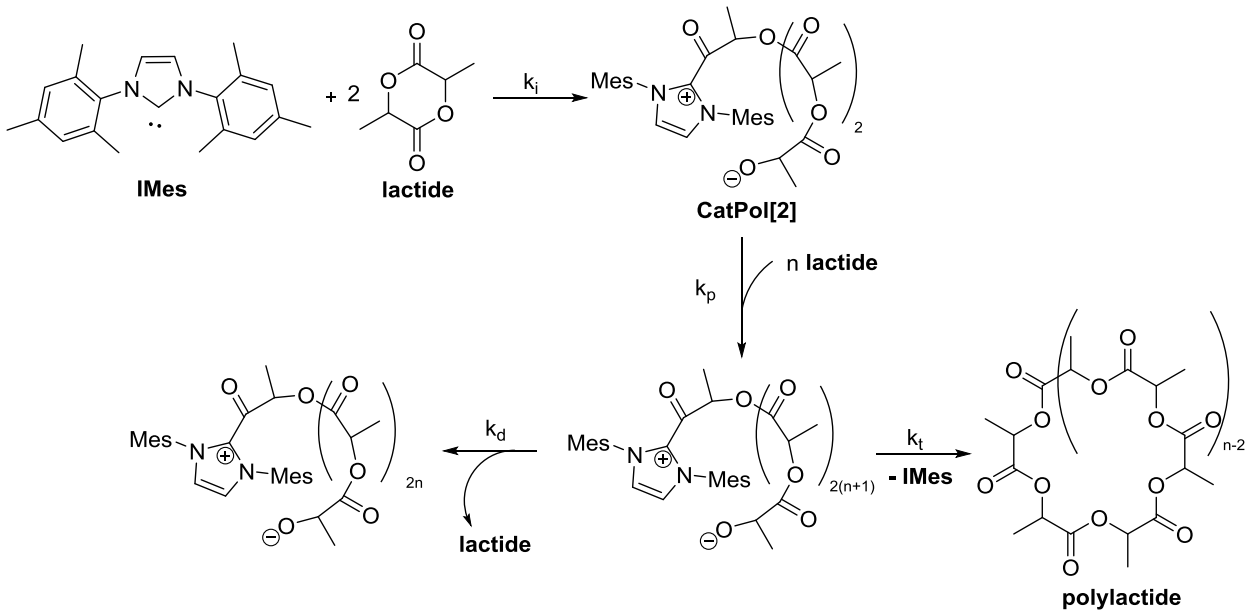

Figure 1. Kinetic model of the polymerization of lactide by IMes as proposed by Waymouth, *et al.*[4,5]

As predicted by Waymouth, *et al.*, up to 65% of the IMes could be active and in the zwitterionic form.[4] We hypothesized that a ^{19}F tag on IMes would allow differentiation of the free and zwitterionic species by ^{19}F NMR spectroscopy due to the larger dispersion of chemical shifts. Additionally, the only ^{19}F NMR peaks in the spectrum would be due to free and zwitterionic carbene, facilitating peak assignments and lowering the probability of peak overlap. Since protio solvents are needed for cost-efficient SF NMR measurements, ^{1}H NMR spectra have a decreased signal to noise ratio due to the large solvent peaks. Since the solvents used in these studies do not contain fluorine atoms, there should be an improved signal to noise ratio in ^{19}F NMR spectra compared to ^{1}H NMR spectra.

Results and Discussion

The fluorinated IMes that was synthesized, 1,3-bis(4-fluoro-2,6-dimethylphenyl)-2-ylidene, was chosen due to minimal expected steric and electronic effects on the catalysis. The synthetic scheme is displayed in Scheme 1.

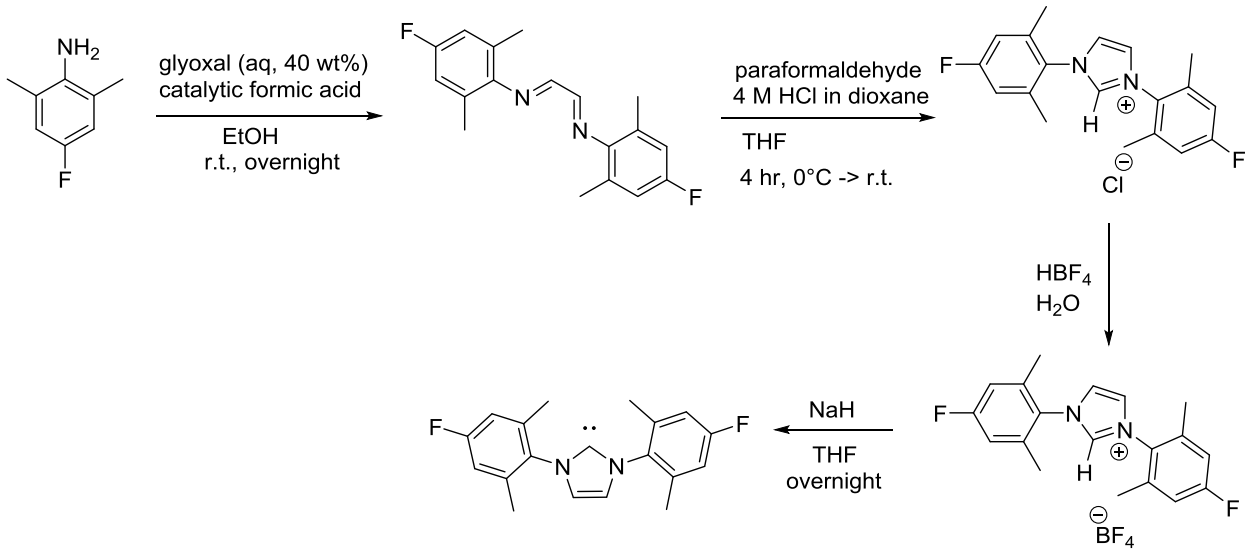

Scheme 1. Synthesis of 1,3-bis(4-fluoro-2,6-dimethylphenyl)-2-ylidene.

The HCl imidazolium salt has been synthesized previously,[6] but this is the first report of the synthesis of free fluorinated IMes. 2,6-dimethyl-4-fluoroaniline undergoes a condensation reaction with glyoxal and catalytic formic acid to yield *N,N'*-bis(2,6-dimethyl-4-fluorophenyl)ethylenediimine in a 64% yield which is cyclized with formaldehyde to yield *N, N'*-bis(2,6-dimethyl-4-fluorophenyl)imidazolium chloride in 47% yield. An anion exchange is performed with aqueous fluoroboric acid to produce *N, N'*-bis(2,6-dimethyl-4-fluorophenyl)imidazolium tetrafluoroborate in 96% yield. The carbene, 1,3-bis(4-fluoro-2,6-dimethylphenyl)-2-ylidene (***p*-F-IMes**), is produced by deprotonation by sodium hydride in 30% yield. Total isolated yield over four steps is 8.6%.

The polymerization of lactide with the fluorine-labeled IMes (***p*-F-IMes**) was observed by alternating ^{1}H and ^{19}F NMR spectra after injection of catalyst solution into monomer solution. The polymerization progress was observed by ^{1}H NMR spectroscopy (Figure 2). The fluorinated catalyst does polymerize lactide, albeit approximately 8 times much more slowly than IMes.

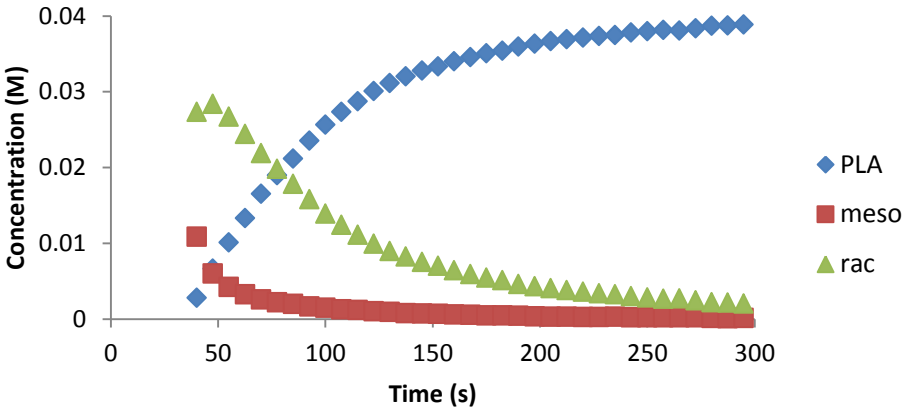

Figure 2. Polymerization of lactide by fluorine-tagged IMes at room temperature. [*meso*-lactide]$_0$ = 37 mM, [*rac*-lactide]$_0$ = 4.7 mM, [*p*-F-IMes] = 10.5 mM.

The stacked ^{19}F NMR spectra are displayed in Figure 3. Only one ^{19}F NMR peak was observed during reaction progression. There was some observed broadening in the peak, but efforts to model the broadening were unsuccessful without any peak separation. Additionally, there could be fast exchange that could not be modeled.

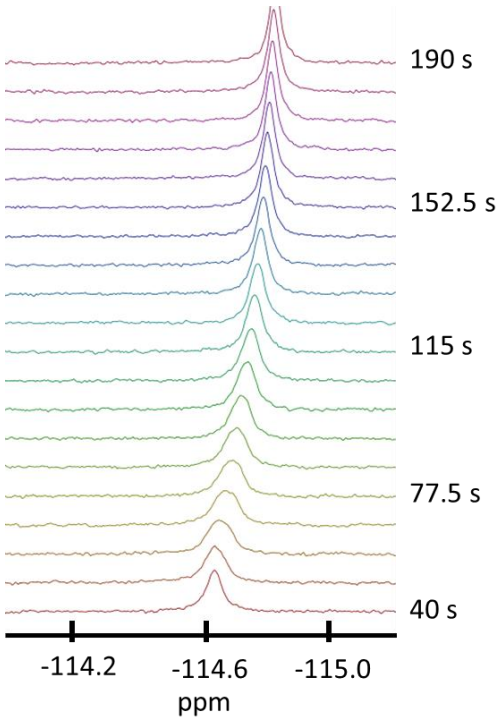

Figure 3. Stacked ^{19}F NMR spectra during polymerization of lactide with fluorine-labeled IMes at room temperature. [*meso*-lactide]$_0$ = 37 mM, [*rac*-lactide]$_0$ = 4.7 mM, [*p*-F-IMes] = 10.5 mM.

Broadening is also observed in the imidazole ^{1}H NMR peak at 6.2 ppm during polymerization (Figure 4). Efforts to model the broadened peak as two overlapping species were unsuccessful.

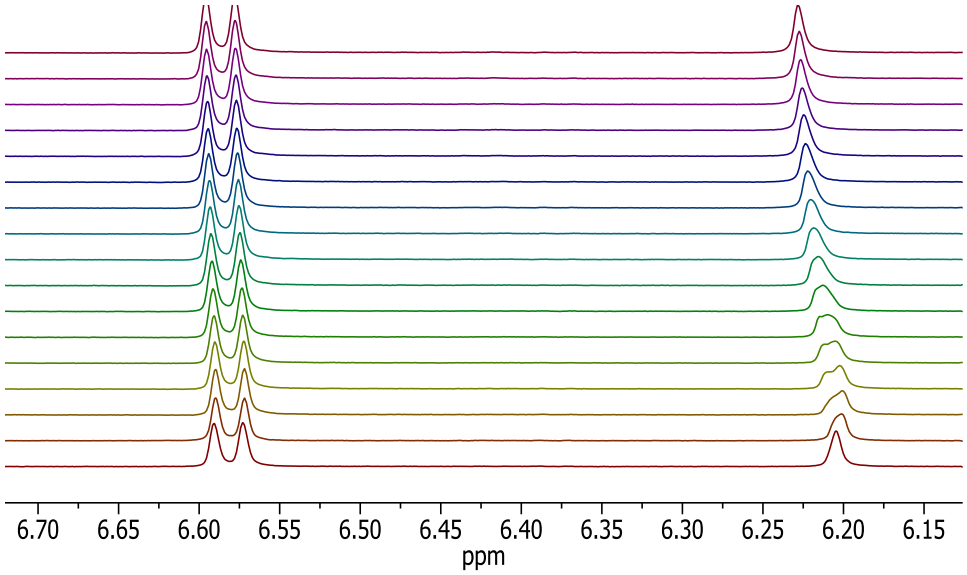

Figure 4. ^{1}H NMR spectra during reaction progression. The bottom spectrum is after 40 s of reaction time, with each subsequent spectrum 7.5 s later. [*meso*-lactide]$_0$ = 37 mM, [*rac*-lactide]$_0$ = 4.7 mM, [*p*-F-IMes] = 10.5 mM.

Conclusion

Although 1,3-bis(4-fluoro-2,6-dimethylphenyl)-2-ylidene does polymerize lactide, catalyst speciation was not observed during polymerization. Peak broadening was observed but attempts to model the peak broadening as two simple overlapping peaks were unsuccessful. There could be fast exchange between the zwitterionic and carbene species causing the observed behavior. Additionally, the fluorine tag may be too far away from the carbene to show a large chemical shift difference between free carbene and zwitterion in ^{19}F NMR. Future work could focus on creating other labeled carbenes in order to observe catalyst speciation. Particularly, labeling the carbene carbon with ^{13}C should give conclusive evidence of catalyst speciation by monitoring the reaction by ^{13}C NMR spectroscopy.

Experimental

Synthesis of N, N'-bis(2,6-dimethyl-4-fluorophenyl)imidazolium tetrafluoroborate

N, N'-bis(2,6-dimethyl-4-fluorophenyl)imidazolium chloride (100 mg, 0.287 mmol) was dissolved in 7 mL H_2O and stirred until mostly dissolved. Aqueous fluoroboric acid (48 wt% in water, 41 μL, 0.315 mmol, 1.1 equivalents) was added and stirred at room temperature for 1.5 h. The product was extracted with CH_2Cl_2 (3 x 25 mL), and the organic layers were combined and dried over $MgSO_4$. The solvent was evaporated, yielding *N, N'*-bis(2,6-dimethyl-4-fluorophenyl)imidazolium tetrafluoroborate as a light yellow solid (110.2 mg, 0.275 mmol, 96.0% yield). ^{1}H NMR (400 MHz, CD_2Cl_2) δ 8.98 (s, 1H), 7.59 (s, 2H), 7.04 (d, J = 8.6 Hz, 4H), 2.19 (s, 12H). ^{19}F NMR (377 MHz, CD_2Cl_2) δ -109.10 (s, 4F), -152.09 (s, 2F).

Synthesis of 1,3-bis(4-fluoro-2,6-dimethylphenyl)-2-ylidene

N, N'-bis(2,6-dimethyl-4-fluorophenyl)imidazolium tetrafluoroborate (100 mg, 0.25 mmol) was dissolved in 5 mL THF. Sodium hydride (12 mg, 0.5 mmol, 2 equiv) was added and stirred at room temperature overnight. The reaction mixture was filtered through celite and the solvent was removed, yielding 1,3-bis(4-fluoro-2,6-dimethylphenyl)-2-ylidene as an off-white solid in a 30% yield (23.4 mg, 0.075 mmol). ^{1}H NMR (400 MHz, Toluene-d_8) δ 6.60 (d, J = 9.0 Hz, 4H), 6.31 (s, 2H), 1.92 (s, 12H). ^{19}F NMR (377 MHz, Toluene-d_8) δ -115.0 (s, 2F). ^{13}C NMR (126 MHz, Toluene-d_8) δ 220.18, 161.95 (d, J = 245.5 Hz), 138.03, 137.96, 120.53, 114.81 (d, J = 22.1 Hz), 18.01.

NMR Procedure

Meso-enriched lactide (89% *meso*-, 11% *rac*-lactide) and bis-trimethylsilylbenzene (BTMSB) were dissolved in toluene-d_8 and placed in an NMR tube. To initiate the reaction, a solution of 1,3-bis(4-fluoro-2,6-dimethylphenyl)-2-ylidene in toluene-d_8 was injected into the NMR tube, which was then inverted twice and placed back into the spectrometer. The initial concentrations were as follows: [*meso*-lactide]$_0$ = 37 mM; [*rac*-lactide]$_0$ = 4.7 mM; [*p*-F-IMes] = 10.5 mM; [BTMSB] = 11.4 mM.

References:

(1) McGee, W. a; Parkhurst, L. J. *Anal. Biochem.* **1990**, *189* (2), 267.

(2) Frieden, C.; Hoeltzli, S. D.; Ropson, I. J. *Protein Sci.* **1993**, *2* (12), 2007.

(3) Hoeltzli, S. D.; Ropson, I. J.; Frieden, C. In *Techniques in Protein Chemistry V*; Crabb, J. W., Ed.; Academic Press: San Diego, CA, 1994; pp 455–465.

(4) Jeong, W.; Shin, E. J.; Culkin, D. a.; Hedrick, J. L.; Waymouth, R. M. *J. Am. Chem. Soc.* **2009**, *131* (13), 4884.

(5) Culkin, D. a.; Jeong, W.; Csihony, S.; Gomez, E. D.; Balsara, N. P.; Hedrick, J. L.; Waymouth, R. M. *Angew. Chemie - Int. Ed.* **2007**, *46* (15), 2627.

(6) Leuthäußer, S.; Schmidts, V.; Thiele, C. M.; Plento, H. *Chem. - A Eur. J.* **2008**, *14* (18), 5465.

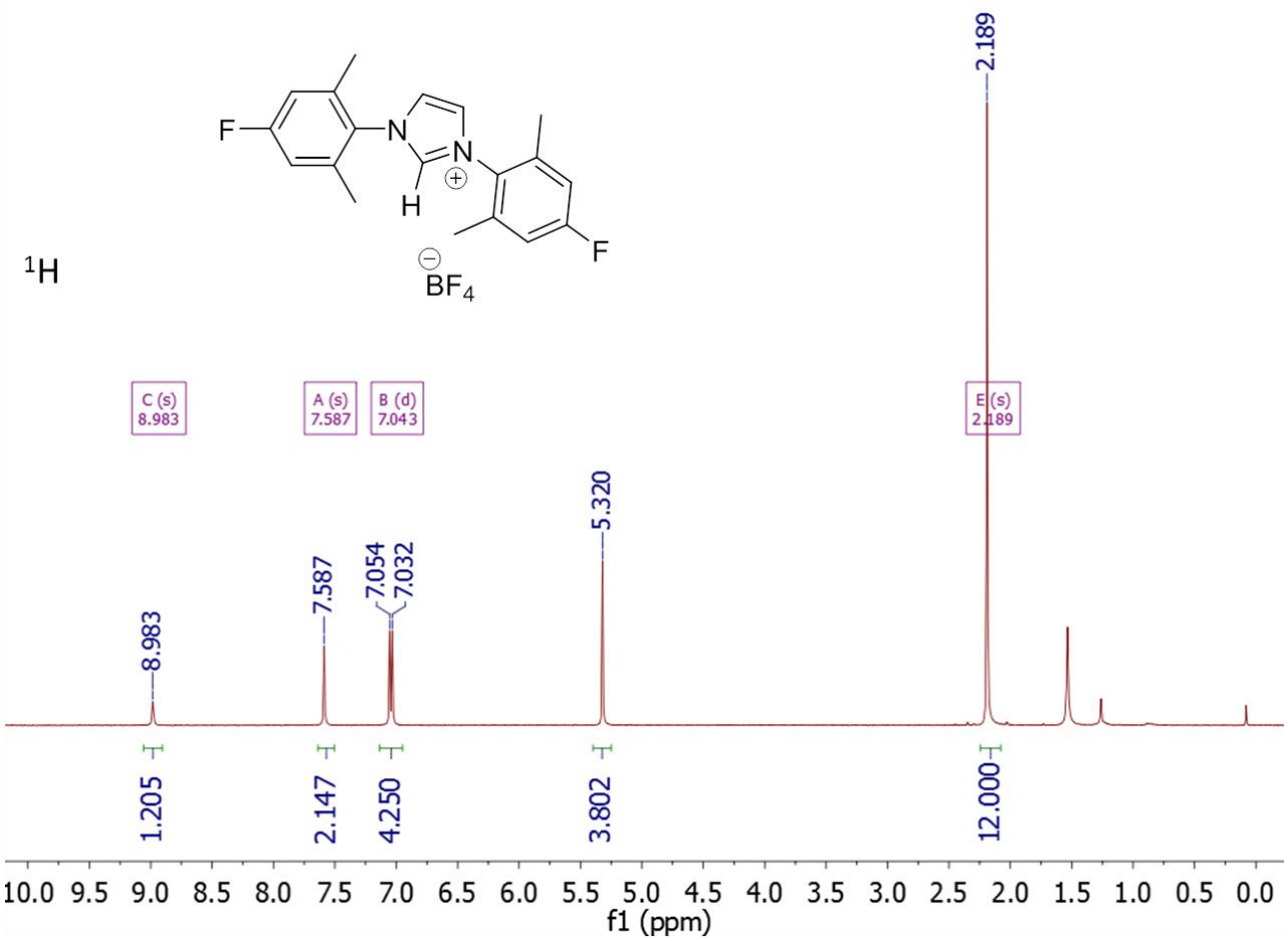
^{1}H
F
N
N
H
F
BF_4
C (s) 8.983
A (s) 7.587
B (d) 7.043
E (s) 2.189
8.983
7.587
7.054
7.032
5.320
2.189
1.205
2.147
4.250
3.802
12.000
10.0 9.5 9.0 8.5 8.0 7.5 7.0 6.5 6.0 5.5 5.0 4.5 4.0 3.5 3.0 2.5 2.0 1.5 1.0 0.5 0.0
f1 (ppm)

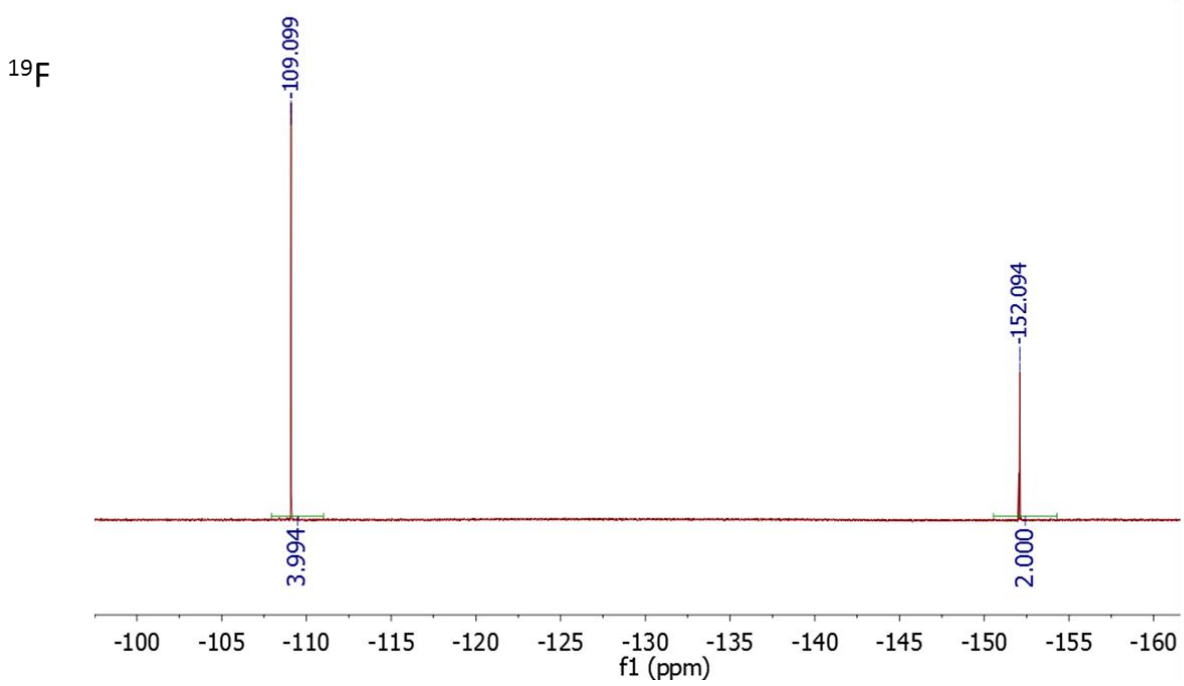
^{19}F
-109.099
-152.094
3.994
2.000
-100 -105 -110 -115 -120 -125 -130 -135 -140 -145 -150 -155 -160
f1 (ppm)

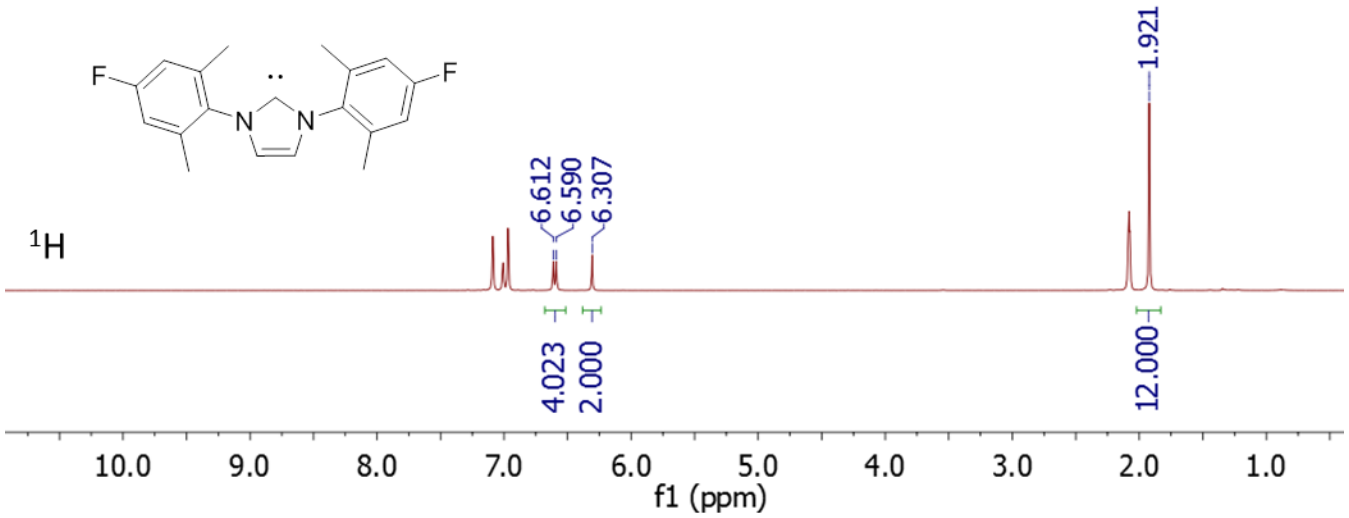
F
F
N
N
1.921
6.612
6.590
6.307
^{1}H
4.023
2.000
12.000
10.0
9.0
8.0
7.0
6.0
5.0
4.0
3.0
2.0
1.0
f1 (ppm)

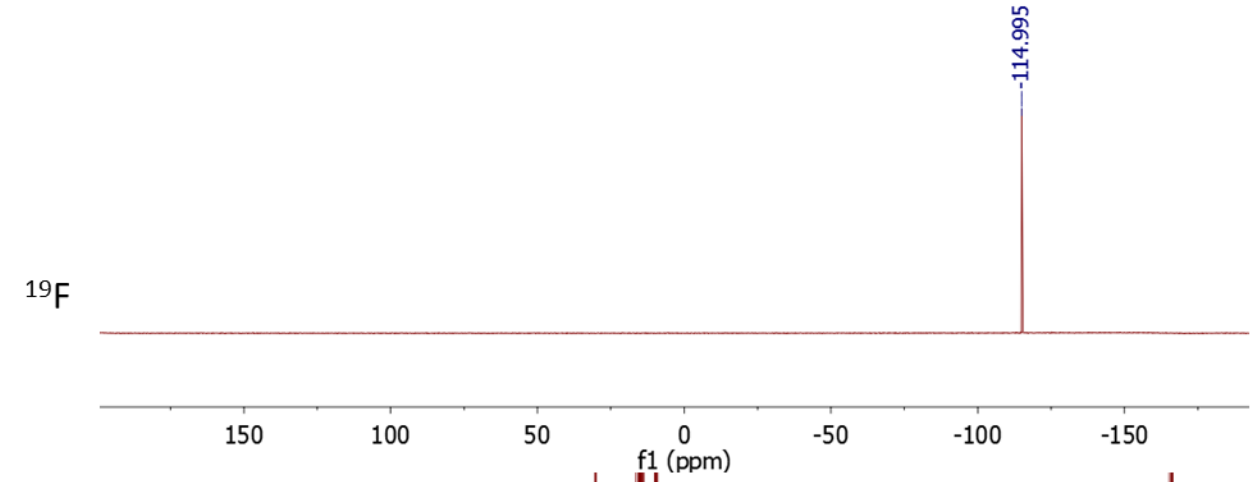
-114.995
^{19}F
150
100
50
0
-50
-100
-150
f1 (ppm)

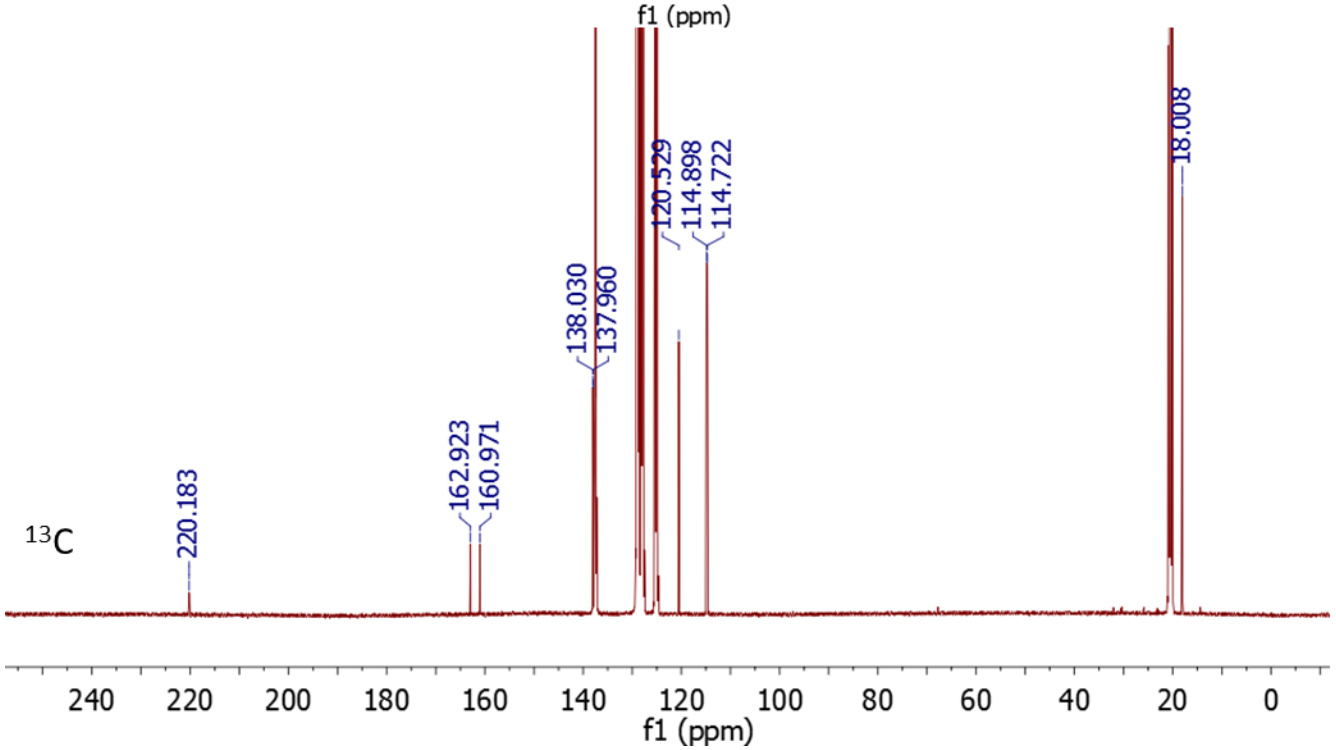
18.008
120.529
114.898
114.722
138.030
137.960
162.923
160.971
220.183
^{13}C
240
220
200
180
160
140
120
100
80
60
40
20
0
f1 (ppm)

Appendix C

Stopped-Flow NMR Pulse Sequence Optimization

Introduction

The pulse sequence used for SF NMR is crucial because quantitative integrations are essential in order to gain high quality, accurate mechanistic and kinetic information. For a series of one-pulse spectra with very short delays between acquisitions, leftover magnetization from the previous pulse can cause non-quantitative integrals. Three pulse sequences were tested for their ability to provide quantitative integrations (Figure 1). A 30° pulse was used because it allows three times faster magnetic relaxation while retaining 87% of the maximum signal intensity of a 90° pulse.

Results and Discussion

The first pulse sequence tested, **A** (Figure 1a) is the standard 30° pulse sequence used when taking ^{1}H 1D NMR data. The second, **B** (Figure 1b), and third, **C** (Figure 1c), pulse sequences utilize spoiler gradient pulses, which cause any transverse (xy plane) magnetization to become incoherent. The pulse sequence **B** uses a sequence of spoiler gradient, 90° pulse, spoiler gradient (Figure 1b). The first spoiler gradient "hsgt" removes any transverse magnetization leftover after the previous acquisition. The 90° pulse moves any magnetization on the z axis to the xy plane, where it is then removed by the second spoiler gradient pulse, resulting in no leftover magnetization from the previous pulse sequence iteration. The next pulse sequence, **C** (Figure 1c), adds one spoiler gradient to the 30° pulse sequence to remove any transverse magnetization from the previous pulse. Pulse sequence **C** does not remove any leftover z magnetization, allowing the entire sample to become fully magnetized on the z axis more quickly, which should result in more accurate integration data for fast reactions.

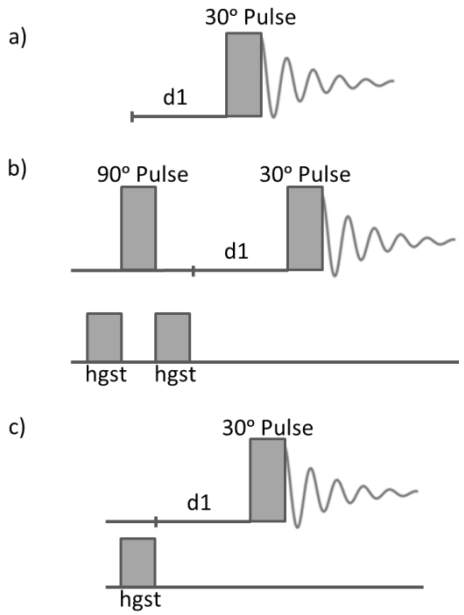

Figure 1. A comparison of SF pulse sequences. a) **A**, a simple 30° pulse sequence b) **B** adds a sequence of spoiler gradient (hgst), 90° pulse, and second spoiler gradient c) **C** adds one spoiler gradient to the 30° pulse. The sequence is repeated after acquisition finishes until the reaction is complete. For b) and c), the top line is the proton detection channel and the bottom line is the gradient channel.

In order to compare each pulse sequence directly, a sample of lactide was placed in protio THF in a standard 5 mm NMR probe and the pulse sequences were ran with different delays prior to the 30° pulse (d1). Since the sample was not reacting, the integrations should be constant with each successive acquisition. The results displayed have d1 set to 0.01 s and acquisition time (aq) to 1 s to highlight any existing problems (Figure 2). The integrals of the methyl (a doublet) and methine (a quartet) protons are normalized to one proton by dividing the integration of the methyl signal by 3. An ideal pulse sequence would result in a straight horizontal line at 1 proton for both methyl and methine signals, showing full magnetization relaxation with no t_1 (spin–lattice relaxation time) dependence, which is apparent if the methine and methyl signals show different integrations after being normalized to 1.

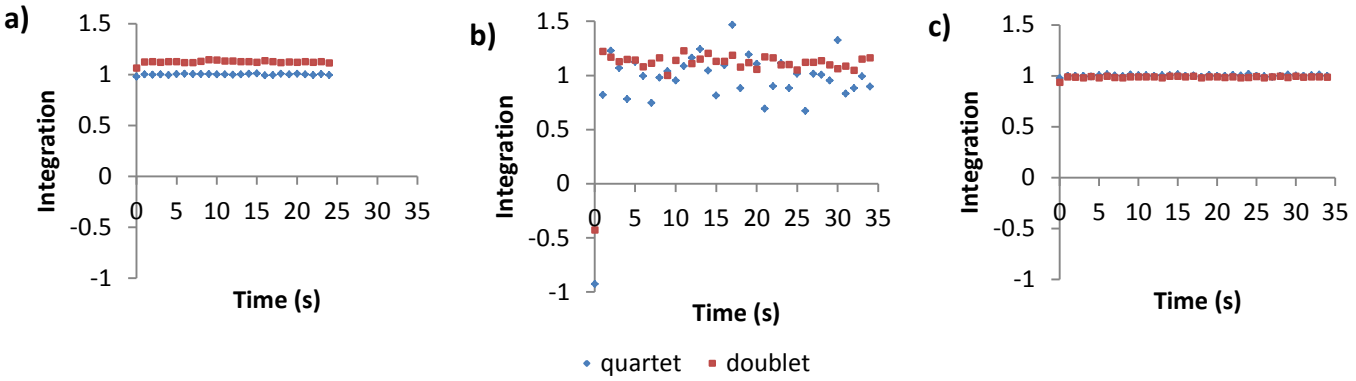

Figure 2. A comparison of the integration values of a static sample of lactide in protonated THF with different pulse sequences. a) **A**, with no spoiler gradients b) **B**, with two spoiler gradients and a 90° pulse c) **C**, with one spoiler gradient. All integrations are normalized to one proton.

The pulse sequence with no gradients, **A**, shows a mostly consistent signal with time (Figure 2a), but the methine quartet and the methyl doublet of lactide are not the same value, indicating t_1 dependence. The pulse sequence with two gradient pulses and a 90° pulse, **B**, shows extremely inconsistent integrations with time (Figure 2b), and the first scan has negative integrations. The pulse sequence **C** shows very consistent integrations with time and no t_1 dependence (Figure 2c). These data clearly show that the pulse sequence with one gradient should be used for SF NMR experiments. With such a short delay time (here we used d1 = 0.01 s), the simple pulse sequence **A** is not able to fully magnetize the transverse signals leftover from the previous pulse, so we see an effect on the methine signals (which have a longer t_1 than the methyl signals). With pulse sequence **B**, all magnetization is removed prior to the delay time, which is too short to allow for magnetization of a completely un-magnetized sample, causing noisy results. Pulse sequence **C**, with one spoiler gradient pulse, removes the leftover transverse magnetization, which takes the most time to be magnetized to the z axis, allowing a short delay time to be used and still obtain consistent integrations with no t_1 dependence.

Conclusion

Under the conditions of a short delay prior to the pulse and quick, successive acquisitions, pulse sequence **C**, which consisted of one spoiler gradient pulse, performed the best of the three pulse sequences tested, showing no t_1 dependence and consistent integrations. Therefore, for stopped-flow NMR spectroscopy where a series of quick acquisitions is desired, a spoiler gradient pulse should be added to the pulse sequence.

Appendix D

Chapter 3 CAD Diagrams

All measurements are in inches. See chapter three for photographs of the machined pieces.

Probe Base:

From above:

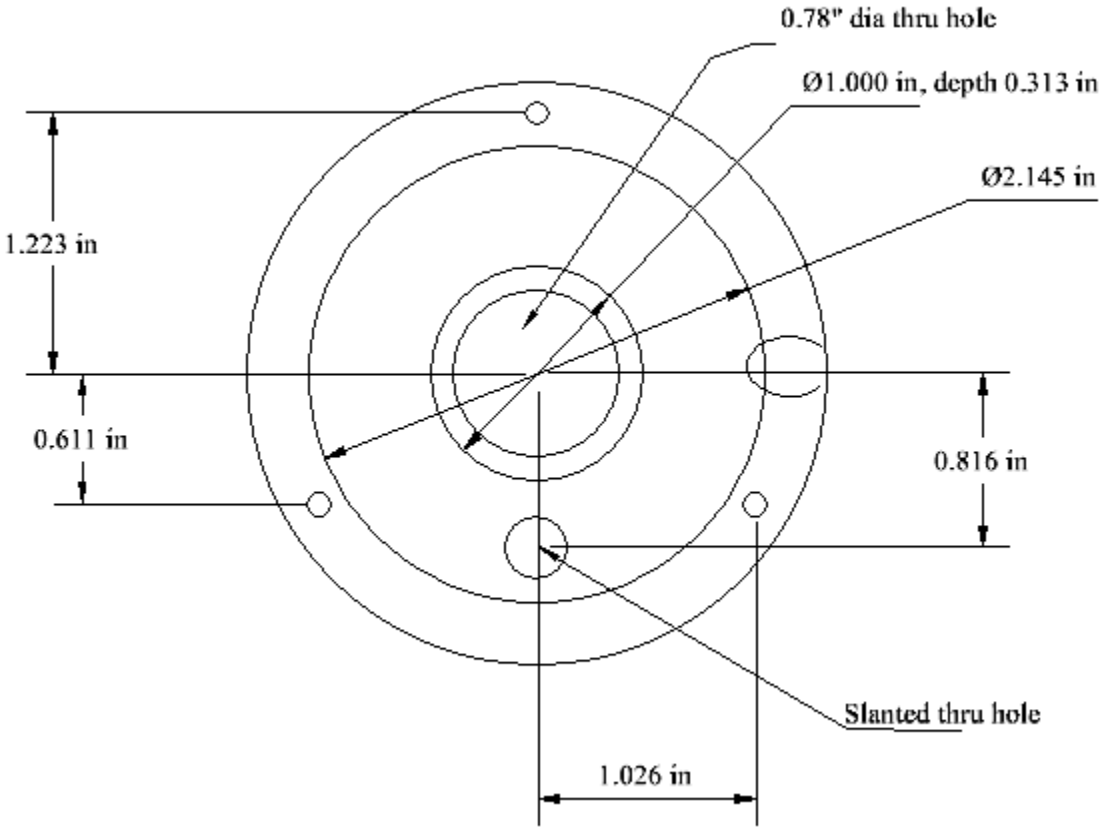

From below:

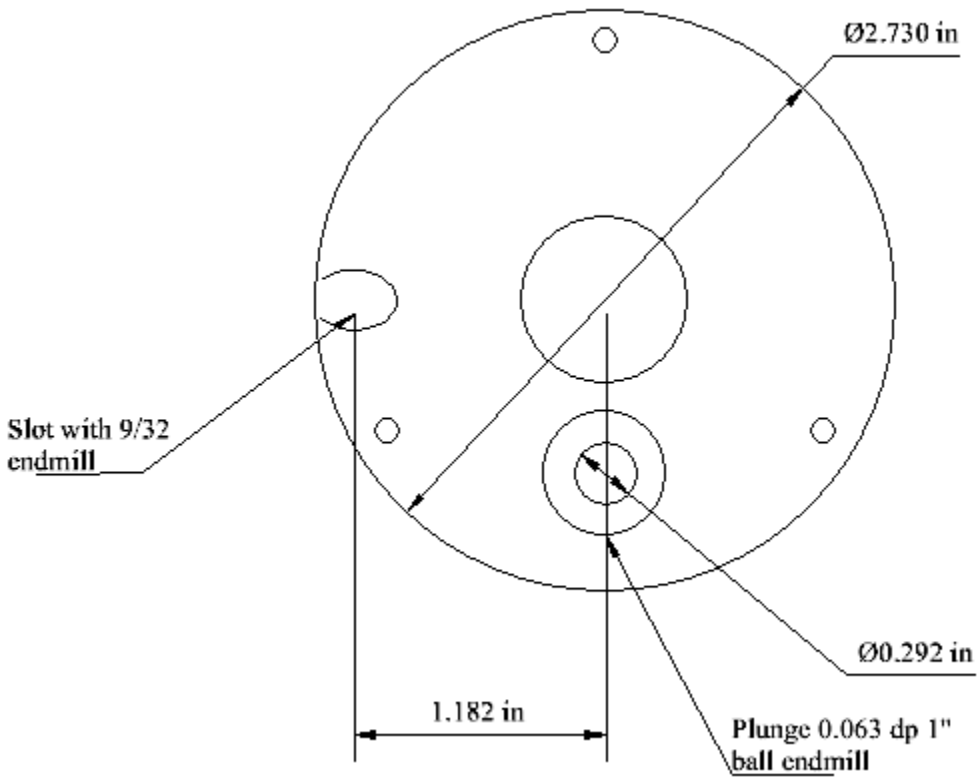
Ø2.730 in
Slot with 9/32
endmill
Ø0.292 in
1.182 in
Plunge 0.063 dp 1"
ball endmill

From side:

View A:

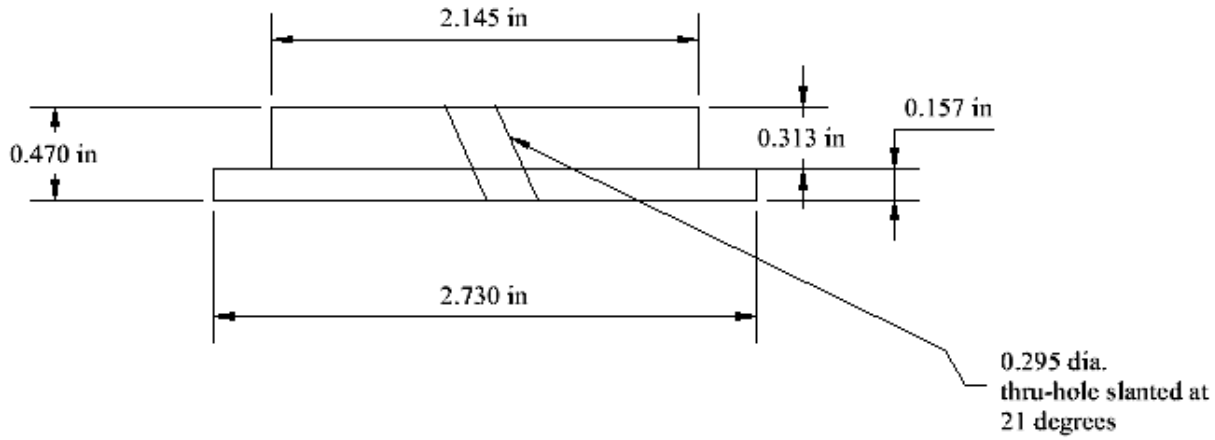

View B:

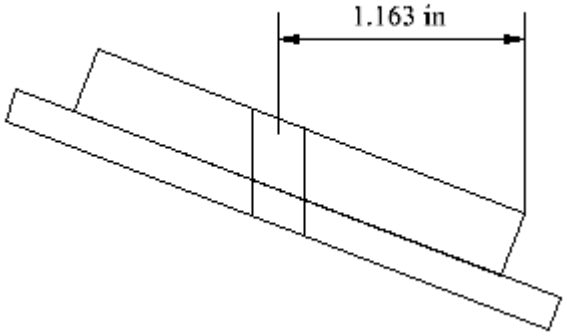

Mixer Body:

From above:

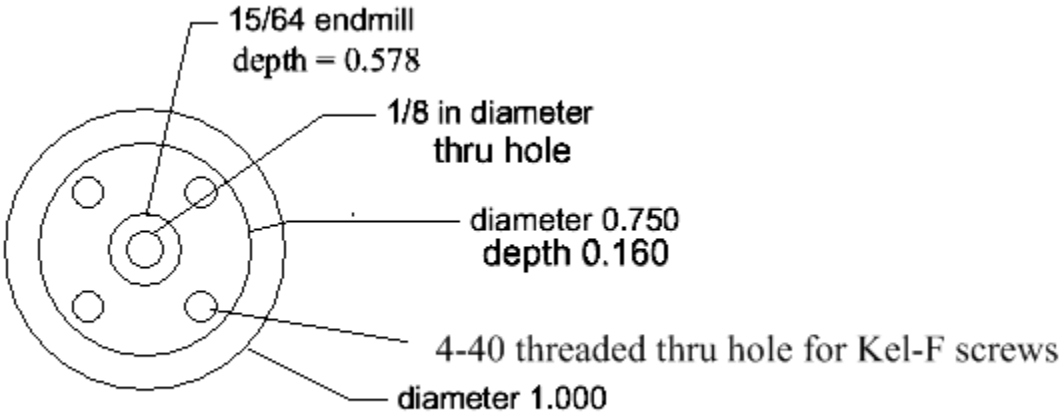

From below:

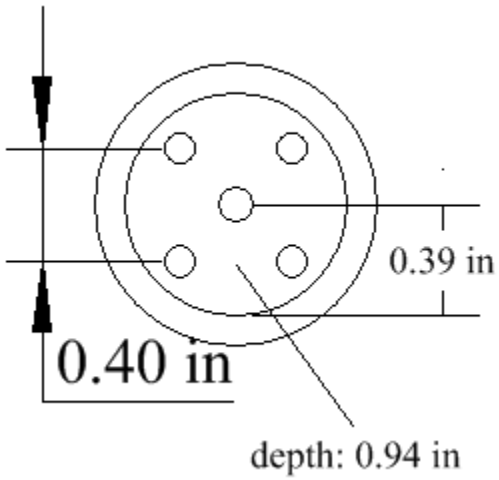

From side:

View A:

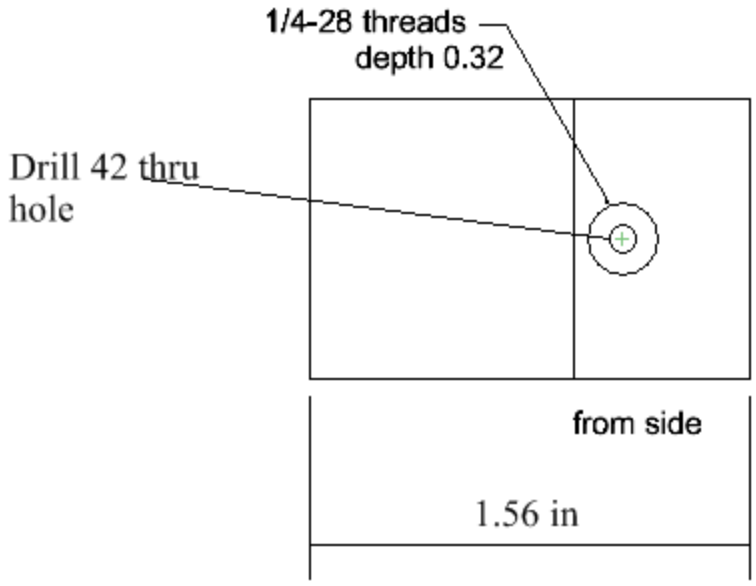

View B:

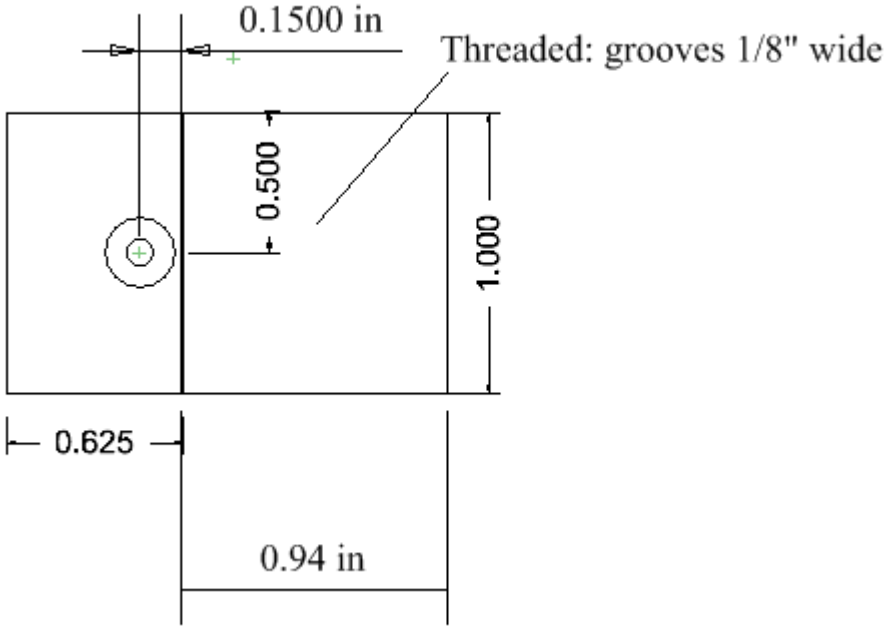

Mixer Cap:

From above:

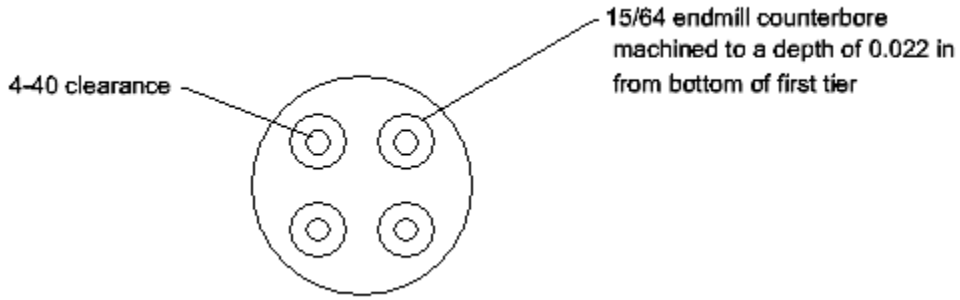

From below:

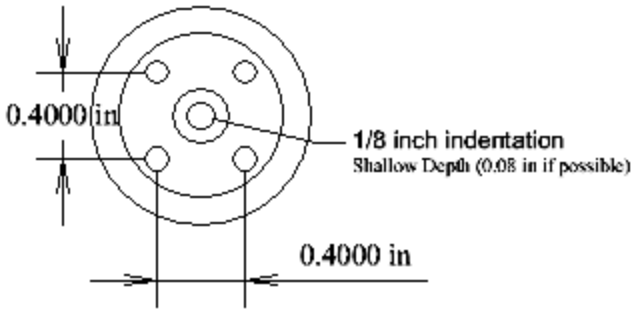

From side:

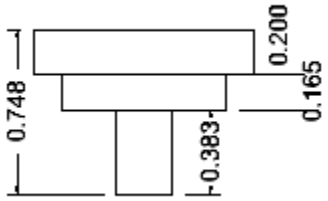

Appendix E

Supporting Information for Chapter 6

The correlation matrix is output by Copasi to display the amount of correlation between each fitted parameter. The closer the value is to 1 or -1 indicates interdependency between rate constants. Highly correlated parameters are marked in red.

Model 1 Correlation Matrix

	k_i	k_p	k_t	k_{-t}	sf	k_d
k_i	1	0.780741	-0.21427	0.02125	-0.8255	-0.12988
k_p	0.780741	1	0.078592	-0.04525	-0.64554	-0.0889
k_t	-0.21427	0.078592	1	-0.15993	0.560818	-0.00509
k_{-t}	0.02125	-0.04525	-0.15993	1	-0.06829	0.302161
K	-0.8255	-0.64554	0.560818	-0.06829	1	0.09515
k_d	-0.12988	-0.0889	-0.00509	0.302161	0.09515	1

Model 2 Correlation Matrix

	k_i	k_p	k_t	k_{-t}	sf	k_d
k_i	1	-0.4557	0.335347	-0.05715	-0.65456	-0.70329
k_p	-0.4557	1	-0.42917	-0.29691	0.479796	0.931946
k_t	0.335347	-0.42917	1	0.609647	-0.06454	-0.50828
k_{-t}	-0.05715	-0.29691	0.609647	1	-0.27995	-0.33467
K	-0.65456	0.479796	-0.06454	-0.27995	1	0.669931
k_d	-0.70329	0.931946	-0.50828	-0.33467	0.669931	1

Model 3 Correlation Matrix

	k_i	k_p	k_t	k_{-t}	sf	k_d
k_i	1	-0.3445	-0.3623	-0.05919	-0.63595	0.228285
k_p	-0.3445	1	0.965089	0.46428	0.091516	-0.41503
k_t	-0.3623	0.965089	1	0.671029	-0.00731	-0.39714
k_{-t}	-0.05919	0.46428	0.671029	1	-0.45109	-0.1805
K	-0.63595	0.091516	-0.00731	-0.45109	1	-0.03996
k_d	0.228285	-0.41503	-0.39714	-0.1805	-0.03996	1

Waymouth Model Correlation Matrix, low conversions

	k_i	k_p	k_t	k_{-t}	sf	k_d
k_i	1	-0.09136	-0.41653	-0.08894	-0.99553	0.110171
k_p	-0.09136	1	0.445481	-0.05172	0.099089	0.778614
k_t	-0.41653	0.445481	1	0.025008	0.431337	-0.19963
k_{-t}	-0.08894	-0.05172	0.025008	1	0.08958	-0.0678
K	-0.99553	0.099089	0.431337	0.08958	1	-0.10608
k_d	0.110171	0.778614	-0.19963	-0.0678	-0.10608	1

Waymouth Model Correlation Matrix, higher conversions

	k_i	k_p	k_t	k_{-t}	sf	k_d
k_i	1	-0.62694	0.744895	-0.0463	-0.89284	-0.91178
k_p	-0.62694	1	-0.43786	-0.29259	0.637518	0.881433
k_t	0.744895	-0.43786	1	-0.13911	-0.43183	-0.62968
k_{-t}	-0.0463	-0.29259	-0.13911	1	0.038449	-0.18513
sf	-0.89284	0.637518	-0.43183	0.038449	1	0.870878
k_d	-0.91178	0.881433	-0.62968	-0.18513	0.870878	1